UNIVERSITY OF OKLAHOMA

GRADUATE COLLEGE

BIOPHYSICAL MECHANISMS FOR THE GENERATION OF ELECTROSENSORY AND COMMUNICATION SIGNALS IN THE WEAKLY ELECTRIC FISH *EIGENMANNIA VIRESCENS*

A DISSERTATION

SUBMITTED TO THE GRADUATE FACULTY

in partial fulfillment of the requirements for the

Degree of

DOCTOR OF PHILOSOPHY

By

YUE BAN
Norman, Oklahoma
2018

BIOPHYSICAL MECHANISMS FOR THE GENERATION OF ELECTROSENSORY AND COMMUNICATION SIGNAL IN THE WEAKLY ELECTRIC FISH *EIGENMANNIA VIRESCENS*

A DISSERTATION APPROVED FOR THE
DEPARTMENT OF BIOLOGY

BY

_____
Dr. Michael R. Markham, Chair

_____
Dr. Ari Berkowitz

_____
Dr. Christian Lemon

_____
Dr. John P. Masly

_____
Dr. Laura Bartley

Acknowledgements

I would like to express my appreciation and thanks to my dissertation advisor, Dr. Michael Markham, for his generous support for my Ph.D. study, for his patience and kindness. I thank him for always being encouraging and offering me the freedom to explore the research projects that I was interested in. I admire him for trying his best to provide me all the resources to conduct research and develop my career. He is a superb mentor. It has been an honor to be his first Ph.D. student.

I am grateful for Dr. Rosemary Knapp's help in applying for funding that supported me to take the "Neural Systems and Behavior" course in the Marine Biological Laboratory. And I thank Dr. Ari Berkowitz for the great deal of knowledge I learned in the "Neural Control of Movement" and "Behavioral Neurobiology" courses. I will forever be thankful to my current and former advisory committee members Drs. Ari Berkowitz, Christian Lemon, J.P. Masly, Laura Bartley, Benjamin Smith, and Bing Zhang for their patient guidance and advice on my research and career development.

I would like to extend my thanks to many people, who generously contributed to work presented in my dissertation. I thank Dr. Rosemary Knapp for use of her cryostat, Dr. J.P. Masly and Dr. Tingting Gu for imaging assistance, Dr. Sharmishtha Shyamal for advice on qRT-PCR experiment, and Tian Yuan for suggestions on molecular cloning. I thank current and previous members of the Markham lab for creating a respectful, supportive, harmonious work environment, our lab manager Rosalie Maltby for assistance in fish care and purchasing reagents, and Mehrnoush Nourbakhsh for help in molecular cloning.

My sincere thanks also go to the Nancy L. Mergler Dissertation Completion fellowship, the Graduate Student Senate Research and Conference Grants, M. Blanche Adams and M. Frances Adams Scholarship and the Biology Department Travel Grants for funding my research and attendance of academic conferences.

To my parents, thank you for raising me to be a good person and supporting my dream to study abroad. To my beloved husband, thank you for your patience, love, constant support and encouragement.

Table of Contents

List of Tables

Chapter 1

Chapter 2

Chapter 3

List of Figures

Chapter 1

Chapter 2

Chapter 3

Abstract

The weakly electric fish *Eigenmannia virescens* generates electric organ discharges (EODs) to navigate and communicate. The EODs are brief monophasic voltage pulses with brief inter-pulse intervals, resulting in a sinusoidal waveform. EODs are produced by the simultaneous action potentials (APs) of ~1000 electric organ (EO) cells (electrocytes). Electrocytes generate APs at steady frequencies of 200-600 Hz with Na^+ currents that exceed 10 microamperes during each AP, creating large energetic demands. The aim of this study was to investigate the biophysical mechanisms that allow fast spiking and manage the large ionic currents in electroctyes.

E.virescens elecrocytes initiate the AP using voltage-gated Na^+ (Na_v) channels and terminate the AP using Na^+-activated K^+ (K_{Na}) channels, rather than voltage-gated K^+ (K_v) channels, as is the case in other electric fish where electrophysiological data are available. The characteristics of K^+ channels are key determinants of an excitable cell's firing pattern. Using degenerate PCR and RACE-PCR, I identified the presence of three types of K_{Na} channel subunit in electrocytes, eSlack1 and eSlick, closely related to K_{Na} channel subunits in other vertebrates, and a shorter isoform, eSlack2. Whole-cell currents recorded from *Xenopus laevis* oocytes expressing these K_{Na} channels revealed that eSlack1 and eSlick can form functional homomeric K^+ channels and eSlick currents activated much more rapidly than eSlack1 currents. eSlack2 could not form functional homomeric ion channels, even though the subunits could be successfully trafficked to the plasma membrane.

To investigate how ion channels coordinate to generate high-frequency APs, I studied the expression pattern of ion channels and Na^+/K^+ ATPases using

immunohistochemistry and by expressing fluorescent protein-tagged ion channels in electrocytes. Cholinergic receptors and Na_v channels are only localized on the posterior side, while all K^+ channels including the three K_{Na} channel subunits and the ATP sensitive $K_{ir}6.2$ are expressed on the anterior side. Na^+/K^+ ATPases are widely distributed on both the posterior and anterior membranes. Two-photon 3D imaging of electrocytes showed the cell's posterior membrane is densely occupied by narrow invaginations providing extensive surface area for the expression of Na^+ channels and Na^+/K^+ ATPases to manage the large ionic currents. Abundant vesicles were present underneath the posterior membrane, which may be associated with the trafficking of Na^+ channels and Na^+/K^+ ATPases to the plasma membrane when the amplitude of AP is under modulation.

Finally, I investigated the ionic mechanisms associated with variations in AP frequency in the fast-spiking electrocytes by measuring the transcription levels of ion channels and ion transporters in EO from fish with different EOD frequencies. EOD frequency is correlated with the transcription levels of Nav1.4a, the fast-activating Slick K_{Na} channel subunits, $K_{ir}6.2$ and Na^+/K^+ ATPases but not $Na_v1.4b$, eSlack1 and eSlack2.

In summary, the fast-activating Slick K_{Na} channels are expressed exclusively in electrocytes to support the generation of sustained high-frequency APs. Among all the ion channels and ion transporters expressed in electrocytes, only Slick K_{Na} channels, $Na_v1.4a$, and Na^+/K^+ ATPases are associated with increased excitability, and these transcripts are expressed predominantly in electrocytes when compared to skeletal muscle. Variations in the transcription levels of eSlick, Nav1.4a and Na^+/K^+ ATPases

are positively correlated with individual differences in EODf, where they likely contribute to the capacity for high-frequency firing.

Key words: weakly electric fish, three-dimensional electrocyte morphology, ion channel compartmentalization, sodium-activated potassium channels

Abbreviations: EO, electric organ, EOD, electric organ discharge; EODf, electric organ discharge frequency; AP, action potential; I_{Na}, Na^+ current; I_K, K^+ current; Na_v channel, voltage-gated Na^+ channel; K_{Na} channel, Na^+-activated K^+ channel; K_v channel, voltage-gated K^+ channel; K_{ir} channel, inward-rectifier K^+ channel; RACE, rapid amplification of cDNA ends; qRT-PCR, quantitative real-time polymerase chain reaction; ELL, electrosensory lateral line lobe; TS, torus semicircularis; ACTH, adrenocorticotropic hormone; RCK, regulator of K^+ conductance; EC_{50}, half maximal effective concentration.

Preface

The main goal of this research was to investigate the biophysical mechanisms that allow the generation of metabolically expensive electrical sensory and communication signals in the weakly electric fish *Eigenmannia virescens*. In this work, I focused on the cellular and molecular features of *E. virescens* electrocytes that enable the sustained generation of high-frequency APs. It was completed under the supervision of Dr. Michael Markham of the Department of Biology at the University of Oklahoma. The dissertation is composed of four chapters. Chapter 1 is an overview of the electrosensory and communication signals in weakly electric fish. Chapters 2 and 3 have been included in the format of two manuscripts. Chapter 4 is general conclusions and directions for future work.

Chapter 2 is an investigation into the morphological characteristics of electrocytes and the subcellular localization of ion channels and ion transporters in electrocytes. I and Dr. Markham conceived the project. I, Dr. Markham, and Dr. Benjamin Smith designed the experiments and wrote the manuscript. I performed all experiments except as noted. Dr. Markham performed the computational simulation of electrocyte function. Dr. Benjamin participated in this project when he was a research scientist at the Samuel Roberts Noble Microscopy Laboratory of the University of Oklahoma. Dr. Benjamin Smith now works as a microscopy specialist at the University of California-Berkeley. He performed and taught me imaging using the Leica® TCS SP8 laser scanning confocal microscope, rendered the images in Avizo® Fire 8.0.1 and quantified the number of nuclei in electrocytes. The work presented in this chapter has been published as Ban, Y., Smith, B. E., & Markham, M. R. (2015). A highly polarized

excitable cell separates sodium channels from sodium-activated potassium channels by more than a millimeter. Journal of Neurophysiology, 114(1), 520-530.

Chapter 3 is an investigation into the ionic mechanisms associated with variations in action potential frequency in the fast-spiking electrocytes. I and Dr. Markham conceived the project and designed the experiments. I performed all experiments (except as noted) and wrote the manuscript. Rosalie Maltby, a researcher in Dr. Markham's lab, performed RACE-PCR to amplify a fragment of eSlack1. Mehrnoush Nourbakhsh, a Ph.D. student at Dr. Markham's lab, helped subclone mCherry-eSlack2 and mCherry-eSlick nucleotide sequence from pOX vectors into pMAX vectors.

Chapter 1: General introduction

Cost of communication signals

Communication occurs when one organism (the signaler) transmits information to a second individual (the receiver) to influence the behavior of the receiver. The information can be carried by a great diversity of signals including visual, acoustic, chemical, electrical and tactile modalities such as the ornamented tail feathers of a peacock, the roar of howler monkeys, the trail pheromones produced by ants, and the electric fields generated by electric fish. Although signaling can bring benefits including winning the competition for mates, warning approaching animals to maintain territories, leading nestmates to the location of food resources, etc., both signalers and receivers incur costs to participate in communication (Bradbury and Vehrencamp, 1998). These costs are represented in various forms: energetic investments in signal emission and anatomical structures required for signal production and receiving, opportunity cost such as the loss of foraging time due to efforts in signaling to attract mates, and risks of predators eavesdropping on the signals (Bradbury and Vehrencamp, 1998).

The cost of signaling determines the reliability of communication. When signalers and receivers experience conflicts of interest, why do animals continue to communicate reliably despite the temptation to manipulate signal receivers with misleading information? Zahavi's "costly signaling" theory provided one explanation to this puzzle (Zahavi, 1975). The production of misleading signals is much more costly than honest signals, thus it is not worthwhile for signalers to deceive receivers. The incentives of honest communication come from the costs of signaling.

Communication signals can be energetically costly or inexpensive depending on the proportion of the organism's energy budget allocated to signal production. Passive visual signals conveying information by the size, shape and color of an animal are thought to require less energy input from the signalers, because most of the energy is provided by extrinsic sources – the sun. Communication signals are costly when they involveactive signal generation such as the emission of ultrasonic echolocation calls of bats and electric organ discharges of weakly electric fish, in which the energy originates from the signalers (Nelson and MacIver, 2006).

Communication signals coupled to active sensory systems

Animals interpret the surrounding world by receiving signals reflected from or generated by objects in the environment. The sensory systems can be either active or passive depending on the origin of the energy carried by the signal. In passive sensory systems, the energy is generated by an extrinsic source, for example, birds use plumage color as a mating signal, in which the energy being received is provided by the sun. Some animals adopted active sensory systems, in which they use self-generated energy to probe the outside environment. Examples include echolocation in bats and dolphins, electrolocation in weakly electric fish, and active movement of whiskers in rodents and antennae in insects (Bullock et al., 2006; DuÈrr et al., 2001; Hartmann, 2001; Thomas et al., 2004).

Animals with active sensory systems have the advantage of precisely controlling the characteristics of signals, such as the magnitude, direction and temporal resolution. In the example of weakly electric fish, they image their environment by generating an electric field, which allows them to operate in environments with low or absent ambient

energy (e.g., light), thereby inhabiting ecological niches other animals cannot (Bullock et al., 2006). Using electricity as the primary sensory modality also reduces the chance of eavesdroppers that target prey by detecting visual or acoustic signals. Additionally, the electric signals are broadly distributed to encompass a full 360° around the body to allow them to maintain sensory contact with targets in any direction (Knudsen, 1975). Some South American species can generate continuous high-frequency electric signals to image their surrounding world with very high temporal resolution. The combination of an omnidirectional emission pattern and a high discharge rate makes it easier for these fish to track moving objects, especially when living in rapidly flowing rivers (Hopkins and Heiligenberg, 1978).

The trade-off for these advantages in active sensory systems is higher energetic demand as active-sensing animals need to allocate energy to generate the signals. Energy carried by the signals will be reduced during propagation by absorption or scattering by objects in the environment before being received by animals. Active-sensing animals pay twice for the attenuation cost, once as the signal is transmitted from the signaler to the target, and again as the signal is returned from the target to the signaler (Nelson and MacIver, 2006). To compensate for the effects of attenuation, the intensity of signals emitted from active-sensing animals is often orders of magnitude higher than the detection threshold of receptors (Nelson and MacIver, 2006). Reducing energetic cost through decreasing the magnitude of signals or ceasing the signal periodically is likely to decrease the animal's sensory and physical performance. Signal cessation is not even possible for those weakly electric fish that generating continuous high-rate electric signals for navigation and communication.

Electrolocation and communication in weakly electric fish

In teleost fishes, electroreception appears in two distantly related clades: the South American siluriformes plus gymnotiformes and the African notopteriformes plus mormyriformes. The presence of ampullary-type receptors allows them to perceive low-frequency electric fields produced by other organisms. In contrast to siluriformes and notopteriformes that are only passively electroreceptive, gymnotiformes and mormyriformes independently evolved EOs which are specialized to generate electric discharges, and tuberous electroreceptors that are tuned to self-produced high-frequency electric fields (Alves-Gomes, 2001; Lavoué et al., 2012). The electrogenic and electroreceptive organs in these two independent lineages have evolved in a convergent manner and developed an effective electric sensory and motor system in these fish. One gymnotiform, *Electrophorus electricus,* generates high-voltage shocks to stun prey and dissuade predators, while all other gymnotiformes and mormyriformes generate weak EODs for locating targets and communicating with conspecifics, thus are commonly called "weakly electric fish."

Most weakly electric fish are nocturnal and live in murky waters where visual perception is almost impossible. Electrical signaling enables them to detect targets in the range of approximately one body length (Von der Emde, 1999). Objects having different electrical properties from the surrounding water will distort the electric field. By monitoring the distortions, these fish are able to determine the location, size, shape and composition of nearby objects. An object that is more conductive than water (e.g., copper) will increase the density of current lines between the object and the fish to create an "electrical bright spot" on the fish's skin. In contrast, an object that is more

resistant than water (e.g., a rock) will decrease the current intensity and give rise to an "electrical shadow" on the fish's skin. Non-conducting objects (e.g., plastics) will slow down the passage of electricity, resulting in a delay in the arrival of electrical signals at the tuberous receptors (Bastian, 1981; Heiligenberg, 1973; von der Emde, 1990; Von Der Emde, 1998; von der Emde and Fetz, 2007). A fish's electrolocation ability deteriorates in the presence of nearby fish generating electrical discharges at similar frequencies. Some species can avoid this jamming of electroreception by shifting their discharge frequency to reduce interference. During this jamming avoidance response, *Eigenmannia* can both increase and decrease its EOD frequency, while *Apteronotus* can only raise its frequency (Bullock et al., 1972; Heiligenberg, 1973; Heiligenberg et al., 1991).

The waveform and frequency of the EOD are species-specific, sexually dimorphic and individually distinct, and therefore can convey information about the fish's species, sex, identity and social status. For example, the glass knifefish *Sternopygus macrurus* discharge at ~ 50-200 Hz (Hopkins, 1974a) while the brown ghost knifefish *Aperonotus leptorhynchus* discharge at much higher frequencies ~600-1100 Hz. Sexual dimorphism in electric signals has been reported in many species. The EOD rates of male *Sternopygus* and *Eigenmannia* are lower than those of females, whereas male *Apteronotus* discharge at higher frequencies than females (Hopkins, 1972, 1974a; Meyer et al., 1987; Zakon et al., 1991). Within each species' range of discharge rates, each individual has its unique frequency and waveform. In *Apteronotus* and *Sternarchorhynchus*, dominant males show higher discharge rates (Fugère et al., 2010; Hagedorn and Heiligenberg, 1985).

These fish can also modify EOD patterns to communicate during social encounters such as aggression and courtship behaviors (Bullock, 1969; Hagedorn and Heiligenberg, 1985). The most-studied modulations are "chirps," which are transient and dramatic increases in EOD frequency, followed by a similarly rapid decrease to baseline frequency. The increase in discharge rate is usually accompanied by a reduction in EOD amplitude. In *Apeteronotus*, chirps could occur spontaneously or be induced by an artificial electric signal mimicking the presence of a nearby fish (Bullock, 1969; Engler et al., 2000; Engler and Zupanc, 2001; Zupanc, 2002; Zupanc and Maler, 1993).

The self-generated electric discharges and any modifications to the electric fields during navigation and communication are sensed by the tuberous receptors. These electroreceptors are densely distributed over the fish's skin, allowing the animal to monitor its outside environment in an almost omnidirectional manner (Carr et al., 1982). Axons of these electroreceptors project to the electrosensory lateral line lobes (ELLs) in the hindbrain. ELL efferent cells project to the midbrain torus semicircularis (TS), neurons of which then convey electrosensory information to higher processing centers (Bell and Maler, 2005; Krahe and Maler, 2014).

Electric organs and the generation of electric organ discharges

The electric signals used for navigation and communication are generated by the EO. In gymnotiformes, the EO usually runs longitudinally along the fish's body extending from just behind the gill to the tail. In mormyriformes, the EO is located between the trunk and the caudal fin (Bennett, 1971a; Stoddard, 2010). The EO is composed of specialized cells, named electrocytes. Except for *Apteronotus*, the EO of

which is neurogenic, all the remaining gymnotiformes and Mormyridae have EOs derived from muscle cells (Kirschbaum, 1977). The development of the EO in *Apteronotus* starts with a myogenic EO in the larval stage, which is then replaced by the axons of electromotor neurons during the juvenile stage (Kirschbaum, 1983).

Compared to muscle fibers, myogenic electrocytes are larger in cell size, more electrically excitable, have enhanced insulation and eliminate the coupling between excitation and contraction. Gallant and colleagues (2014) identified the transcriptional changes accompanying the evolution of myogenic EOs from muscle tissues by transcriptome profiling of myogenic EOs and skeletal muscles in several species of gymnotifomes and mormyriformes. EOs downregulate several transcription factors to prevent further differentiate into muscle; enhance expression of the α subunit of Na^+/K^+ ATPases (*atp1a2a* and *atp1a3a*) and voltage-gated Na^+ channels (*scn4aa*) to increase excitability; increase expression of two collagen genes, *col6a6 and col141a1* to ensure insulation; and upregulate genes involved in the insulin-like growth factor signaling pathway to increase cell size (Gallant et al., 2014).

Electrocytes in the EO are usually organized in orderly rows (Ban et al., 2015; Paul et al., 2015; Schwartz et al., 1975a). The firing frequency of electrocytes is controlled by the medullary pacemaker nucleus via spinal motor neurons that innervate each cell on one face (Bennett et al., 1967a; Bennett et al., 1967b). All the electrocytes fire APs simultaneously to generate a current that moves forward toward the head then returns to the tail through the surrounding water. The EOD waveform can be monophasic, biphasic or more complex, depending on the biophysical properties of electrocytes. For example, the electrocytes of *Eigenmannia* and *Sternopygus* only

express voltage-gated Na^+ (Na_v) channels on the innervated posterior face and are able to fire a single AP, resulting in a monophasic EOD (Ban et al., 2015; Patterson and Zakon, 1996). In contrast, the electrocytes of *Brachyhypopomus* express Na_v channels on both the posterior and anterior faces. Upon stimulation, the innervated posterior face first generates an AP creating a headward flux of Na^+ ions, which depolarizes the anterior face and generates a second AP with a tailward flow of Na^+ ions. The two APs together create a biphasic EOD wave (Fig. 1) (Markham and Stoddard, 2005; Stoddard et al., 1999).

Based on the frequency and regularity of EOD waveforms, weakly electric fish are classified into two categories. All mormyriformes (except *Gymnarchus niloticus*) and the gymnotiform families *Gymnotidae, Hypopomidae, and Rhamphichthyidae* are pulse-type fish producing low-rate EODs (10-120 Hz) separated by long and irregular intervals. In contrast, fish that generate continuous high-frequency EODs (50-1100Hz) with intervals almost equal to the duration of a single EOD, such as *Gymnarchus niloticus* and the gymnotiform families *Apteronotidae and Sternopygidae* are defined as wave-type fish (Fig. 1) (Bennett, 1970a; Hopkins, 1986). Pulse-type fish can modulate their discharge rate, whereas wave-type fish maintain a constant high-frequency EOD, making it impossible to regulate energy expenditure by modulation of discharge rate.

Metabolic cost of EOD generation

The metabolic cost of electrogenesis in weakly electric fish has been addressed in a few studies with contrasting results. Earlier studies suggested that the energetic cost of electrogenesis was negligible. Hopkins (Hopkins, 1999) estimated the cost of EOD generation in the pulse-type fish *Gnathonemus petersii* based on previous current and

voltage recordings from the EO (Bell et al., 1976), and suggested that the energy allocated to electrogenesis is only ~1% of the total energy budget. Julian et al. found that the oxygen consumption rates of 34 gymnotiformes were only half of that estimated for non-electric teleost fishes having similar sizes (Julian et al., 2003). Whether the generation of communication signals is energetically costly or inexpensive should primarily depend on the proportion of energy budget that are allocated to signal production. It is important to focus on the cost of EOD production other than the metabolic cost of the whole animal. Salazar and Stoddard combined pharmacological approaches and respirometry to partition the cost of electrogenesis from other metabolic costs in the pulse-types fish *Brachyhypopomus pinnicaudatus,* and found that males consumed 11-22% of the total energy for electrical signaling (Salazar and Stoddard, 2008b). Lewis et al. used respirometry to measure the animal's oxygen consumption during the jamming avoidance response and estimated that an individual EOD in the wave-type fish *Eigenmannia virescens* cost 7×10^{13} to 4×10^{14} ATP molecules, consistent with Markham's estimation based on the cost of AP generation in electrocytes (Lewis et al., 2014; Markham et al., 2013). Incorporating the cost of the entire pacemaker network, Salazar et al. suggested that EOD generation consumed ~30% of routine energetic cost (Salazar et al., 2013). These recent experimental and theoretical estimates indicate that EOD production is energetically expensive.

Recent analyses comparing the cost of electric signaling to that of other communication signals also suggest that EOD production creates high energetic demand. Markham et al. (2016) compared the cost of electrical signaling in the wave-type fish Eigenmannia virescens to the cost of other energetically expensive

communication signals, the mate attraction signals from trilling katydid and the loud calls from Carolina wren are the most expensive communication signals on a second-to-second basis (Stoddard and Salazar, 2011). These signals are only emitted for a brief period during a day, while the wave-type fish *Eigenmannia virescens* generate EOD at a constant frequency (200-600 Hz) 24 hours per day. When comparing the metabolic cost of communication signals on a daily basis, the cost of EOD generation becomes approximately equal to the most expensive acoustic signals (Table 1) (Markham et al., 2016). Markham et al. also compared the metabolic cost of EO and other tissues that are composed of excitable cells such as muscle, brain, heart and retina, and indicated that the energy consumed by EO was similar to that of other comparison tissues except skeletal muscle, which consumed a higher level of energy under exercise conditions (Ames et al., 1992; Gibala et al., 1997; Haworth et al., 1983; Lewis et al., 2014a; Sokoloff, 1969). Brain, heart and retina comprise only a small fraction of whole body weight, whereas EO comprises ~10% of the fish's total weight, which would make the relative cost of EO higher than other comparison tissues (Markham et al., 2016).

Behavioral adaptations in electrical signaling to conserve energy

Plasticity in EOD waveforms plays an important role in regulating the energy expenditure of electrical signaling. Many species are nocturnal and the modulation of EOD waveforms has been shown to follow a circadian rhythm. Pulse-type fish can reduce both the rate and amplitude of EOD during the day to save energy (Franchina and Stoddard, 1998; Silva et al., 2007). However, reducing EOD frequency is not possible for wave-type fish. The only strategy available for them to save energy during the resting time is to produce smaller-amplitude EODs (Markham et al., 2009; Sinnett

and Markham, 2015). When socially isolated, these fish will also reduce the amplitude of the EOD (Franchina and Stoddard, 1998).

The circadian and social modulations of EOD amplitude occur through the action of adrenocorticotropic hormone (ACTH). *In vivo* injection of ACTH into the pulse-type fish *Brachyhypopomus pinnicaudatus* and the wave-type fish *Sternopygus macrurus* increases EOD amplitude within minutes. And *in vitro* application of ACTH to electrocytes increased the amplitude of the discharge generated by an individual electrocyte (the μEOD) (Markham et al., 2009; Markham and Stoddard, 2005). The rapid modulation of EOD waveform mediated by ACTH is through the trafficking of Na_v channels into and out of the plasma membrane of electrocytes to regulate the influx of Na^+ ions in each electrocyte and the overall EOD amplitude (Markham et al., 2009b).

Under extreme conditions such as hypoxia and food deprivation, weakly electric fish have shown behavioral adaptations similar to the energy-saving adaptations during resting periods. Without the ability of aerobic respiration, wave-type fish have low tolerance to aquatic hypoxia. *Apteronotus leptorhynchus* and *Eigenmannia virescens* were found to decrease their EOD amplitudes to reduce the energetic cost in response to hypoxic stress (Reardon et al., 2011b). The EOD amplitude of *E. virescens* was reduced under food deprivation and recovered after feeding (Sinnett and Markham, 2015). The modulation of EOD amplitude under food deprivation was suggested to be mediated by the level of leptin hormone (Sinnett and Markham 2015). It appears that these fish respond to energy-limiting conditions by reducing EOD amplitude but not frequency. Modulating EOD frequency may be an energetically expensive process. The inability to

change discharge rate further ensures the honesty of EOD frequency as a signal representing the organism's identity.

Cellular and molecular adaptations in electrical signaling to conserve energy

EODs are generated by the summed simultaneous APs of electrocytes. Thus the energy consumed by EOD production should arise from the maintenance of membrane potentials, synaptic transmission and especially AP generation in electrocytes. APs are usually initiated by the opening of Na^+ channels, allowing the influx of Na^+ ions, which depolarize the cell and cause the opening of K^+ channels. K^+ efflux competing with Na^+ influx results in cell repolarization. Cells are eventually hyperpolarized and APs are terminated by the closing of Na^+ channels and K^+ channels. After each AP, Na^+/K^+ ATPases restore the ionic gradients by importing two K^+ ions and simultaneously extruding three Na^+ ions at the cost of one ATP (Bean, 2007a). When both Na^+ channels and K^+ channels are open during repolarization, only a small portion of the K^+ efflux is used to repolarize the cell, because most is cancelled by the simultaneous Na^+ influx. This overlap between Na^+ influx and K^+ efflux reduces the energetic efficiency (Fig. 2) (Carter and Bean, 2009).

The kinetics as well as the densities of ion channels determine the shape and frequency of APs. To achieve fast-spiking, neurons usually express fast-activating K^+ channels. However, faster K^+ channels will increase the overlap between Na^+ and K^+ currents, further magnifying the energetic cost. If minimizing energy consumption is one constraint governing the types of ion channels expressed in neurons (Hasenstaub et al., 2010a), neurons with faster K^+ channels should also express Na^+ channels with a faster inactivation speed in order to reduce the overlap between Na^+ and K^+ currents

(Fig. 2). This strategy was adopted by the electrocytes of wave-type fish *Sternopygus macrurus* to improve energetic efficiency of AP generation.

The activation speed of K^+ currents and the inactivation speed of Na^+ currents is highly correlated in electrocytes of *Sternopygus macrurus*. Electrocytes from fish with higher EOD frequencies express fast-activating K^+ currents as well as Na^+ currents with a faster inactivation speed (Ferrari et al., 1995; McAnelly and Zakon, 2000). The increased inactivation speed of Na^+ currents is achieved by the upregulation of Na_v channels' β1 subunit, which has been shown to affect the channel's gating properties (Liu et al., 2007b). And the faster activation of K^+ currents is supported by the increased expression level of two types of K^+ channels, $K_v1.1a$ and $K_v1.2a$ (Few and Zakon, 2007).

***Eigenmannia virescens* as a model to study energy-saving adaptations**

Eigenmannia virescens is a gymnotiform weakly electric fish that lives in the freshwater rivers of South America. *E. virescens* electrocytes generate APs at constant, high frequencies of 200-600 Hz with the influx of Na^+ ions during each AP exceeding 10 μA (Markham et al., 2013). The number of ATP molecules required by the Na^+/K^+ ATPases to export the Na^+ ions than enter the cell during each AP was estimated to be two orders of magnitude more than that estimated for mammalian neurons (Attwell and Laughlin, 2001a; Howarth et al., 2012b; Lewis et al., 2014b). The combination of high firing rates and large ionic currents creates extreme energetic demands for each electrocyte individually, and for the EO as a whole. Unlike the electrocytes of other gymnotiform electric fish, in which APs are terminated by classical K_v channels, *E. virescens* electrocytes express a novel K_{Na} channel to repolarize the AP. Computational

simulation to compare the ability of model electrocytes with K_{Na} or K_v channels to maintain the high-frequency firing pattern found that only K_{Na} channels can support the cell to fire at 500 Hz without truncating the amplitude of APs, more importantly, K_{Na} channels can make the AP ~30% energetically more efficient by reducing the overlap between inward Na^+ currents and outward K^+ currents (Markham et al., 2013).

K_{Na} channels, widely expressed in cardiac cells, neurons and muscles of other vertebrates (Kaczmarek, 2013), are encoded by two highly similar paralog genes, *Slack* (*Slo2.2*, *kcnt1*) and *Slick* (*Slo2.1*, *kcnt2*) belonging to the *Slo* gene family (Bhattacharjee et al., 2003; Joiner et al., 1998). K_{Na} channels are tetramers consisting of four subunits. Each Slack and Slick subunit is approximately 1200 amino acids long, containing six membrane-spanning domains, with a pore-forming region between the fifth and sixth membrane-spanning domain, and an extensive cytoplasmic C-terminus, composed of two RCK domains regulating the conductance of K^+ ions (Fig. 3) (Yuan et al., 2003).

A short motif located within the second RCK domain coordinates the binding of Slack and Slick subunits with Na^+ ions (Thomson et al., 2015; Zhang et al., 2010a). Based on patch-clamp recordings, the concentration of Na^+ ions required to activate K_{Na} channels was estimated to far exceed that normally occuring in bulk cytoplasm (EC_{50} of Na^+ activation: ~7-80 mM) (Dryer, 1994b). Hage and Salkoff determined that persistent Na^+ currents provided the source of Na^+ ions that activate K_{Na} channels in mammalian neurons. They suggested that K_{Na} channels were closely clustered with channels carrying the persistent Na^+ currents allowing the accumulation of Na^+ ions just beneath the plasma membrane to activate K_{Na} channels without changing the concentration of Na^+ ions in bulk cytoplasm (Hage and Salkoff, 2012).

Mammalian Slack and Slick subunits are ~74% identical in protein sequences, but with slightly different characteristics. The activation of Slack channels requires binding with Na^+ ions, whereas Slick channels have shown a basal level of activity in the absence of Na^+ ions. Slick channels are more sensitive to $[Cl^-]_i$ than Slack channels and have been shown to be inhibited by an increased level of intracellular ATP (Bhattacharjee et al., 2003; Joiner et al., 1998). In rats, RNA alternative splicing gives rise to two amino-termini isoforms of Slack: Slack-A and Slack-B. Slack-A and Slick have similar amino-terminus and express currents activating much faster than that of Slack-B, which has a much larger amino-terminus (Brown et al., 2008). Slick can form heteromeric K_{Na} channels with Slack-B and the amino-terminus of Slack-B has been shown to facilitate the trafficking of Slick subunits to the plasma membrane (Chen et al., 2009).

The physiological roles of K_{Na} channels in excitable cells are not fully understood. In quail trigeminal ganglion neurons, K_{Na} channels activated very rapidly during a depolarization step (Bader et al., 1985), suggesting their participation in fast repolarization, which is important for fast-spiking cells. Additionally, since the activation of K_{Na} channels depends on binding with Na^+ ions, they may serve as a negative feedback mechanism in response to increases in intracellular Na^+ $[Na^+]_i$ (Yuan et al., 2013). Under hypoxia or ischemia, inhibition of Na^+/K^+ ATPases increases $[Na^+]_i$, which would activate K_{Na} channels. Thus K_{Na} channels may play an important role in ameliorating the detrimental effects caused by osmotic imbalance and enhancing the ability of neurons and cardiomyocytes to react to hypoxic stress.

The main goal of this research was to investigate the biophysical mechanisms allowing the generation of metabolically expensive electrical signals in *E. virescens.* This study focused specifically on the cellular and molecular features of *E. virescens* electrocytes that maintain the high-frequency APs and manage the large ionic currents. The firing pattern of APs and the resulting metabolic cost are mainly determined by cell morphology, intrinsic properties, and densities as well as subcellular localization of ion channels involved in AP generation. Chapter 2 is an investigation into the morphology of electrocytes as well as the subcellular localization of cholinergic receptors, ion channels and Na^+/K^+ ATPases in electrocytes using confocal laser-scanning fluorescence microscopy and immunohistochemistry (Ban et al., 2015). Chapter 3 focuses primarily on the role of K_{Na} channels in facilitating high-frequency firing of electrocytes by exploring their molecular identity, expression pattern, densities and kinetic properties.

References

Alves-Gomes, J., 2001. Alves-Gomes, J., 2001. The evolution of electroreception and bioelectrogenesis in teleost fish: a phylogenetic perspective. Journal of Fish Biology 58, 1489-1511.

Ames, A., Li, Y.-Y., Heher, E., Kimble, C.R., 1992. Energy metabolism of rabbit retina as related to function: high cost of Na^+ transport. J. Neurosci. 12, 840-853.

Attwell, D., Laughlin, S.B., 2001. An energy budget for signaling in the grey matter of the brain. Journal of Cerebral Blood Flow & Metabolism 21, 1133-1145.

Bader, C., Bernheim, L., Bertrand, D., 1985. Sodium-activated potassium current in cultured avian neurones. Nature 317, 540.

Ban, Y., Smith, B.E., Markham, M.R., Ban, Y., 2015. A highly-polarized excitable cell separates sodium channels from sodium-activated potassium channels by more than a millimeter. Journal of neurophysiology, jn. 00475.02014.

Bastian, J., 1981. Electrolocation. Journal of comparative physiology 144, 465-479.

Bean, B.P., 2007. The action potential in mammalian central neurons. Nature Reviews Neuroscience 8, 451-465.

Bell, C., Bradbury, J., Russell, C., 1976. The electric organ of a mormyrid as a current and voltage source. Journal of comparative physiology 110, 65-88.

Bell, C.C., Maler, L., 2005. Central neuroanatomy of electrosensory systems in fish, Electroreception. Springer, pp. 68-111.

Bennett, M., 1971. Electric organs, Fish physiology. Elsevier, pp. 347-491.

Bennett, M., Pappas, G., Aljure, E., Nakajima, Y., 1967a. Physiology and ultrastructure of electrotonic junctions. II. Spinal and medullary electromotor nuclei in mormyrid fish. Journal of neurophysiology 30, 180-208.

Bennett, M., Pappas, G., Gimenez, M., Nakajima, Y., 1967b. Physiology and ultrastructure of electrotonic junctions. IV. Medullary electromotor nuclei in gymnotid fish. Journal of neurophysiology 30, 236-300.

Bennett, M.V., 1970. Comparative physiology: electric organs. Annual review of physiology 32, 471-528.

Bhattacharjee, A., Joiner, W.J., Wu, M., Yang, Y., Sigworth, F.J., Kaczmarek, L.K., 2003. Slick (Slo2. 1), a rapidly-gating sodium-activated potassium channel inhibited by ATP. The Journal of neuroscience 23, 11681-11691.

Bradbury, J.W., Vehrencamp, L., 1998. Principles of animal communication. Sinauer Associates.

Brown, M.R., Kronengold, J., Gazula, V.R., Spilianakis, C.G., Flavell, R.A., Von Hehn, C.A., Bhattacharjee, A., Kaczmarek, L.K., 2008. Amino-termini isoforms of the Slack K^+ channel, regulated by alternative promoters, differentially modulate rhythmic firing and adaptation. The Journal of physiology 586, 5161-5179.

Bullock, T.H., 1969. Species Differences in Effect of Electroreceptor Input on Electric Organ Pacemakers and Other Aspects of Behavior in Electric Fish; pp. 102–118. Brain, Behavior and Evolution 2, 102-118.

Bullock, T.H., Hamstra, R.H., Scheich, H., 1972. The jamming avoidance response of high frequency electric fish, How do Brains Work? Springer, pp. 509-534.

Bullock, T.H., Hopkins, C.D., Fay, R.R., 2006. Electroreception. Springer Science & Business Media.

Carr, C.E., Maler, L., Sas, E., 1982. Peripheral organization and central projections of the electrosensory nerves in gymnotiform fish. Journal of Comparative Neurology 211, 139-153.

Carter, B.C., Bean, B.P., 2009. Sodium entry during action potentials of mammalian neurons: incomplete inactivation and reduced metabolic efficiency in fast-spiking neurons. Neuron 64, 898-909.

Chen, H., Kronengold, J., Yan, Y., Gazula, V.-R., Brown, M.R., Ma, L., Ferreira, G., Yang, Y., Bhattacharjee, A., Sigworth, F.J., 2009. The N-terminal domain of Slack determines the formation and trafficking of Slick/Slack heteromeric sodium-activated potassium channels. The Journal of Neuroscience 29, 5654-5665.

Dryer, S.E., 1994. Na^+-activated K^+ channels: a new family of large-conductance ion channels. Trends in neurosciences 17, 155-160.

DuÈrr, V., KoÈnig, Y., Kittmann, R., 2001. The antennal motor system of the stick insect Carausius morosus: anatomy and antennal movement pattern during walking. Journal of Comparative Physiology A 187, 131-144.

Eberhardt, L.S., 1994. Oxygen-Consumption during Singing by Male Carolina Wrens (Thryothorus-Ludovicianus). Auk 111, 124-130.

Engler, G., Fogarty, C., Banks, J., Zupanc, G., 2000. Spontaneous modulations of the electric organ discharge in the weakly electric fish, Apteronotus leptorhynchus: a biophysical and behavioral analysis. Journal of Comparative Physiology A 186, 645-660.

Engler, G., Zupanc, G., 2001. Differential production of chirping behavior evoked by electrical stimulation of the weakly electric fish, Apteronotus leptorhynchus. Journal of Comparative Physiology A 187, 747-756.

Ferrari, M., McAnelly, M., Zakon, H., 1995. Individual variation in and androgen-modulation of the sodium current in electric organ. Journal of Neuroscience 15, 4023-4032.

Few, W.P., Zakon, H.H., 2007. Sex differences in and hormonal regulation of K_v1 potassium channel gene expression in the electric organ: molecular control of a social signal. Developmental neurobiology 67, 535-549.

Franchina, C., Stoddard, P., 1998. Plasticity of the electric organ discharge waveform of the electric fish Brachyhypopomus pinnicaudatus I. Quantification of day-night changes. Journal of Comparative Physiology A 183, 759-768.

Fugère, V., Ortega, H., Krahe, R., 2010. Electrical signalling of dominance in a wild population of electric fish. Biology letters, rsbl20100804.

Gallant, J.R., Traeger, L.L., Volkening, J.D., Moffett, H., Chen, P.-H., Novina, C.D., Phillips, G.N., Anand, R., Wells, G.B., Pinch, M., 2014. Genomic basis for the convergent evolution of electric organs. Science 344, 1522-1525.

Gibala, M.J., MacLean, D.A., Graham, T.E., Saltin, B., 1997. Anaplerotic processes in human skeletal muscle during brief dynamic exercise. The Journal of physiology 502, 703-713.

Hage, T.A., Salkoff, L., 2012. Sodium-activated potassium channels are functionally coupled to persistent sodium currents. The Journal of Neuroscience 32, 2714-2721.

Hagedorn, M., Heiligenberg, W., 1985. Court and spark: electric signals in the courtship and mating of gymnotoid fish. Animal Behaviour 33, 254-265.

Hartmann, M.J., 2001. Active sensing capabilities of the rat whisker system. Autonomous Robots 11, 249-254.

Hasenstaub, A., Otte, S., Callaway, E., Sejnowski, T.J., 2010. Metabolic cost as a unifying principle governing neuronal biophysics. Proceedings of the National Academy of Sciences 107, 12329-12334.

Haworth, R.A., Hunter, D.R., Berkoff, H.A., Moss, R.L., 1983. Metabolic cost of the stimulated beating of isolated adult rat heart cells in suspension. Circul. Res. 52, 342-351.

Heiligenberg, W., 1973. Electrolocation of objects in the electric fish Eigenmannia (Rhamphichthyidae, Gymnotoidei). Journal of comparative physiology 87, 137-164.

Heiligenberg, W., Keller, C.H., Metzner, W., Kawasaki, M., 1991. Structure and function of neurons in the complex of the nucleus electrosensorius of the gymnotiform fish Eigenmannia: detection and processing of electric signals in social communication. Journal of Comparative Physiology A 169, 151-164.

Hopkins, C., 1986. Behavior of mormyridae. Electroreception.

Hopkins, C.D., 1972. Sex differences in electric signaling in an electric fish. Science 176, 1035-1037.

Hopkins, C.D., 1974a. Electric communication in the reproductive behavior of Sternopygus macrurus (Gymnotoidei). Ethology 35, 518-535.

Hopkins, C.D., 1974b. Electric communication: functions in the social behavior of Eigenmannia virescens. Behaviour, 270-305.

Hopkins, C.D., 1999. Design features for electric communication. Journal of experimental Biology 202, 1217-1228.

Hopkins, C.D., Heiligenberg, W.F., 1978. Evolutionary designs for electric signals and electroreceptors in gymnotoid fishes of Surinam. Behavioral Ecology and Sociobiology 3, 113-134.

Howarth, C., Gleeson, P., Attwell, D., 2012. Updated energy budgets for neural computation in the neocortex and cerebellum. Journal of Cerebral Blood Flow & Metabolism 32, 1222-1232.

Joiner, W.J., Tang, M.D., Wang, L.-Y., Dworetzky, S.I., Boissard, C.G., Gan, L., Gribkoff, V.K., Kaczmarek, L.K., 1998. Formation of intermediate-conductance calcium-activated potassium channels by interaction of Slack and Slo subunits. Nature neuroscience 1, 462-469.

Julian, D., Crampton, W.G., Wohlgemuth, S.E., Albert, J.S., 2003. Oxygen consumption in weakly electric Neotropical fishes. Oecologia 137, 502-511.

Kaczmarek, L.K., 2013. Slack, Slick, and Sodium-Activated Potassium Channels. ISRN neuroscience 2013.

Kavanagh, M.W., 1987. The Efficiency of Sound Production in 2 Cricket Species, Gryllotalpa-Australis and Teleogryllus-Commodus (Orthoptera, Grylloidea). J. Exp. Biol. 130, 107-119.

Kirschbaum, F., 1977. Electric-organ ontogeny: distinct larval organ precedes the adult organ in weakly electric fish. Naturwissenschaften 64, 387-388.

Kirschbaum, F., 1983. Myogenic electric organ precedes the neurogenic organ in apteronotid fish. Naturwissenschaften 70, 205-207.

Knudsen, E.I., 1975. Spatial aspects of the electric fields generated by weakly electric fish. Journal of Comparative Physiology A: Neuroethology, Sensory, Neural, and Behavioral Physiology 99, 103-118.

Kotiaho, J.S., Alatalo, R.V., Mappes, J., Nielsen, M.G., Parri, S., Rivero, A., 1998. Energetic costs of size and sexual signalling in a wolf spider. Proceedings of the Royal Society of London B: Biological Sciences 265, 2203-2209.

Krahe, R., Maler, L., 2014. Neural maps in the electrosensory system of weakly electric fish. Current opinion in neurobiology 24, 13-21.

Lavoué, S., Miya, M., Arnegard, M.E., Sullivan, J.P., Hopkins, C.D., Nishida, M., 2012. Comparable ages for the independent origins of electrogenesis in African and South American weakly electric fishes. PLoS one 7, e36287.

Lewis, J.E., Gilmour, K.M., Moorhead, M.J., Perry, S.F., Markham, M.R., 2014. Action Potential Energetics at the Organismal Level Reveal a Trade-Off in Efficiency at High Firing Rates. The Journal of Neuroscience 34, 197-201.

Liu, H., Wu, M.M., Zakon, H.H., 2007. Individual variation and hormonal modulation of a sodium channel β subunit in the electric organ correlate with variation in a social signal. Developmental neurobiology 67, 1289-1304.

Markham, M.R., Ban, Y., McCauley, A.G., Maltby, R., 2016. Energetics of sensing and communication in electric fish: A blessing and a curse in the Anthropocene? Oxford University Press.

Markham, M.R., Kaczmarek, L.K., Zakon, H.H., 2013. A sodium-activated potassium channel supports high-frequency firing and reduces energetic costs during rapid modulations of action potential amplitude. Journal of neurophysiology 109, 1713-1723.

Markham, M.R., McAnelly, M.L., Stoddard, P.K., Zakon, H.H., 2009. Circadian and social cues regulate ion channel trafficking. PLoS biology 7, e1000203.

Markham, M.R., Stoddard, P.K., 2005. Adrenocorticotropic hormone enhances the masculinity of an electric communication signal by modulating the waveform and timing of action potentials within individual cells. Journal of Neuroscience 25, 8746-8754.

McAnelly, M.L., Zakon, H.H., 2000. Coregulation of voltage-dependent kinetics of Na^+ and K^+ currents in electric organ. Journal of Neuroscience 20, 3408-3414.

Meyer, J.H., Leong, M., Keller, C.H., 1987. Hormone-induced and maturational changes in electric organ discharges and electroreceptor tuning in the weakly electric fishApteronotus. Journal of Comparative Physiology A 160, 385-394.

Nelson, M.E., MacIver, M.A., 2006. Sensory acquisition in active sensing systems. Journal of Comparative Physiology A 192, 573-586.

Niven, J.E., Laughlin, S.B., 2008. Energy limitation as a selective pressure on the evolution of sensory systems. Journal of Experimental Biology 211, 1792-1804.

Patterson, J.M., Zakon, H.H., 1996. Differential expression of proteins in muscle and electric organ, a muscle derivative. Journal of Comparative Neurology 370, 367-376.

Paul, C., Mamonekene, V., Vater, M., Feulner, P.G., Engelmann, J., Tiedemann, R., Kirschbaum, F., 2015. Comparative histology of the adult electric organ among four species of the genus Campylomormyrus (Teleostei: Mormyridae). Journal of Comparative Physiology A 201, 357-374.

Prestwich, K.N., Brugger, K.E., Topping, M., 1989. Energy and Communication in 3 Species of Hylid Frogs - Power Input, Power Output and Efficiency. J. Exp. Biol. 144, 53-80.

Reardon, E.E., Parisi, A., Krahe, R., Chapman, L.J., 2011. Energetic constraints on electric signalling in wave-type weakly electric fishes. Journal of Experimental Biology 214, 4141-4150.

Salazar, V.L., Krahe, R., Lewis, J.E., 2013. The energetics of electric organ discharge generation in gymnotiform weakly electric fish. The Journal of experimental biology 216, 2459-2468.

Salazar, V.L., Stoddard, P.K., 2008. Sex differences in energetic costs explain sexual dimorphism in the circadian rhythm modulation of the electrocommunication signal of the gymnotiform fish Brachyhypopomus pinnicaudatus. Journal of Experimental Biology 211, 1012-1020.

Salkoff, L., Butler, A., Ferreira, G., Santi, C., Wei, A., 2006. High-conductance potassium channels of the SLO family. Nature Reviews Neuroscience 7, 921-931.

Schwartz, I., Pappas, G., Bennett, M., 1975. The fine structure of electrocytes in weakly electric teleosts. Journal of neurocytology 4, 87-114.

Silva, A., Perrone, R., Macadar, O., 2007. Environmental, seasonal, and social modulations of basal activity in a weakly electric fish. Physiology & behavior 90, 525-536.

Sinnett, P.M., Markham, M.R., 2015. Food deprivation reduces and leptin increases the amplitude of an active sensory and communication signal in a weakly electric fish. Hormones and behavior 71, 31-40.

Sokoloff L. 1969. Cerebral circulation and behavior in man: Strategy and findings. In: Mandell AJ, Mandell MP, editors. Psychochemical research in man. New York: Academic. p. 237–52.

Stevens, E.D., Josephson, R.K., 1977. Metabolic-Rate and Body-Temperature in Singing Katydids. Physiol. Zool. 50, 31-42.

Stoddard, P., 2010. Electrical signals.

Stoddard, P., Rasnow, B., Assad, C., 1999. Electric organ discharges of the gymnotiform fishes: III. Brachyhypopomus. Journal of Comparative Physiology A 184, 609-630.

Stoddard, P.K., 1999. Predation enhances complexity in the evolution of electric fish signals. Nature 400, 254.

Stoddard, P.K., Salazar, V.L., 2011. Energetic cost of communication. Journal of Experimental Biology 214, 200-205.

Thomas, J.A., Moss, C.F., Vater, M., 2004. Echolocation in bats and dolphins. University of Chicago Press.

Thomson, S.J., Angela, H., Sanguinetti, M.C., 2015. Identification of the Intracellular Na^+ Sensor in Slo2. 1 Potassium Channels. Journal of Biological Chemistry, jbc. M115. 653089.

von der Emde, G., 1990. Discrimination of objects through electrolocation in the weakly electric fish, Gnathonemus petersii. Journal of Comparative Physiology A 167, 413-421.

Von Der Emde, G., 1998. Capacitance detection in the wave-type electric fish Eigenmannia during active electrolocation. Journal of Comparative Physiology A 182, 217-224.

Von der Emde, G., 1999. Active electrolocation of objects in weakly electric fish. Journal of experimental biology 202, 1205-1215.

Von der Emde, G., Fetz, S., 2007. Distance, shape and more: recognition of object features during active electrolocation in a weakly electric fish. Journal of Experimental Biology 210, 3082-3095.

Yuan, A., Santi, C.M., Wei, A., Wang, Z.-W., Pollak, K., Nonet, M., Kaczmarek, L., Crowder, C.M., Salkoff, L., 2003. The Sodium-Activated Potassium Channel Is Encoded by a Member of the Slo Gene Family. Neuron 37, 765-773.

Zahavi, A., 1975. Mate selection—a selection for a handicap. Journal of theoretical Biology 53, 205-214.

Zakon, H.H., Thomas, P., Yan, H.-Y., 1991. Electric organ discharge frequency and plasma sex steroid levels during gonadal recrudescence in a natural population of the weakly electric fish Sternopygus macrurus. Journal of Comparative Physiology A: Neuroethology, Sensory, Neural, and Behavioral Physiology 169, 493-499.

Zhang, Z., Rosenhouse-Dantsker, A., Tang, Q.-Y., Noskov, S., Logothetis, D.E., 2010. The RCK2 domain uses a coordination site present in Kir channels to confer sodium sensitivity to Slo2. 2 channels. The Journal of Neuroscience 30, 7554-7562.

Zupanc, G.K., 2002. From oscillators to modulators: behavioral and neural control of modulations of the electric organ discharge in the gymnotiform fish, Apteronotus leptorhynchus. Journal of Physiology-Paris 96, 459-472.

Zupanc, G.K., Maler, L., 1993. Evoked chirping in the weakly electric fish Apteronotus leptorhynchus: a quantitative biophysical analysis. Canadian Journal of Zoology 71, 2301-2310.

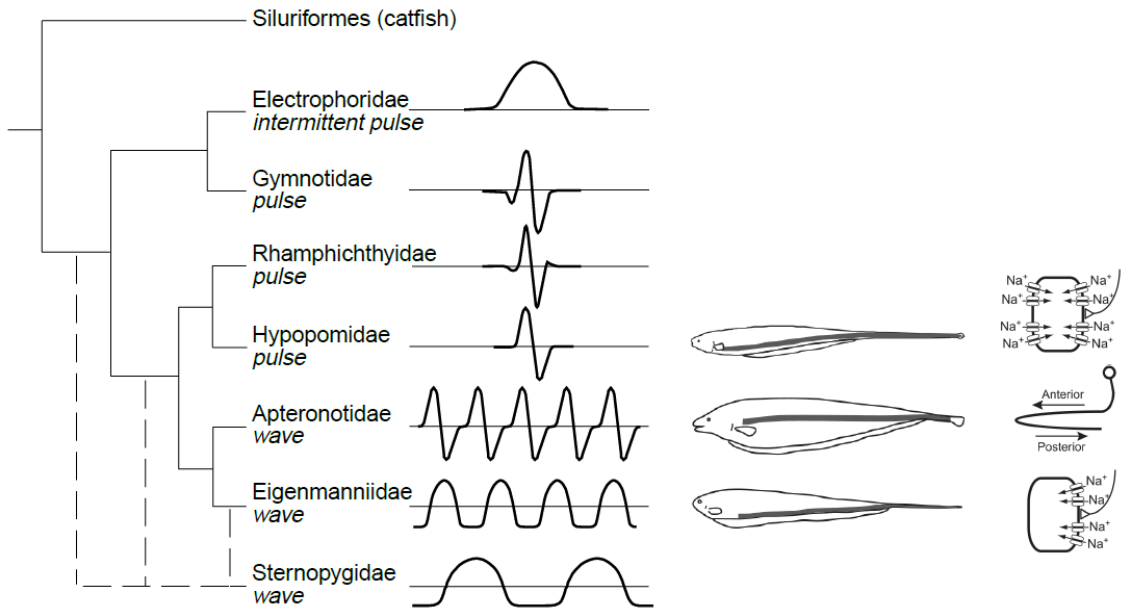

Figure 1. EOs, EOD waveforms and electrocytes of the gymnotiform families. Left: "molecular-morphological consensus phylogeny of the gymnotiform families" and their EOD waveforms (Stoddard, 1999). Middle: outlines of *Brachyhypopomus gauderio* (a pulse-type fish in the family of Hypopomidae, EOD frequency: 2-115 Hz), *Apteronotus albifrons* (a wave-type fish in the family of Apteronotidae, EOD frequency: 600-1100 Hz), and *Eigenmannia virescens* (a wave-type fish in the family of Eigenmanniidae, EOD frequency: 200-600 Hz). The location of EO in each fish is shown in grey. Right: Sketch of electrocytes indicating the expression pattern of Na_v channels and the direction of current flow. This figure is adapted from Figure 1 of Stoddard, 1999 and Figure 1 of Salazar et al., 2013.

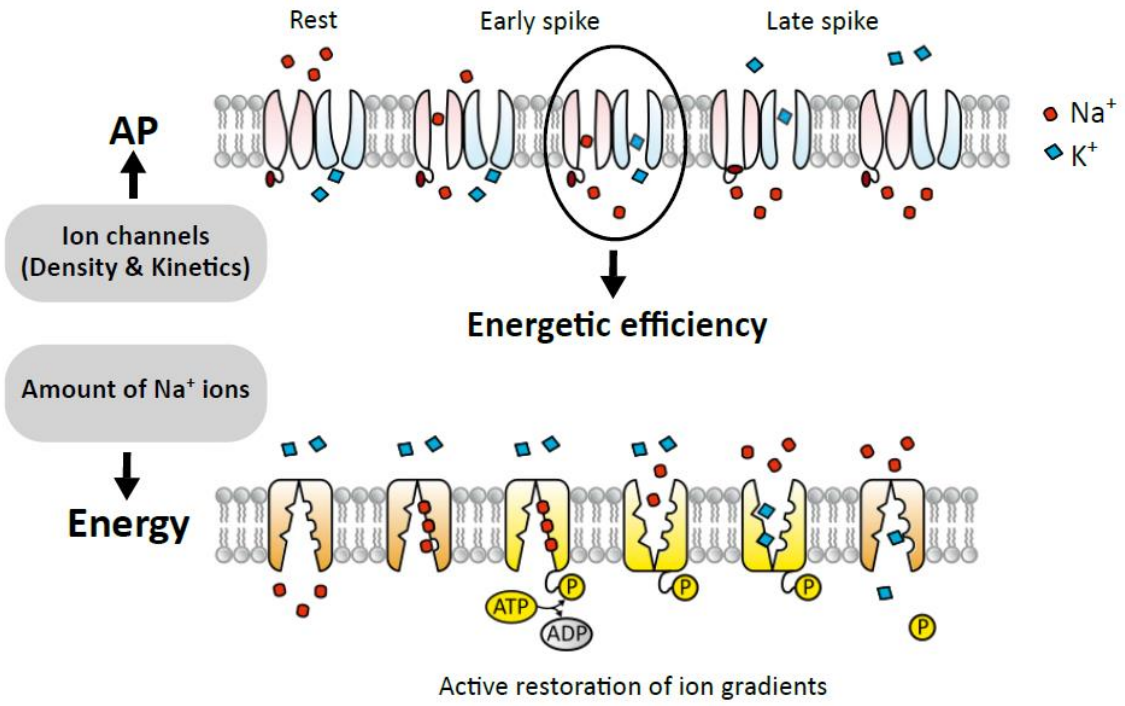

Figure 2. The generation of APs and the active restoration of ionic gradients by Na^+/K^+ ATPases. Top: AP generation. At resting membrane potential, both Na^+ channels and K^+ channels are closed. There is a higher concentration of Na^+ ions in the extracellular space and higher concentration of K^+ ions inside cells. In the first stage of AP, depolarization causes Na^+ channels to open, allowing the influx of Na^+ ions, which further depolarizes the cell and cause the opening of K^+ channels. Simultaneously, Na^+ channels start to inactivate as the cell becomes more depolarized. During the next phase, K^+ efflux competes with Na^+ influx and repolarizes the cell. Eventually, cells are hyperpolarized and APs are terminated by the closing of Na^+ channels and K^+ channels. The shape and frequency of APs are determined by the densities and kinetics of ion channels. Bottom: after each AP, Na^+/K^+ ATPase restores the ionic gradients by importing two K^+ ions and simultaneously extruding three Na^+ ions at the cost of one ATP molecule. The energy consumed by Na^+/K^+ ATPases is determined by the number of Na^+ ions that enter the cell during each AP. When both Na^+ channels and K^+ channels are open during repolarization, most K^+ efflux is cancelled by the simultaneous Na^+ influx, leaving a small portion used to repolarize the cell. The overlap between Na^+ and K^+ currents reduces the energetic efficiency. This figure is adapted from figure 1 of Hasenstaub et al., 2010.

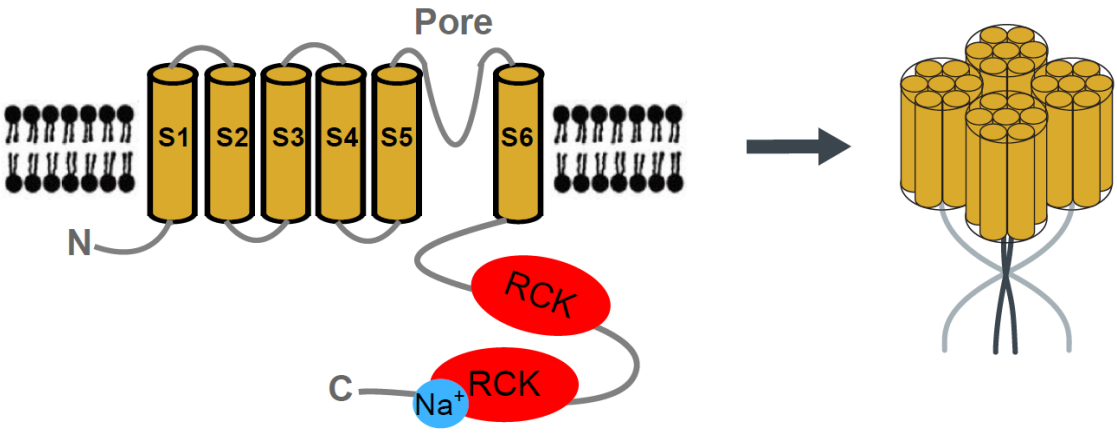

Figure 3. Schematic representation of mammalian K_{Na} channel. K_{Na} channels are tetramers consisting four subunits. Each Slack and Slick subunit is approximately 1200 amino acids long, containing six membrane-spanning domains, with a pore-forming region between the fifth and sixth membrane-spanning domain, and an extensive cytoplasmic C-terminus, composed of two RCK domains regulating the conductance of K^+ ions. This figure is adapted from figure 1 of Salkoff et al., 2006.

Table 1: The metabolic cost of EOD production in gymnotiform electric fish compared to the costs of other animal's communication signals. This table is adapted from Markham et al., 2016.

Organism	Source	Signal ATP g^{-1} s^{-1}	Duration (hours day^{-1})	Signal ATP g^{-1} d^{-1}
Arachnids				
Wolf Spider *Hygrolycosa rubrofasciata*	Kotiaho et al. (1998)	1.71×10^{17}	2	1.23×10^{21}
Insects				
Trilling Katydid *Euconocephalus nasutus*	Stevens and Josephson (1997)	5.89×10^{17}	2	4.24×10^{21}
Trilling cricket *Gryllotalpa australis*	Kavanagh (1987)	1.82×10^{17}	2	1.31×10^{21}
Amphibians				
Squirrel treefrog *Hyla squirella*	Prestwich et al. (1989)	7.88×10^{16}	2	5.67×10^{20}
Birds				
Carolina Wren *Thryothorus ludovicianus*	Eberhardt (1994)	3.37×10^{17}	2	2.43×10^{21}
Gymnotiform weakly electric fish				
Feathertail knife fish (female) *Brachyhypopomus gauderio*	Salazar and Stoddard (2008)	5.97×10^{14}	24	5.16×10^{19}
Feathertail knife fish (male) *Brachyhypopomus gauderio*	Salazar and Stoddard (2008)	4.74×10^{15}	24	4.10×10^{20}
Glass knife fish (200 Hz) *Eigenmannia virescens*	Lewis et al. (2014)	4.82×10^{14}	24	3.69×10^{19}
Glass knife fish (300 Hz) *Eigenmannia virescens*	Lewis et al. (2014)	1.30×10^{15}	24	1.12×10^{20}
Glass knife fish (500 Hz) *Eigenmannia virescens*	Lewis et al. (2014)	3.47×10^{15}	24	3.01×10^{20}

Table 2: The metabolic cost of EO compared to the cost of other excitable tissues. This table is adapted from Markham et al., 2016.

Tissue	Organism	Condition	ATP g^{-1} s^{-1}	Source
Electric organ	*E. virescens*	400 Hz rate	3.47×10^{16}	Lewis et al. (2014)
Skeletal muscle	Human	resting	1.10×10^{16}	Gibala et al. (1997)
Skeletal muscle	Human	exercising	6.02×10^{17}	Gibala et al. (1997)
Brain	Human	alert	7.40×10^{16}	Sokoloff (1969)
Brain	Human	sleeping	4.48×10^{16}	Sokoloff (1969)
Heart	Rat	60 beats min^{-1}	1.26×10^{16}	Haworth et al. (1983)
Retina	Rabbit	darkness	9.89×10^{16}	Ames et al. (1992)
Retina	Rabbit	light	6.92×10^{16}	Ames et al. (1992)

Chapter 2: A highly polarized excitable cell separates sodium channels from sodium-activated potassium channels by more than a millimeter

[This chapter has been published as Ban, Y., Smith, B. E., & Markham, M. R. (2015). A highly polarized excitable cell separates sodium channels from sodium-activated potassium channels by more than a millimeter. Journal of Neurophysiology, 114(1), 520-530.]

SUMMARY

The bioelectrical properties and resulting metabolic demands of electrogenic cells are determined by their morphology and the subcellular localization of ion channels. The electric organ cells (electrocytes) of the electric fish Eigenmannia virescens generate action potentials (APs) with Na^+ currents >10 microamperes and repolarize the AP with Na^+-activated K^+ (K_{Na}) channels. To better understand the role of morphology and ion channel localization in determining the metabolic cost of electrocyte APs, we used two-photon 3D imaging to determine the fine cellular morphology and immunohistochemistry to localize the electrocytes' ion channels, ionotropic receptors, and Na^+/K^+ ATPases. We found that electrocytes are highly polarized cells ≈1.5 mm in anterior-posterior length and ≈0.6 mm in diameter, containing approximately 30,000 nuclei along the cell periphery. The cell's innervated posterior region is deeply invaginated and vascularized with complex ultrastructural features while the anterior region is relatively smooth. Cholinergic receptors and Na^+ channels are restricted to the innervated posterior region, while inward rectifier K^+ channels and the K_{Na} channels that terminate the electrocyte AP are localized to the

anterior region, separated by >1 millimeter from the only sources of Na^+ influx. In other systems submicron spatial coupling of Na^+ and K_{Na} channels is necessary for K_{Na} channel activation. However, our computational simulations showed that K_{Na} channels at a great distance from Na^+ influx can still terminate the AP suggesting that K_{Na} channels can be activated by distant sources of Na^+ influx and overturning a long-standing assumption that AP-generating ion channels are restricted to the electrocyte's posterior face.

INTRODUCTION

Action potentials (APs) are transient changes in membrane voltage that are typically initiated by inward Na^+ current (I_{Na}) and terminated by outward K^+ current (I_K). These currents are driven by ionic concentration gradients across the cell membrane (Bean, 2007b) and transmembrane Na^+/K^+ ATPases consume energy to restore the ionic gradients after each AP. Total Na^+ influx during the AP determines ATPase activity and therefore the resulting metabolic cost of the AP (Attwell and Laughlin, 2001a; Howarth et al., 2012a; Niven and Laughlin, 2008). Any temporal overlap of inward I_{Na} and outward I_K reduces energy efficiency, but this overlap is often necessary in fast-spiking cells where the need to maintain brief APs requires that I_K begins while I_{Na} is still active to terminate the AP quickly. This incomplete inactivation of Na^+ channels during AP repolarization can result in the entry of twice as much Na^+ as the theoretical minimum, significantly reducing energy efficiency at high AP frequencies (Carter and Bean, 2009).

The weakly electric fish *Eigenmannia virescens* generates electric organ discharges (EODs) to navigate and communicate in darkness (Hopkins, 1974). Because

they generate APs at steady frequencies of 200-600Hz (Scheich, 1977) with underlying Na^+ currents that can exceed 10 microamperes (Markham et al., 2013), the electric organ cells (electroctyes) create extremely high metabolic demands (Lewis et al., 2014b). High rates of ATP hydrolysis by the Na^+/K^+ ATPases are therefore necessary to remove Na^+ from the cell between APs. The simultaneous APs of >1000 electrocytes during each EOD further magnify the metabolic cost of signal production and as a result EOD amplitude is highly sensitive to metabolic stress (Reardon et al., 2011).

E. virescens electrocytes are large cells >1mm in length, each innervated by spinal motoneurons at a cholinergic synapse on the morphologically complex posterior membrane (Fig. 1B) (Schwartz et al., 1975b). Only the posterior membrane generates an AP with the anterior membrane presumed to be electrically passive (Bennett, 1961, 1971). These findings together led to a long-standing assumption that the ion channels responsible for producing the AP are restricted to the posterior region of the cell. Electrocytes express an inwardly rectifying K^+ current, a voltage-gated Na^+ current and a Na^+-activated K^+ (K_{Na}) current that terminates the AP. The expression of K_{Na} channels instead of voltage-gated K^+ (K_v) channels increases AP energy efficiency by reducing the overlap of I_{Na} and I_K during the electrocyte AP (Markham et al., 2013). Early biochemical studies identified Na^+/K^+ ATPases expressed on both the anterior and posterior membranes (Denizot, 1982), but the spatial distribution of the cholinergic receptors and ion channels is not yet known. A full account of the electrocyte's fine morphology and distribution of ionotropic receptors and ion channels is a crucial first step toward understanding the interplay of the ionic currents that determine the

spatiotemporal dynamics of intracellular Na^+ concentrations which regulate K_{Na} channel activation, ATPase activity, and ultimately the metabolic burden of EOD production.

We therefore used confocal laser-scanning fluorescence microscopy and immunohistochemistry to identify the electrocyte's fine 3D structure and the subcellular localization of their cholinergic receptors, ion channels, and ion transporters. We found that cholinergic receptors and Na^+ channels were restricted to the innervated posterior region, while inward rectifier K^+ channels and K_{Na} channels were localized over 1 mm away in the anterior region. Confirming earlier results (Denizot, 1982), Na^+/K^+ ATPases were densely expressed on both the posterior and anterior membranes. These findings are unexpected because K_{Na} channels that terminate the electrocyte AP and the anterior-membrane Na^+/K^+ ATPases are separated by more than a millimeter from the only sources of Na^+ influx that would activate them. Our computational simulations of electrocyte APs and Na^+ dynamics confirm that K_{Na} channels, even at a distance of more than 1mm from Na^+ influx, can terminate the electrocyte AP and maintain high-frequency firing. This discovery is particularly surprising in light of data from other systems where micron-scale spatial coupling of K_{Na} and Na^+ channels is necessary for K_{Na} channel activation (Budelli et al., 2009b; Hage and Salkoff, 2012a).

MATERIALS AND METHODS

Animals

Fish were wild-caught male and female *Eigenmannia virescens* (Glass Knife-fish). Animals were from tropical South America, obtained from tropical fish importers and ranging in size from 12 to 19 cm. Fish were housed in groups of 4-10 in 40-liter or 10-liter tanks in a recirculating aquarium system at 28 ± 1 °C with water conductivity of

200-500 μS/cm. The EOD of *E. virescens* is a sinusoidal wave with a frequency of 250-600 Hz (Fig. 1F). Each positive-going pulse of the wave is a single EOD (Fig. 1D, E), and these occur at regular intervals under the control of a medullary pacemaker nucleus (Fig.1A, B).

We harvested electric organ (EO) tissue from *E. virescens* by cutting off a small (1-2 cm) piece of the narrow tail filament, consisting of only soft tissue and composed almost entirely of the EO (Fig.1C). This brief procedure lasts less than 15 seconds and is performed without anesthesia because induction and recovery from immersion anesthesia are more harmful to the fish than the tail-clip itself. The tail and EO regenerate within two months.

To obtain mouse brains for validating antibodies used in the present study, five C57BL/6J mice (The Jackson Laboratory, stock #664) were deeply anesthetized by isoflurane inhalation (5% (v/v) isoflurane in oxygen), then decapitated and brains were quickly removed and frozen in liquid nitrogen.

All methods were approved by the Institutional Animal Care and Use Committee of The University of Oklahoma, and complied with the guidelines given in the Public Health Service Guide for the Care and Use of Laboratory Animals.

Microinjection

We harvested a ≈2 cm section of the tail, removed the overlying skin, and pinned the exposed EO tissue in a Sylgard® (Dow Corning Corporation) coated petri dish containing normal saline (114 mM NaCl, 2 mM KCl, 4 mM $CaCl_2 \cdot 2H_2O$, 2 mM $MgCl_2 \cdot 6H_2O$, 2 mM HEPES, and 6 mM glucose; pH to 7.2 with NaOH). Temperature of the preparation was stable at room temperature (22±1°C). Rhodamine B or Alexa

Fluor® 594 dextran (10,000MW) (Life Technologies) were prepared as a 1% w/v solution in water. Precipitate within the dextran solution was removed by centrifugation at 12,000 × g for 5 min. Microinjections were performed using an automatic nanoliter injector ("Nanoject II", Drummond Scientific Company). Micropipettes for injection were drawn from borosilicate glass capillaries (Drummond Scientific Company) with a laser micropipette puller (Model P-2000, Sutter Instruments). We injected 13.8 nL dextran solution into the cytoplasm of 4-5 electrocytes in each sample of EO with the constant injection speed of 23 nL/sec. The EO tissue with Rhodamine B or Alexa Fluor® 594 dextran-injected electroctyes was then held in normal saline at room temperature (22±1°C) for 15 minutes until the dextran fully diffused into injected electrocytes. We then proceeded immediately to image the live cells directly, or fix and section the tissue before mounting and imaging.

Vibratome sectioning

We fixed the Alexa Fluor® 594 dextran-injected EO tissue in 2% paraformaldehyde buffered with 1× phosphate-buffered saline (PBS) overnight at 4°C, and washed six times for 15 min each in 1× PBS. The EO tissue was then embedded in 3% agar, trimmed and glued to a vibratome chuck with cyanoacrylate. The chuck was mounted on a vibratome (Leica Series 1000) and 100-μm sections were cut and mounted on microscope slides with VectaShield® with DAPI (Vector Laboratories).

Confocal imaging

Live electrocytes were imaged *in situ* on a Leica® TCS SP8 laser scanning confocal microscope, with a Coherent Chameleon mode-locked Ti:sapphire laser and a 25x/0.95NA dipping objective. The images were acquired as serial sections through the

entire electrocyte using intensity compensation via increasing detector gain. The entire electrocyte was imaged using a 2×4 tiled scan with a 30% overlap between adjacent images. The images were then rendered using a 3D shaded projection in Avizo® Fire 8.0.1 (FEI Visualization Sciences Group).

Fixed electrocyte sections were imaged on a Leica® TCS SP8 laser scanning confocal microscope, using a 63x/1.3NA glycerol objective with a correction collar and an argon laser, 488nm laser line to observe tissue autofluorescence, and a DPSS 561nm laser line to excite the Alexa® 594. The images were acquired via serial sections with a voxel size of 160nm × 160nm × 160nm and intensity compensation via increasing laser output. The images were then rendered using Imaris® x64 7.6.5(Bitplane). Electrocyte nuclei were counted by determining the number of DAPI-stained nuclei colocalized with Alexa 594 within an image series from the anterior end, posterior end, or cell body, and then extrapolating to the total observed volume of each electrocyte region.

Western Blot

EOs and mouse brains were isolated from animals and flash frozen in liquid nitrogen. Tissues were ground into fine powder using a pre-chilled pestle in a mortar filled with liquid nitrogen. 15 mg mouse brain and 100 mg *E. virescens* EO tissue powder were dissolved in 1 mL 1× NuPAGE® LDS sample buffer (Life Technologies) containing 2.5 % (v/v) 2-mercaptoethonal (Amresco), then heated at 70°C for 10 min. After heating, protein samples were centrifuged at 17,000 × g for 10 min to remove DNA. The collected supernatants were run on a NuPAGE® Novex® 4-12% Bis-Tris protein gradient gel (Life Technologies) then transferred onto a PVDF membrane using an iBlot® dry blotting system (Life Technologies). Membranes were blocked in 1× Tris-

buffered saline (TBS) containing 0.1% Tween20 (Sigma-Aldrich) (TBST) and 5% nonfat dry milk for 1 h at room temperature under agitation. After blocking, membranes were sequentially incubated with primary antibodies diluted in TBST containing 5% nonfat dry milk and 0.02% Sodium Azide (Sigma-Aldrich) including rabbit polyclonal anti-kcnt1(Aviva Systems Biology) 1:200, rabbit polyclonal anti-Pan Na_v (Alomone Labs) 1:200, and mouse monoclonal antibody against the α subunit of Na^+/K^+ ATPase (a5, developed by D.M. Fambrough (Lebovitz et al., 1989), and obtained from the Developmental Studies Hybridoma Bank (DSHB) at University of Iowa) 1:1000 at room temperature for 2 h under agitation. After primary antibody incubation, membranes were washed three times for 5 min with TBST. Then membranes were incubated with secondary antibodies conjugated with horseradish peroxidase (HRP) (Santa Cruz Biotechnology) diluted in TBST containing 5% nonfat dry milk (1:5000 and 1:2000 for goat anti-rabbit IgG-HRP and goat anti-mouse IgG-HRP respectively) for1 h at room temperature. After washing, proteins on the membrane were detected using the Amersham™ ECL™ prime western blotting detection reagent (GE Healthcare) and imaged with a Chemi Doc™ XRS+ imaging system (Bio-Rad). Exposure time was selected manually depending on the observed signal intensity. The membranes stained with polyclonal anti-Pan Na_v and mouse monoclonal antibody against the α subunit of Na^+/K^+ ATPase were cut to separate the EO and mouse brain strips then exposed separately due to the large difference in signal intensity between *E. virescens* EO and mouse brain. Molecular weights of the detected protein were determined by loading Precision Plus Protein™ Kaleidoscope™ standards (Bio-Rad)

together with protein samples into the same gel. Final processing of the images was performed with ImageJ-win64 version 1.44B (National Institutes of Health).

Immunohistochemistry

Sections of EO were embedded completely in OCT compound, flash frozen in liquid nitrogen-chilled isopentane (Sigma-Aldrich) and stored at -80°C until further processing. Serial longitudinal sections (15-20 µm thick) were cut at -25°C using a cabinet cryostat (Leica CM 1900), mounted on gelatin-subbed slides and air-dried overnight at room temperature. Tissue sections were then fixed in 4% paraformaldehyde (Electron Microscopy Sciences) buffered with 1×PBS for 20 min, subsequently washed three times for 5 min each in 1× PBS containing 0.05% Tween-20 (Sigma-Aldrich) (PBST) and blocked in PBST containing 2% bovine serum albumin (BSA) and 5% goat normal serum (Jackson ImmunoResearch) for 1 h at room temperature and then incubated overnight at 4°C with primary antibodies diluted in PBST. After primary antibody incubation, tissue sections were washed as above, and incubated with Alexa Fluor® 488 or 594-conjugated secondary antibodies (Jackson ImmunoReseach) 1:200 diluted in PBST for 1 h at room temperature in a humidified chamber. Sections were then washed and air dried. Slides were mounted using VectaShield® with DAPI (Vector Laboratories) and kept in the dark at 4°C.

A rabbit polyclonal antibody (1:100) against an intracellular epitope of $Na_v1.x$ channels (Anti-Pan Na_v, obtained from Alomone Labs) was used to label voltage-gated Na^+ channels. A mouse monoclonal antibody (1:100) against the α subunit of Na^+/K^+ ATPase (a5, developed by D.M. Fambrough(Lebovitz et al., 1989), and obtained from the Developmental Studies Hybridoma Bank (DSHB) at University of Iowa) was used

to label Na^+/K^+ ATPase. A rat antibody (1:10) against the muscle-type acetylcholine nicotinic receptor (mAb 35, developed by J. Lindstrom (Tzartos et al., 1981), and obtained from DSHB at University of Iowa) was used to label acetylcholine receptors. A mouse monoclonal antibody (1:100) against neurofilament-associated antigen (3A10, developed by T. Jessel and J. Dodd, and obtained from DSHB at University of Iowa) was used to label axon terminals. A rabbit polyclonal antibody (1:200) against K_{Na} channel (anti-Kcnt1, obtained from Aviva Systems Biology) was used to label K_{Na} channels. A mouse monoclonal antibody (1:100) against inward-rectifier K^+ channel 6.2 (B-9, obtained from Santa Cruz Biotechnology), was used to label ATP-sensitive inward rectifier K^+ channels.

Immunohistochemistry slides were imaged on a Zeiss ApoTome.2 microscope with 5X/0.16NA and 10X/0.45NA dry objectives. Images were acquired with a Zeiss AxioCam MRm camera, then processed by Zeiss AxioVision Rel.4.8. We used structured illumination to create optical sections of our fluorescent samples. Final processing of the images was performed with ImageJ-win64 version 1.44B (National Institutes of Health).

Computational Simulations

We modeled the *E. virescens* electrocyte as a three-compartment cell consisting of an active posterior compartment, a passive central compartment, and an active anterior compartment. We used the Hodgkin-Huxley formalism to simulate ionic currents and changes in membrane voltage. We also applied a simplified model of Na^+ entry, diffusion, and pumping to simulate changes in Na^+ concentrations in the three compartments. Simulated cholinergic synaptic current was applied only to the posterior

compartment. The capacitance for the posterior compartment was 48.0 nF and the anterior-compartment capacitance was 18.0 nF. We based these values on the surface areas of the posterior 0.35 mm and anterior 0.2 mm of the electrocyte, respectively, with surface areas determined from confocal 3D reconstructions of electrocytes. The central-compartment capacitance was 18 nF, estimated as the surface area of a cylinder 0.95 mm long and 0.6 mm in diameter, dimensions determined by our imaging data. Differential equations were coded in Matlab (Mathworks, Inc. Natick MA) and integrated using Euler's method with integration time steps of 5×10^{-8} sec. All model parameters are shown in Table 1.

The passive central compartment's current balance equation included only passive leak (I_L) fixed at 5 μS, and coupling to the two active compartments:

$$C_m \frac{dV_c}{dt} = -I_L + g_w(V_a - V_c) + g_w(V_p - V_c) \qquad (1)$$

where g_w is the coupling conductance, fixed at 322 μS.

The current balance equations for the posterior and anterior active compartments were, respectively:

$$C_m \frac{\mathrm{dV_p}}{\mathrm{dt}} = I_{Syn}(t) - \mathrm{I_{Na}} - \mathrm{I_L} + g_w(V_c - V_p) \qquad (2)$$

$$C_m \frac{\mathrm{dV_a}}{\mathrm{dt}} = -\mathrm{I_{KNa}} - \mathrm{I_R} - \mathrm{I_L} + g_w(V_c - V_a) \qquad (3)$$

where I_{Syn} represents synaptic current, I_{Na} is Na^+ current, I_{KNa} is the Na^+-activated K^+ current, and I_R is the inward rectifier K^+ current. For all three compartments, I_L is the leak current, which was given by Equation 4.

$$I_L = \bar{g}_{\mathrm{L}}(\mathrm{V} + 95) \qquad (4)$$

The posterior-compartment synaptic current, I_{Syn}, was given by Equation 5

$$I_{Syn} = \bar{g}_{Syn}\, g_{Syn(t)}(V_p - 15) \qquad (5)$$

where the time series $g_{Syn(t)}$ was a series of 10 alpha waveforms generated using the discrete time equation:

$$g_{Syn(n+2)} = 2\left(1 - \frac{T}{\tau}\right) g_{Syn(n+1)} - \left(1 - \frac{T}{\tau}\right)^2 g_{Syn(n)} + \left(\frac{T}{\tau}\right)^2 x(n) \qquad (6)$$

(Graham and Redman, 1993) where *T* is the integration time step and τ is the time constant. The binary series *x(n)* specified the onset times of the synaptic inputs, and the resulting time-series $g_{Syn(n)}$ was normalized such that $0 \leq g_{Syn(n)} \leq 1$.

The equation for I_{Na} was divided into a transient component (I_{NaT}) and a persistent component (I_{NaP}) as in Equations 7 and 8,

$$I_{NaT} = \bar{g}_{Na} m^3 (1 - \gamma) h (V_p - E_{Na}) \qquad (7)$$

$$I_{NaP} = \bar{g}_{Na} m^3 \gamma (V_p - E_{Na}) \qquad (8)$$

where $0 < \gamma < 1$. E_{Na}, the Na^+ equilibrium potential, was allowed to vary with changing Na^+ concentrations in the posterior compartment (Na_P) according to the equation $E_{Na} = 25.7ln(114/[Na_P])$, assuming 114 mM extracellular Na^+ and temperature of 25 °C.

The anterior-compartment K^+ currents were given by equations 9 and 10.

$$I_{KNa} = \bar{g}_{KNa} n^4 s^4 (V_a + 95) \qquad (9)$$

$$I_R = \bar{g}_R \left(\frac{1}{1 + \exp(\eta_R (Vm + 110))}\right) (V_a + 95) \qquad (10)$$

The gating variables *m*, *n*, and *h* in Equations 7 - 9 are given by Equations 11-13 where *j* = *m*, *n*, or *h*.

$$\frac{dj}{dt} = \alpha_j (1 - j) - \beta_j (j) \qquad (11)$$

$$\alpha_j = k_{\alpha j} \exp(\eta_{\alpha j} V) \qquad (12)$$

$$\beta_j = k_{\beta j} \exp(\eta_{\beta j} V) \qquad (13)$$

We modeled the Na^+-dependence of I_{KNa} with the gating variable, *s*, which is determined by the Na^+ concentration in the bulk cytoplasm in the anterior compartment (Na_A), according to Equation 14.

$$\frac{ds}{dt} = k_f[Na_A](1 - s) - k_b s \qquad (14)$$

We modeled Na^+ concentrations in each compartment based on the compartmental volumes which were 4.2×10^7 μm^3, 2.7×10^8 μm^3, and 1.7×10^7 μm^3 for the posterior, central, and anterior compartments, respectively. The posterior and anterior compartment volumes were measured from our 3D reconstructions of electrocytes, while the central compartment volume was estimated as the volume of a cylinder 0.95 mm long and 0.6 mm in diameter. The initial Na^+ concentration in all three compartments was 15 mM. The equation for Na^+ concentration in the posterior compartment was:

$$\frac{d[Na_P]}{dt} = p + \frac{q}{Vol_P} - \delta([Na_P] - [Na_C])\frac{\lambda_P}{\lambda_C} - b_P[Na_P] \qquad (15)$$

where *p* represents sodium leak and *q* is moles of Na^+ ions entering through the cholinergic receptors and Na^+ channels, given by Equation 16:

$$q = \frac{dt(2\,I_{Syn} + I_{Na})10^{-12}}{eL} \qquad (16)$$

wherein the integrated Na^+ current, *dt(2ISyn+ INa) in nA*ms*, is multiplied by 10^{-12} to yield Coulombs, divided by the elementary charge on a monovalent cation, *e*, to yield number of Na^+ ions, and divided by Avogadro's constant, *L*, to yield moles of Na^+. I_{Syn} was multiplied by 2 in Equation 16 to account for Na^+ entry associated with I_{Syn} where g_{Syn} arises from cholinergic receptors, assuming the Na^+ permeability is twice that of the K^+ permeability. Diffusion of Na^+ between compartments is governed by δ (the diffusion rate constant), the difference in Na^+ concentration between the compartments,

and the ratio of their volumes (λ). Na^+ removal is modeled by the fractional pumping rate b_P, representing the rate at which Na^+ is pumped out of the posterior compartment to the extracellular space.

The central compartment's Na^+ concentration was affected only by diffusion to and from the posterior and anterior compartments as in Equation 17.

$$\frac{d[Na_C]}{dt} = \delta([Na_P] - [Na_C])\frac{\lambda_P}{\lambda_C} - \delta([Na_C] - [Na_A])\frac{\lambda_C}{\lambda_A} \quad (17)$$

The posterior compartment Na^+ concentration was given by Equation 18

$$\frac{d[Na_P]}{dt} = \delta([Na_C] - [Na_A])\frac{\lambda_C}{\lambda_A} - b_A[Na_A] \quad (18)$$

which includes diffusion to and from the central compartment as well as b_A which gives the fractional rate at which Na^+ is pumped from the anterior compartment to the extracellular space.

RESULTS

Gross electrocyte morphology

In *E. virescens*, the EO runs longitudinally along the body and extends into the caudal tail filament (Fig.1A). Several rows of electrocytes are densely packed in the EO (Fig. 1C). We injected Rhodamine B dextran (10,000 MW) into single electrocytes within an isolated section of EO, allowed 15 minutes for the dextran to fully diffuse, then imaged the cell on a Leica® TCS SP8 laser scanning confocal microscope. 3D reconstructions of these cells showed that electrocytes are large cylinder-like cells approximately 1.5 millimeter in length and 600 μm in diameter (Fig. 2A). The electrocyte's surface structure was not uniform, and based on differences in surface structure we divided the cell into three regions: the posterior face, the main body, and the anterior face (Fig. 2A). The space between adjacent electrocytes along the rostral-

caudal axis is ≈30 μm, and the posterior face of each electrocyte is surrounded by the anterior face of the adjacent cell (Fig. 2B).

The surface of the posterior face was densely occupied by narrow invaginations that extended longitudinally into the cell approximately 300 μm, resulting in a pronounced increase in membrane surface area (Fig. 2C). The anterior face usually contained three large lobes with smaller papillary extensions. Additionally, a network of capillaries was observed embedded immediately underneath the ruffled anterior membrane (Fig. 2D, Fig. 3B2). In contrast to the posterior and anterior faces, the surface of the main body is relatively smooth, with an array of spherical structures just beneath the membrane (Fig. 2E).

Electrocytes are multi-nucleated cells formed by the fusion of skeletal myocytes during development (Bennett, 1970; Unguez and Zakon, 1998a, 2002; Zakon and Unguez, 1999) resulting in a syncytium with nuclei localized to the surface of the electrocyte (Machado, et al., 1976). Our images of DAPI stained nuclei colocalized with Alexa Fluor® 594 within our 3D reconstruction confirmed that the nuclei of *E. virescens* electroctyes are densely distributed in a thin layer near the membrane (Fig. 2F; see Fig. 3A for colocalization). The combination of whole cell 3D imaging and high-resolution imaging of smaller electrocyte sections in the present study allowed us to estimate the number of nuclei within a single electrocyte by two distinct methods, both of which indicated that each electrocyte has approximately 30,000 nuclei.

The first method we used was to create an isosurface around the whole-cell image of the electrocyte (Fig. 2A). This allowed us to measure the surface area of the entire electrocyte, which was 4.5×10^6 μm^2. We then counted the number of nuclei per

unit surface area in a single high-resolution image of the cell body, and found that there were 220 nuclei per 2.8×10^4 μm^2 of cell surface area. This method thereby yielded 4.5×10^6 μm^2 $\left(\frac{220 \text{ nuclei}}{2.8 \times 10^4 \text{ μm}^2}\right) = 35{,}000$ nuclei in the electrocyte. To validate the above estimation, we used an alternate approach to estimating the number of nuclei within an electrocyte by modelling the electrocyte with simple geometries, with the anterior end and cell body approximated as a hollow cylinder with a paraboloid scooped out at the anterior end, and the posterior end as a solid paraboloid. The anterior end had a cupped shape, with nuclei along the surface, so the surface area was approximated as a paraboloid with a measured radius of 365μm and a depth of 144 μm, giving a surface area of 4.8×10^5 μm^2. We then counted the number of nuclei in a single high resolution image of the anterior region with 1.5×10^4 μm^2 of surface area and found 170 nuclei, giving a total of 4.8×10^5 μm^2 $\left(\frac{170 \text{ nuclei}}{1.5 \times 10^4 \text{ μm}^2}\right) = 5.4 \times 10^3$ nuclei in the anterior end. The central compartment end was approximated as a hollow cylinder with a measured length of 1.0×10^3 μm and a measured diameter of 600 μm. Therefore, the total number of nuclei on the cell body would be $(600\text{μm})(\pi)(1000\text{μm})\left(\frac{220 \text{ nuclei}}{2.8 \times 10^4 \text{ μm}^2}\right) = 1.5 \times 10^4$ nuclei in the central compartment. For the posterior end, since the invaginations penetrate back to the cell body resulting in nuclei being located throughout the posterior end, we modelled the posterior end as a solid paraboloid. The paraboloid had a measured length of 590 μm and a radius of 215 μm giving a total volume of 8.6×10^7 μm^3. We then measured the number of nuclei in a 7.0×10^6 μm^3 image. To ensure that we only measured electrocyte nuclei, we only counted nuclei that were colocalized with Alexa Fluor®

594. In the sample volume, we counted 1000 nuclei. Extrapolated over the whole posterior end, there would therefore be $8.6 \times 10^7\ \mu m^3 \left(\frac{1000\ \text{nuclei}}{1.2 \times 10^4\ \mu m^3}\right) = 1.2 \times 10^4$ nuclei in the posterior region. Taken together, these quantities sum to 32,000 nuclei per electrocyte, which is in close concordance with our estimate based on the first method.

Fine structure of the electrocyte

We investigated the fine structure of the posterior and anterior faces by imaging 100-µm thick serial sections of a paraformaldehyde-fixed EO sample that contained a single target electrocyte filled with Alexa Fluor® 594 dextran. Electrocytes, vasculature, and pigment cells within the EO also emit a broad autofluorescence spectrum when excited by a 488 nm laser line. We took advantage of this autofluorescence to image tissue adjoining the Alexa Fluor® 594 dextran injected cell.

Our images of the posterior face showed that the surface of each invagination contained many small spine-like structures approximately 50 µm in length. The spines terminate in an enlarged sphere approximately 20 µm in diameter (Fig. 3A). Blood vessels occupy the space between electroctyes with the majority penetrating into the invaginations of the posterior face, while a smaller number contact the anterior face (Fig. 3 A2 and B2, respectively). Capillaries occupy much of the space within each posterior-face invagination, and the spines within the invaginations are largely enveloped by these capillaries. The fine structure of the anterior face (Fig. 3B) is generally less complex than the posterior face, with the unique feature that capillaries appear to reside within enclosed, tube-like structures proximal to the anterior face membrane (Fig. 3B2). An additional and striking difference between the anterior and

posterior faces is that the posterior-face membrane is densely occupied by vesicles, which are exceedingly less abundant on the anterior face (Fig. 3C, D).

Subcellular localization of cholinergic receptors, ion channels, and ion transporters

In gymnotiformes, electrocyte APs are controlled by a medullary pacemaker nucleus via spinal electromotor neurons that innervate each electrocyte (Fig. 1A). Labeling of spinal nerves with the antibody 3A10 against neurofilament-associated antigen (Unguez and Zakon, 1998) showed that only the posterior face is innervated and the innervation occurs throughout the posterior face (Fig. 4A). We also found that acetylcholine receptors were clustered only on the posterior face (Fig. 4B). Given that the cholinergic synapses are restricted to the posterior membrane, we hypothesized that the other ion channels would be localized also on the posterior membrane.

We labeled voltage-gated Na^+ channels (Na_v) with a pan-Na_v antibody raised against an epitope identical in all isoforms of Na_v1 and found that Na_v channels were expressed only on the electrocyte's posterior face (Fig.4C). To ensure these signals are not from the innervating axons, we costained Na_v channels with 3A10 and found no colocalization between them (Fig.4 D). The expression pattern of acetylcholine receptors and Na_v channels indicates that the posterior face is the only entrance site for Na^+ influx and the site of AP initiation.

Based on electrophysiological and molecular evidence that electrocytes express inward-rectifier and K_{Na} channels (Markham et al., 2013), we immunolabeled both channels and to our surprise, found that both are localized only to the anterior face (Fig. 4E, F). Immunolabeling of Na^+/K^+ ATPase alpha subunits showed that these are found

on both the anterior and posterior faces, another unusual arrangement given that the sources of Na^+ influx are restricted to the posterior membrane (Fig. 4G).

Given the counterintuitive spatial separation of the Na^+ channels, K_{Na} channels, and Na^+/K^+ATPases, we performed western blot analyses to ensure that these antibodies indeed specifically labeled the proteins of interest. Western blot of *E. virescens* EO and mouse brain whole-cell lysate labeled with polyclonal anti-Na_v detected specific bands of approximately 250 kDa (the predicted molecular weight of Na_v channels) in both tissues (Fig. 4H). Similarly, polyclonal anti-kcnt1 (K_{Na}) and monoclonal anti Na^+/K^+ ATPase-α subunit labeled bands of approximately 130 kDa and 100 kDa, respectively, in both EO and mouse brain (Fig. 4H). These molecular weights correspond with the predicted molecular weights of K_{Na} channels and Na^+K^+ATPase -α subunits.

Numerical simulations of electrocyte function

Given the unusually large separation of K_{Na} channels from potential Na^+ sources revealed by our imaging data, we used computational simulations of electrocyte action potentials and Na^+ dynamics to test whether the high-frequency firing typical of *E. virescens* electrocytes could be reproduced in a model cell where the spatial arrangement of ion channels matched our imaging data. Our model cell had three compartments, an active posterior compartment, a passive central compartment, and an active anterior compartment. The passive properties of these compartments were guided by morphological measurements of their volumes and membrane areas. We estimated the coupling conductances between compartments based on our measurements of the electrocyte's length and diameter.

The posterior compartment had linear leak current, synaptic current via cholinergic receptors, and voltage-gated Na^+ current (I_L, I_{Syn}, and I_{Na}, respectively). The central compartment had only I_L, and the anterior compartment had I_L, inwardly rectifying K^+ current (I_R) and K_{Na} current (I_{KNa}). Unlike previous simulations of I_{KNa} where the Na^+ sensitivity of the current arises from direct access to a localized persistent Na^+ current (Brown et al., 2008; Markham et al., 2013), we modeled I_{KNa} here such that its Na^+ sensitivity was determined by the Na^+ concentration in the bulk cytoplasm of the anterior compartment. Our model also simulated changes in intracellular Na^+ in each compartment based on Na^+ influx resulting from a static Na^+ leak, I_{Syn} and I_{Na} in the posterior compartment, a fractional Na^+ pumping rate in both the posterior and anterior compartments, and Na^+ diffusion between all three compartments.

In the full model with all currents present according to the parameters in Table 1, the model cell maintained repetitive firing in response to 500 Hz synaptic stimulation (Fig. 5A). During these action potentials, I_{Na} reached peak currents of approximately 15 μA, consistent with earlier experimental results (Lewis et al., 2014a), and I_{KNa} exhibited current magnitudes exceeding 5 μA (Fig. 5B) suggesting an important role in shaping the cell's firing pattern. Na^+ concentrations in the three compartments did vary in response to Na^+ influx, pumping, and diffusion, but only over a range of 1-2 mM (Fig. 5C). As a result, the fractional activation of I_{KNa} due to Na^+ concentrations in the anterior compartment remained fairly steady around 0.7 throughout the action potential train.

To evaluate whether I_{KNa} is a necessary component of AP repolarization in the model cell, we made a model cell with all of the same parameters as in Fig. 5A-C, but

set the conductance for I_{KNa} to zero. This model cell could not maintain repetitive firing at 500Hz (Fig. 5D-E) and instead remained in a state of depolarized oscillation. These results provide evidence that I_{KNa} in our model cell is necessary for AP repolarization and plays a role in AP termination even when the K_{Na} channels are at a great distance from transient Na^+ sources.

DISCUSSION

The most striking finding from this study is the extreme compartmentalization of ion channels and ion transporters across vast distances in *E. virescens* electrocytes. The K_{Na} channels that repolarize the electrocyte AP and a substantial portion of the Na^+/K^+ ATPases responsible for removing Na^+ after each AP are separated by more than a millimeter from the only identified sources of Na^+ influx.

The presence of K_{Na} channels at such a great distance from Na^+ sources raises the important question of how these channels are activated during the AP. In previous work with K_{Na} channels from other taxa, channel activation required intracellular Na^+ concentrations ($[Na^+]_i$) that far exceed those normally found in bulk cytoplasm (Dryer et al., 1989; Kameyama et al., 1984; Yuan et al., 2003). In mammalian neurons, K_{Na} channels are clustered within just a few μm of Na^+ channels in microdomains that allow localized elevation of Na^+ concentrations sufficient to activate K_{Na} channels without changing $[Na^+]_i$ in the bulk cytoplasm (Budelli et al., 2009b; Hage and Salkoff, 2012a) . However, we show here that Na^+ and K_{Na} channels are separated by great distances in *E. virescens* electrocytes, suggesting that K_{Na} channels in *E. virescens* electrocytes do not require proximal sources of Na^+ influx.

One hypothesis as to how K_{Na} channels are activated in electroctyes is that electrocytes experience a significant increase in $[Na^+]_i$ during each AP or during sustained high-frequency firing, a distinct possibility given the magnitude of I_{Na} during the AP. We found a high density of Na^+/K^+ ATPases on the anterior face consistent with earlier biochemical data (Denizot, 1982), suggesting that Na^+ influx from the posterior face ultimately increases $[Na^+]_i$ in the anterior region. Our computational simulations suggest that only small changes in $[Na^+]_i$ occur during high-frequency firing in *E. virescens* electrocytes. This suggests instead a second hypothesis, that the electrocyte's K_{Na} channels are more sensitive to $[Na^+]_i$ than most other K_{Na} isoforms identified to date. Indeed, our simulated I_{KNa} was based on Na^+-dependent rate constants that created partial activation with Na^+ concentrations of approximately 15 mM. Multiple factors determine the Na^+ sensitivity of K_{Na} channels. Single amino-acid substitutions can shift the Na^+ sensitivity of K_{Na} channels over a range of 200 mM (Zhang et al., 2010). Given the elevated rates of evolution for other ion channels in gymnotiform electrocytes (Zakon et al., 2006; Zakon et al., 2008), it seems possible that K_{Na} channels also could have undergone evolutionary changes that would enhance Na^+ sensitivity. Additionally, intracellular factors such as NAD^+ can modulate the Na^+ sensitivity of K_{Na} channels such that the EC_{50} is approximately 17 mM (Tamsett et al., 2009). It is possible that such molecular evolution or functional modulation in *E. virescens* K_{Na} channels could allow their activation at Na^+ concentrations in the 15 mM range. These possibilities can only be directly addressed through cloning and heterologous expression of *E. virescens* electrocyte K_{Na} channels.

Our numerical simulations in the present study suggest that the electrocyte K_{Na} channels remain in a state of partial activation during repetitive firing, rather than responding to transient increases in $[Na^+]_i$ as concluded in earlier work (Markham et al., 2013). If electrocyte K_{Na} channels indeed are maintaining a steady level of activation during normal repetitive firing, this raises the question of what function the channels' Na^+ sensitivity serves in this system. Further experimental investigation and computational simulations of Na^+ dynamics in the electrocyte are needed to clarify the functional significance of K_{Na} channels' Na^+ sensitivity in *E. virescens* electrocytes.

Additionally, the finding that ion channels are expressed on both the anterior and posterior electrocyte faces contradicts a long-standing assumption, originating with some of the earliest electrophysiological studies of *E. virescens* electrocytes, that only the innervated face is active (Bennett, 1961, 1971) and that all ion channels which produce the AP should therefore be localized to the posterior face (e.g., Assad et al., 1998). The presence of K_{Na} and inward-rectifier K^+ channels on the electrocyte anterior membrane indicates that both the posterior and anterior faces of the electrocyte are involved in AP production.

A second important finding here is the sheer magnitude and complexity of the electrocyte's morphology. Our two-photon live-cell and fixed-tissue imaging of *E. virescens* electroctyes extends earlier electron microscopy studies (Schwartz et al., 1975b) that first reported the 2D morphological polarization of these cells. Our 3D reconstructions of *E. virescens* electrocytes also show that they are extremely large multi-nucleated cells with striking differences in the ultrastructural features of the posterior and anterior faces. Because of the electrocytes' large diameter, the laser

scanning confocal microscope could not resolve the submicron detail of the medial region of the cells, preventing us from obtaining a detailed 3D reconstruction of this region of the electrocyte. However, we observed a discrete lower boundary of the fluorescence on the medial side of the electrocyte at a depth of 600 µm, suggesting that the cell is 600 µm across on both the lateral-medial axis and the ventral-dorsal axis.

The deep invaginations of the posterior region create a significant expansion of membrane surface area in a comparatively small volume. This membrane area is almost entirely occupied by vascularization on the extracellular surface, and vesicles on the intracellular surface. It is perhaps possible that some of the fibrillary structures we identified as capillaries were instead portions of the innervating spinal nerves, but this is unlikely because blood vessel walls, unlike nerve, contain autofluorescent elastin and collagen (Deyl et al., 1980) and the narrowest vessels we observed were ≈3 µm in diameter with a hollow center. Additionally, the vessels branched from a large central hollow tube that was almost 20 µm in diameter (Fig. 3B2), making it extremely unlikely that these are axons. The dense vascularization of the posterior face is likely necessary to provide efficient nutrient supply and waste removal consistent with reports that high concentrations of mitochondria are present in the posterior region (Schwartz et al., 1975b). We hypothesize that the densely packed vesicles on the posterior membrane are associated with constitutive trafficking of Na^+ channels and Na^+/K^+ ATPases. In a related electric fish, Na^+ channels are constitutively cycled into and out of the electrocyte membrane, and upregulation of channel exocytosis by hormonal factors can increase I_{Na} magnitude by more than 50% within minutes (Markham et al., 2009a), as has been reported for *E. virescens* (Markham et al., 2013).

The proliferation of membrane surface area on the posterior face also provides a substrate for high numbers of Na^+/K^+ ATPases which are expressed throughout the posterior membrane. Active transport of Na^+ by the Na^+/K^+ ATPase occurs at the rate of $\approx 10^3$ ions per second (Holmgren et al., 2000) while selective ion channels pass 10^7 to 10^8 ions per second (Morais-Cabral et al., 2001). In *E. virescens* electrocytes $\approx 6 \times 10^{10}$ Na^+ ions enter the electrocyte with each AP (Lewis et al., 2014b) with only one millisecond between APs at 500 Hz. Accordingly, efficient removal of Na^+ during the brief interspike interval would depend on extremely high densities of Na^+/K^+ ATPases. The extensive posterior-face membrane area also would increase membrane capacitance and decrease resistance (assuming a constant membrane resistivity). This combination of high capacitance and low resistance would increase current flow during the AP (Schwartz et al., 1975b) and the tuning of resistance relative to capacitance would determine the membrane time constant potentially influencing AP duration (Mills et al., 1992).

The complex organization of the posterior face in *E. virescens* electrocytes contrasts sharply with the morphology of the anterior face which is relatively featureless with sparse vascularization and few detectable vesicles. Within the relatively simple organization of the anterior face, K_{Na} channels, inward-rectifier K^+ channels, and Na^+/K^+ ATPases were densely and apparently evenly distributed across the membrane surface. The paucity of anterior-face exocytotic vesicles suggests that K_{Na} channels are perhaps not cycled or trafficked in the same manner as Na^+ channels on the posterior-face. These results are consistent with our earlier studies of the hormonal regulation of ionic currents in *E.virescens* electrocytes. Application of adrenocorticotropic hormone

(ACTH) increased the magnitudes of I_{Na} and I_{KNa}. The increase in I_{Na} was a direct effect of ACTH application regulating vesicular trafficking of Na^+ channels, but the increased conductance of K_{Na} channels was found to be a secondary effect of the hormone-induced increase in I_{Na} magnitude (Markham et al., 2013).

The bioelectrical properties of all excitable cells are determined by their morphology and the subcellular localization of ion channels. Electrocyte morphology is an important determinant of species-specific and individual-specific EOD waveforms (Bass, 1986; Gallant et al., 2011; Hopkins et al., 1990; Mills et al., 1992) and the subcellular distributions and densities of ionic currents also help determine EOD waveform (Ferrari and Zakon, 1993; Markham and Zakon, 2014; Shenkel and Sigworth, 1991). Some of the ion channels, ionotropic receptors, and ion transporters responsible for electrocytes' biophysical properties have been localized in other gymnotiform and mormyriform electric fish (Cuellar et al., 2006; Gallant et al., 2011; Liu et al., 2007). The present work is, to our knowledge, the first comprehensive presentation of detailed electrocyte morphology together with subcellular localization of all ionic mechanisms responsible for an electrocyte's electrical excitability. It is of course possible that additional key membrane proteins are present but not yet detected. Of particular concern is the possibility that a second undetected isoform of K_{Na} channel is expressed in proximity to the voltage-gated Na^+ channels. We believe this is unlikely because an earlier study detected only a single isoform of K_{Na} channel in *E. virescens* electrocytes by RT-PCR, the KCNT1/Slack isoform (Markham et al., 2013), supporting the conclusion that our immunolabeling in the present study detected all K_{Na} channels expressed in electrocytes. Moreover, the present immunolabeling study detected ion

channels corresponding to all known ionic currents in *E. virescens* electrocytes, and these ionic currents are sufficient to reproduce completely the electrical behavior of these cells as shown by our computational simulations in this study and in earlier work (Markham et al., 2013).

Ultimately, the energetic demands of electrocyte APs and the ability to maintain firing rates exceeding 500 Hz throughout the animal's lifespan stem from the spatiotemporal dynamics of Na^+ entry during the AP and the subsequent Na^+ removal within a millisecond by the Na^+/K^+ ATPases. For these peripheral excitable cells the metabolic cost of AP generation is likely a major force governing their biophysical properties as is the case for central neurons (Hasenstaub et al., 2010). Future studies on the temporal and spatial dynamics of Na^+ entry and removal in electrocytes will be necessary for understanding how the ion channels and Na^+/K^+ ATPases coordinate to maintain high firing rates while managing the extremely large inward Na^+ currents. Further, additional exploration of the interaction between electrocyte Na^+ channels and K_{Na} channels will likely lead to new insights on the many important roles that K_{Na} channels play in excitable cell physiology (Bhattacharjee and Kaczmarek, 2005).

REFERENCES

Assad, C., Rasnow, B., Stoddard, P.K., Bower, J.M., 1998. The electric organ discharges of the gymnotiform fishes: II. Eigenmannia. J. Comp. Physiol. A 183, 419-432.

Attwell, D., Laughlin, S.B., 2001. An energy budget for signaling in the grey matter of the brain. J. Cereb. Blood Flow Metab. 21, 1133-1145.

Bass, A.H., 1986. Species differences in electric organs of mormyrids: substrates for species-typical electric organ discharge waveforms. J. Comp. Neurol. 244, 313-330.

Bean, B.P., 2007. The action potential in mammalian central neurons. Nat. Rev. Neurosci. 8, 451-465.

Bennett, M.V., 1970. Comparative physiology: electric organs. Annu. Rev. Physiol. 32, 471-528.

Bennett, M.V.L., 1961. Modes of operation of electric organs. Ann. N. Y. Acad. Sci. 94, 458-509.

Bennett, M.V.L., 1971. Electric Organs, in: Hoar, W.S., Randall, D.J. (Eds.), Fish Physiology. Academic Press, New York, pp. 347-491.

Bhattacharjee, A., Kaczmarek, L.K., 2005. For K^+ channels, Na^+ is the new $Ca2^+$. Trends Neurosci. 28, 422-428.

Brown, M.R., Kronengold, J., Gazula, V.R., Spilianakis, C.G., Flavell, R.A., von Hehn, C.A., Bhattacharjee, A., Kaczmarek, L.K., 2008. Amino-termini isoforms of the Slack K^+ channel, regulated by alternative promoters, differentially modulate rhythmic firing and adaptation. J. Physiol. 586, 5161-5179.

Budelli, G., Hage, T.A., Wei, A., Rojas, P., Jong, Y.J., O'Malley, K., Salkoff, L., 2009. Na^+-activated K^+ channels express a large delayed outward current in neurons during normal physiology. Nat. Neurosci. 12, 745-750.

Carter, B.C., Bean, B.P., 2009. Sodium entry during action potentials of mammalian neurons: incomplete inactivation and reduced metabolic efficiency in fast-spiking neurons. Neuron 64, 898-909.

Cuellar, H., Kim, J.A., Unguez, G.A., 2006. Evidence of post-transcriptional regulation in the maintenance of a partial muscle phenotype by electrogenic cells of S. macrurus. FASEB J. 20, 2540-.

Denizot, J.P., 1982. The cytochemical demonstration of NaK dependent adenosine triphosphatase at electrocyte level in Eigenmannia virescens (Gymnotidae). Histochemistry 74, 213-221.

Deyl, Z., Macek, K., Adam, M., 1980. Studies on the chemical nature of elastin fluorescence. Biochimica et Biophysica Acta (BBA)-Protein Structure 625, 248-254.

Dryer, S.E., Fujii, J.T., Martin, A.R., 1989. A Na^+-activated K^+ current in cultured brain stem neurones from chicks. J. Physiol. 410, 283-296.

Ferrari, M.B., Zakon, H.H., 1993. Conductances contributing to the action potential of Sternopygus electrocytes. J. Comp. Physiol. A 173, 281-292.

Gallant, J.R., Arnegard, M.E., Sullivan, J.P., Carlson, B.A., Hopkins, C.D., 2011. Signal variation and its morphological correlates in Paramormyrops kingsleyae provide insight into the evolution of electrogenic signal diversity in mormyrid electric fish. J. Comp. Physiol. A 197, 799-817.

Graham, B.P., Redman, S.J., 1993. Dynamic Behavior of a Model of the Muscle Stretch Reflex. Neural Networks 6, 947-962.

Hage, T.A., Salkoff, L., 2012. Sodium-activated potassium channels are functionally coupled to persistent sodium currents. J. Neurosci. 32, 2714-2721.

Hasenstaub, A., Otte, S., Callaway, E., Sejnowski, T.J., 2010. Metabolic cost as a unifying principle governing neuronal biophysics. Proc Natl Acad Sci U S A 107, 12329-12334.

Holmgren, M., Wagg, J., Bezanilla, F., Rakowski, R.F., De Weer, P., Gadsby, D.C., 2000. Three distinct and sequential steps in the release of sodium ions by the Na^+/K^+-ATPase. Nature 403, 898-901.

Hopkins, C.D., 1974. Electric Communication: Functions in the Social Behavior of Eigenmannia virescens. Behaviour 50, 270-305.

Hopkins, C.D., Comfort, N.C., Bastian, J., Bass, A.H., 1990. Functional analysis of sexual dimorphism in an electric fish, Hypopomus pinnicaudatus, order Gymnotiformes. Brain. Behav. Evol. 35, 350-367.

Howarth, C., Gleeson, P., Attwell, D., 2012. Updated energy budgets for neural computation in the neocortex and cerebellum. J. Cereb. Blood Flow Metab. 32, 1222-1232.

Kameyama, M., Kakei, M., Sato, R., Shibasaki, T., Matsuda, H., Irisawa, H., 1984. Intracellular Na^+ activates a K^+ channel in mammalian cardiac cells. Nature 309, 354-356.

Lebovitz, R.M., Takeyasu, K., Fambrough, D.M., 1989. Molecular characterization and expression of the (Na^+/K^+)-ATPase alpha-subunit in Drosophila melanogaster. EMBO J. 8, 193-202.

Lewis, J.E., Gilmour, K.M., Moorhead, M.J., Perry, S.F., Markham, M.R., 2014. Action potential energetics at the organismal level reveal a trade-off in efficiency at high firing rates. J. Neurosci. 34, 197-201.

Liu, H., Wu, M.M., Zakon, H.H., 2007. Individual variation and hormonal modulation of a sodium channel beta subunit in the electric organ correlate with variation in a social signal. Dev. Neurobiol. 67, 1289-1304.

Markham, M.R., Kaczmarek, L.K., Zakon, H.H., 2013. A sodium-activated potassium channel supports high-frequency firing and reduces energetic costs during rapid modulations of action potential amplitude. J. Neurophysiol. 109, 1713-1723.

Markham, M.R., McAnelly, M.L., Stoddard, P.K., Zakon, H.H., 2009. Circadian and social cues regulate ion channel trafficking. PLoS Biol 7, e1000203.

Markham, M.R., Zakon, H.H., 2014. Ionic Mechanisms of Microsecond-Scale Spike Timing in Single Cells. J. Neurosci. 34, 6668-6678.

Mills, A., Zakon, H.H., Marchaterre, M.A., Bass, A.H., 1992. Electric organ morphology of Sternopygus macrurus, a wave-type, weakly electric fish with a sexually dimorphic EOD. J. Neurobiol. 23, 920-932.

Morais-Cabral, J.H., Zhou, Y., MacKinnon, R., 2001. Energetic optimization of ion conduction rate by the K^+ selectivity filter. Nature 414, 37-42.

Niven, J.E., Laughlin, S.B., 2008. Energy limitation as a selective pressure on the evolution of sensory systems. J. Exp. Biol. 211, 1792-1804.

Reardon, E.E., Parisi, A., Krahe, R., Chapman, L.J., 2011. Energetic constraints on electric signalling in wave-type weakly electric fishes. J. Exp. Biol. 214, 4141-4150.

Scheich, H., 1977. Neural basis of communication in the high frequency electric fish,Eigenmannia virescens (Jamming Avoidance Response). J. Comp. Physiol. A 113, 181-206.

Schwartz, I.R., Pappas, G.D., Bennett, M.V.L., 1975. The fine structure of electrocytes in weakly electric teleosts. J. Neurocytol. 4, 87-114.

Shenkel, S., Sigworth, F.J., 1991. Patch recordings from the electrocytes of Electrophorus electricus. Na currents and PNa/PK variability. J. Gen. Physiol. 97, 1013-1041.

Tamsett, T.J., Picchione, K.E., Bhattacharjee, A., 2009. NAD^+ activates KNa channels in dorsal root ganglion neurons. The Journal of Neuroscience 29, 5127-5134.

Tzartos, S.J., Rand, D.E., Einarson, B.L., Lindstrom, J.M., 1981. Mapping of surface structures of electrophorus acetylcholine receptor using monoclonal antibodies. Journal of Biological Chemistry 256, 8635-8645.

Unguez, G.A., Zakon, H.H., 1998a. Phenotypic conversion of distinct muscle fiber populations to electrocytes in a weakly electric fish. J. Comp. Neurol. 399, 20-34.

Unguez, G.A., Zakon, H.H., 1998b. Reexpression of myogenic proteins in mature electric organ after removal of neural input. The Journal of neuroscience 18, 9924-9935.

Unguez, G.A., Zakon, H.H., 2002. Skeletal muscle transformation into electric organ in S. macrurus depends on innervation. J. Neurobiol. 53, 391-402.

Yuan, A., Santi, C.M., Wei, A., Wang, Z.W., Pollak, K., Nonet, M., Kaczmarek, L., Crowder, C.M., Salkoff, L., 2003. The sodium-activated potassium channel is encoded by a member of the Slo gene family. Neuron 37, 765-773.

Zakon, H.H., Lu, Y., Zwickl, D.J., Hillis, D.M., 2006. Sodium channel genes and the evolution of diversity in communication signals of electric fishes: convergent molecular evolution. Proc Natl Acad Sci U S A 103, 3675-3680.

Zakon, H.H., Unguez, G.A., 1999. Development and regeneration of the electric organ. J. Exp. Biol. 202, 1427-1434.

Zakon, H.H., Zwickl, D.J., Lu, Y., Hillis, D.M., 2008. Molecular evolution of communication signals in electric fish. J. Exp. Biol. 211, 1814-1818.

Zhang, Z., Rosenhouse-Dantsker, A., Tang, Q.Y., Noskov, S., Logothetis, D.E., 2010. The RCK2 domain uses a coordination site present in Kir channels to confer sodium sensitivity to Slo2.2 channels. J. Neurosci. 30, 7554-7562.

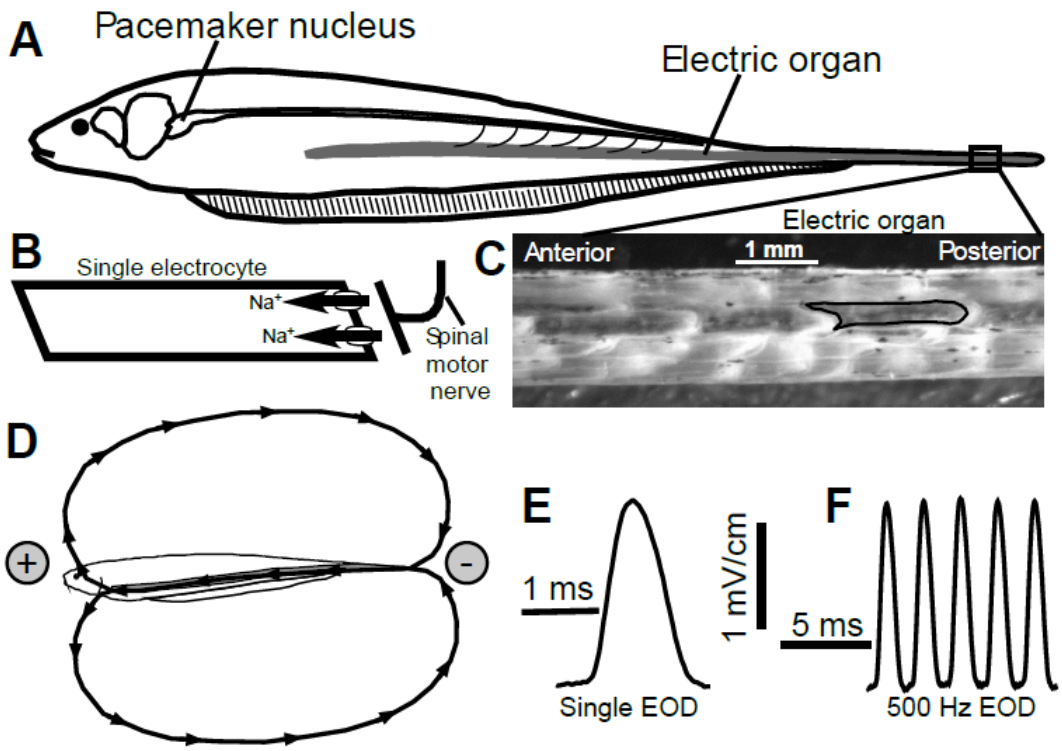

Figure 1. The electric organ discharge in *E.virescens*. (A) The electric organ discharge (EOD) is produced by the coordinated action potentials (APs) of the electrocytes in the electric organ (EO). A medullary pacemaker nucleus controls the electrocyte APs via spinal electromotor neurons which innervate the electrocytes. (B) Simplified schematic of an electrocyte. These are large cells, greater than 1 millimeter in length, innervated by a cholinergic synapse on the posterior end of the cell. Activation of the cholinergic synapse initiates the AP when sodium enters the cell via voltage-gated sodium channels. The cell geometry causes the Na^+ current to move along the rostral-caudal body axis. (C) A section of EO from the tail, with skin removed to expose the electrocytes, which are densely packed within the EO. A single electrocyte is outlined in black. (D) The simultaneous APs of all electrocytes in the EO generate current that moves forward toward the head, following a return path through the water to the tail. By convention, current moving toward the head is measured as positive (upward). (E) A single EOD waveform corresponds to one cycle of APs in the EO. (F) The EOD waveform from a fish with EOD frequency of ≈500 Hz.

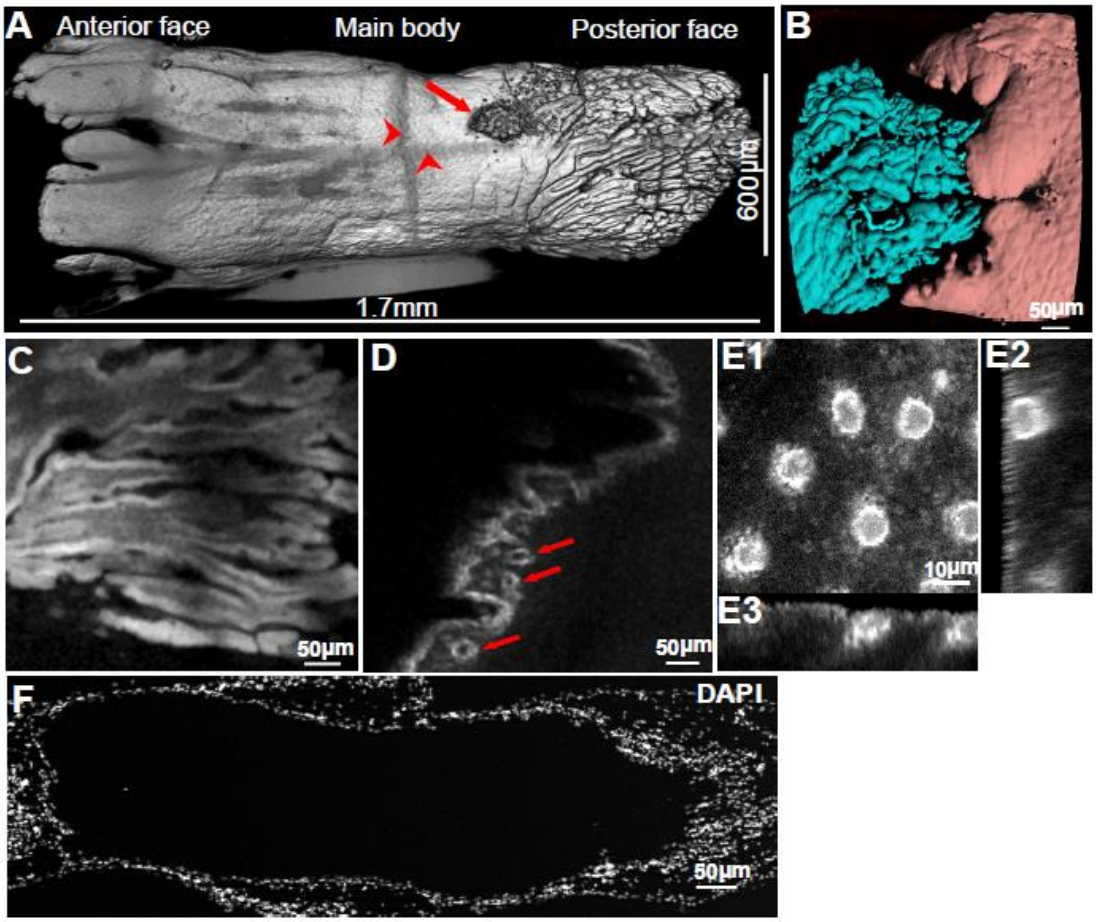

Figure 2. Gross morphology of *E. virescens* electrocytes. (A) 3D reconstruction from serial confocal scanning through a live electrocyte injected with Rhodamine B dextran (10,000 MW). Arrow indicates site of dextran injection. Darkened horizontal and vertical lines (arrowheads) are artifacts caused by the image tile overlap. (B) A segmented autofluorescence image of the junction between two adjoining electrocytes with the posterior face of one electrocyte on the left (cyan) and the anterior face of the adjacent electrocyte (pink) on the right. (C) A single optical section of the posterior face from a Rhodamine B dextran-injected electrocyte. The posterior face contains deep invaginations, dramatically increasing the surface area of the cell. (D) A single optical section of the anterior face from a Rhodamine B dextran-injected electrocyte. Arrows indicate penetrating capillary structures within the anterior face. (E) Orthogonal sectional views of the spherical structures beneath the membrane of the cell body. E1 is looking down at the cell surface. E2 is a single Y-Z image orthogonal to E1, and E3 is a single X-Z image orthogonal to E1 and E2. (F) A single 20 µm-thick electrocyte section stained with DAPI to label nuclei (posterior is to the right).

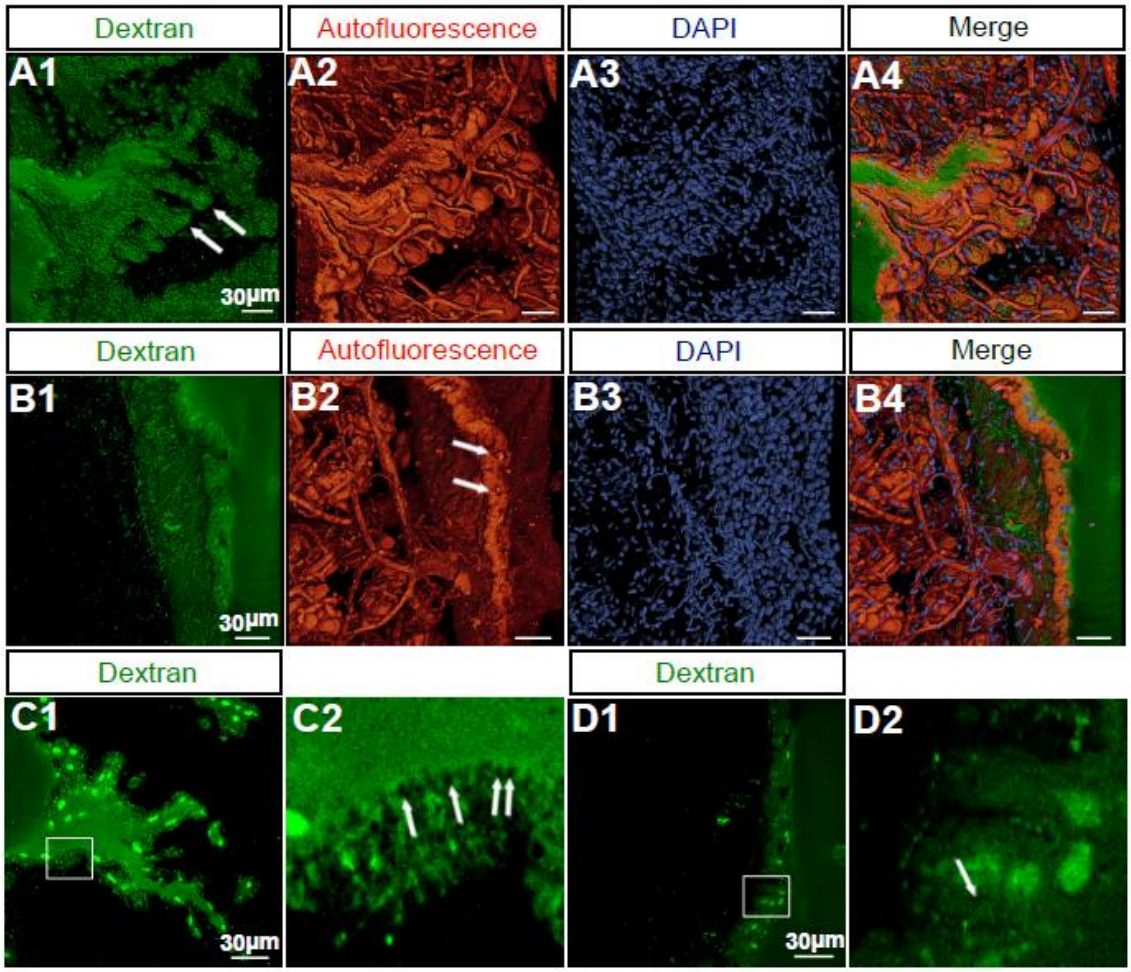

Figure 3. Fine structure of *E. virescens* electrocytes. (A) 3D reconstruction of membrane papillae within a single invagination from serial confocal scans through a fixed 100 µm-thick section of EO tissue. A1 shows the intracellular structure identified by injection of Alexa Fluor® 594 dextran (10,000 MW). Arrows point to the spines projecting from membrane papillae. In A2, tissue autofluorescence reveals that the spines shown in A1are wrapped by capillaries. DAPI stains the multiple nuclei in A3. Images taken in channels A1-A3 opaquely superimposed in A4. (B) 3D reconstruction of the junction between adjacent electrocytes from serial confocal scans through a 100 µm-thick section of fixed EO tissue. B1 shows the anterior face of the electrocyte injected with Alexa Fluor® 594 dextran. Blood vessels occupy the space between adjacent electrocytes in B2 and arrows indicate the capillaries penetrating the anterior face. DAPI labels nuclei in B3. Images taken in channels B1-B3 are merged in B4. (C) The posterior face membrane is mostly occupied by vesicles. C1 is an optical section from the serial confocal scans of the posterior face shown in (A1). The region outlined in white in C1 is enlarged in C2. Arrows indicate vesicles. (D) Few vesicles are found on the surface of the anterior face. D1 is an optical section from the serial confocal scans of the anterior face shown in (B1). Region outlined in white in D1 is enlarged in D2. Green circular structures in C-D are nuclei. Arrows indicate vesicles.

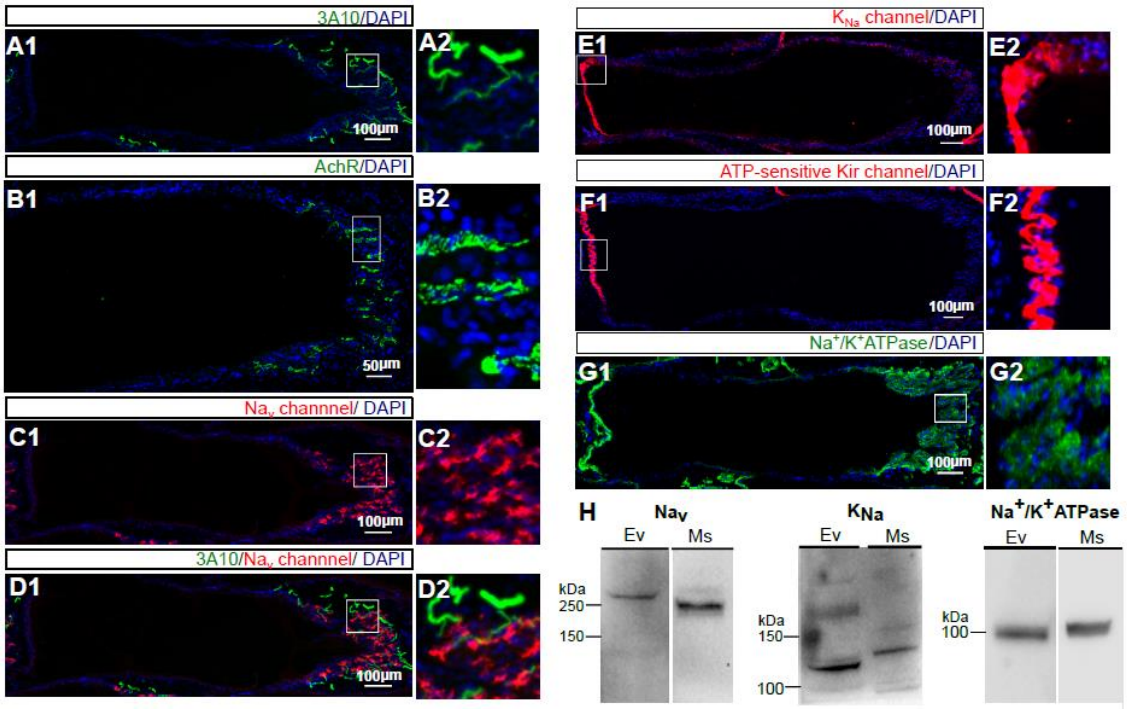

Figure 4. Western blot analysis and immunohistochemistry staining of acetylcholine receptors, ion channels and Na^+/K^+ ATPases in *E. virescens* electrocytes. (A-G) Expression pattern of acetylcholine receptors, ion channels and Na^+/K^+ATPases. (A) Only the posterior face (right) is innervated by spinal electromotor neurons. The axons of innervating neurons are labeled with 3A10 (green). (B) Acetylcholine receptors (green) are clustered only on the posterior face (right). (C) Voltage-gated Na^+ channels (red) are localized only on the posterior face (right). (D) An electrocyte is co-labeled with 3A10 (green) and voltage-gated Na^+ channels (red). (E) Na^+-activated K^+ (K_{Na}) channels (red) are only expressed on the anterior face (left). (F) ATP-sensitive inward rectifier K^+ channels (red) are localized on the anterior face (left). (G) Na^+/K^+ ATPases (green) are expressed in both anterior and posterior faces. DAPI (blue) labels the electrocyte's nuclei in A-G. The region outlined in white in A-G1 is enlarged in A-G2. (H) western blot analysis to confirm the specificity of rabbit polyclonal anti-Na_v (left), rabbit polyclonal anti-kcnt1(middle) and mouse monoclonal anti-α subunit of Na^+/K^+ ATPase (right) in *E.virescens* electric organ and mouse brain. In electric organ, a band around 250 kDa was labeled with anti-Na_v which is slightly larger than that in mouse brain (left). Anti-kcnt1 detected a band around 130 kDa in electric organ which is slightly smaller than that in mouse brain (middle). A band at 100 kDa was detected with anti- α subunit of Na^+/K^+ATPase in both electric organ and mouse brain (right).

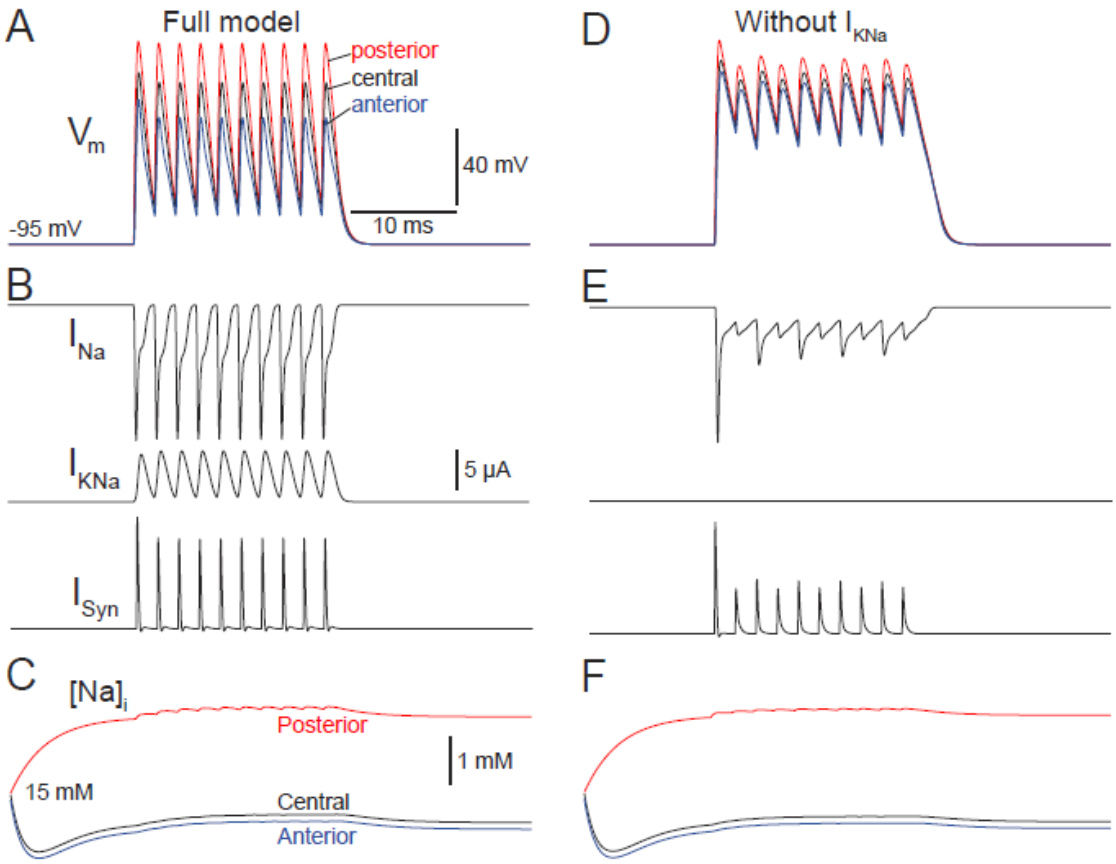

Figure 5. Computational simulations of electrocyte action potentials in a model electrocyte with K_{Na} channels (A-D) and without K_{Na} channels (E-G). (A) Membrane potential of the posterior (red), central (black), and anterior (blue) compartments of a model cell with K_{Na} during a train of 10 action potentials elicited at 500 Hz by simulated synaptic conductances. (B) Time course of the Na^+ current (I_{Na}), K_{Na} current (I_{KNa}) and synaptic current (I_{Syn}) during the action potential train shown in *A*. (C) Timecourse of internal Na^+ concentrations in the posterior (red), central (black), and anterior (blue) compartments during the action potential train shown in Panel A. The different initial Na^+ concentrations reflect the equilibrium of resting Na^+ leak, pumping, and diffusion rates as shown in *D*. (D) Posterior membrane potential and time course of internal Na^+ concentrations in the posterior (red), central (black), and anterior (blue) compartments during the same simulation shown in *A*, but on an expanded timescale that shows the initial changes in Na^+ concentrations as the Na^+ leak, pumping, and diffusion processes reach equilibrium. (E) Membrane potential of the posterior (red), central (black), and anterior (blue) compartments of a model cell without K_{Na} during a train of 10 action potentials elicited at 500 Hz by simulated synaptic conductances. (F) Time course of the Na^+ current (I_{Na}), K_{Na} current (I_{KNa}) and synaptic current (I_{Syn}) during the action potential train shown in *E*. (G) Time course of internal Na^+ concentrations in the posterior (red), central (black), and anterior (blue) compartments during the action potential train shown in *E*. The different initial Na^+ concentrations reflect the equilibrium of resting Na^+ leak, pumping, and diffusion rates as shown in *D*.

Table 1. Parameter values for the electrocyte model

Posterior Compartment		Anterior Compartment	
Parameter	**Value**	**Parameter**	**Value**
g_L	40 μS	g_L	20 μS
$\bar{g}_{Syn}$	600 μS	$\bar{g}_{KNa}$	8000 μS
τ	0.07 ms	k_{an}	1.209 ms^{-1}
		η_{an}	0.00948 mV^{-1}
$\bar{g}_{Na}$	700 μS	$k_{\beta n}$	0.4448 ms^{-1}
γ	0.05	$\eta_{\beta n}$	-0.01552 mV^{-1}
k_{am}	13.6 ms^{-1}	k_f	50 $mM^{-1} \cdot ms^{-1}$
η_{am}	0.0037 mV^{-1}	k_b	200 ms^{-1}
$k_{\beta m}$	0.6894 ms^{-1}		
$\eta_{\beta m}$	-0.0763 mV^{-1}	$\bar{g}_R$	100 μS
k_{ah}	0.00165 ms^{-1}	η_R	0.22 mV^{-1}
η_{ah}	-0.1656 mV^{-1}		
$k_{\beta h}$	1.493 ms^{-1}	δ	0.0019 $mm^2\ s^{-1}$
$\eta_{\beta h}$	0.11 mV^{-1}	b_A	0.7 mM ms^{-1}
p	5 mM ms^{-1}		
δ	0.0019 $mm^2\ s^{-1}$		
b_P	0.3 mM ms^{-1}		

Chapter 3: Ionic mechanisms and a novel sodium-activated potassium channel associated with variations in action potential frequency in fast spiking cells

SUMMARY

The density and kinetic properties of potassium channels in the plasma membrane are key determinants of an excitable cell's functional capacity and the resulting metabolic cost. The electric organ cells (electrocytes) of electric fish *Eigenmannia virescens* generate action potentials (APs) at 200-600 Hz. To better understand the role of potassium channels in endowing electrocytes with the ability to spike quickly and unremittingly, we cloned the cDNAs encoding the Na^+-activated K^+ (K_{Na}) channels which are used to terminate APs in electrocytes. Three types of K_{Na} channel subunits were identified, eslack1, eslack2 and eslick, all of which were expressed on the anterior side of electrocytes, separated by >1 mm from the voltage-gated Na^+ (Na_v) channels, which are restricted to the posterior membrane. Transcripts for eslack1 and eslack2 are found in both skeletal muscle and electric organ (EO) while eslick is expressed only in EO. Whole-cell currents recorded from *Xenopus laevis* oocytes expressing *E. virescens* K_{Na} channels revealed that eslick currents are activated more rapidly than eslack1 currents. In *E. virescens*, each fish has its individual-specific baseline EOD frequency (EODf). Using qRT-PCR to measure the mRNA levels of the three K_{Na} channel genes in EO from fish with various EOD frequencies, we found that transcription levels of eslick correlated with EODf, but transcription levels of eslack1 and eslack2 were not correlated with EODf. We also found that transcription levels of

the inward rectifier K^+ channel $K_{ir}6.2$, Na^+/K^+-ATPase and voltage-gated Na^+ channel $Na_v1.4a$ were correlated with EODf while the transcription level of $Na_v1.4b$ was not.

INTRODUCTION

Individual variation in the properties of communication signals is common among many animal species and serves an important role in animals' social behaviors. Individual differences have been reported in the acoustic characters of the calling song of cicadas (Seabra et al., 2008), songbirds (Fitzsimmons et al., 2008), frogs (Bee, 2004; Bee et al., 2001), and monkeys (Kitchen et al., 2003); in the frequency of bats' echolocation calls (Davidson and Wilkinson, 2002; Jiang et al., 2010); and in the flash pattern of fireflies (Forrest and Eubanks, 1995). Variations in these communication signals are often used for individual discrimination, contain information regarding the animal's dominance status, and facilitate effective communication in variable environments (Bee, 2004; Hahn et al., 2013; Kazial et al., 2001; Kitchen et al., 2003; Medina and Francis, 2012). The causes and molecular mechanisms controlling these individual variations in social signals are, surprisingly, not well understood.

The weakly electric fish *Eigenmannia virescens* relies on self-generated electric organ discharges (EODs) to navigate and communicate in darkness (Hopkins, 1974). *E. virescens* has a considerable animal-to-animal variability in EOD frequency (EODf) (200-500 Hz) (Scheich, 1977) (Fig. 1E). Early studies on the behavior of *E. virescens* suggested that EODf conveys information about individual identity, gender and dominance rank (Helfman et al., 2009; Hopkins, 1974). The EODf is set by the medullary pacemaker nucleus and the EOD is generated by the summed action potentials (APs) of >1000 electrocytes in the EO (Fig.1). The experimental tractability

of *E. virescens*'s electrogeneration system makes it a good model system for studying the molecular mechanisms giving rise to the individual variations in the frequency of communication signals.

Electrocytes are highly polarized cells approximately 1.5 mm in length and 600 µm in diameter. APs are initiated with the activation of cholinergic receptors and Na_v channels on the innervated posterior membrane to allow the influx of Na^+ (Fig. 1). Electrocytes in *E.virescens* terminate APs with K_{Na} channels rather than the voltage-gated K^+ (K_v) channels that are predominantly expressed in the electrocytes of closely related species (Few and Zakon, 2007; Markham et al., 2013). Numerous studies have suggested that the density and kinetic properties of potassium channels in the plasma membrane are key determinants of an excitable cell's functional capacity (Bean, 2007; Coetzee et al., 1999; Erisir et al., 1999; Few and Zakon, 2007; Kaczmarek et al., 2005; Shao et al., 1999). Therefore, we cloned the cDNAs encoding the K_{Na} channels in *E. virescens* EOs and identified three different types of K_{Na} channel subunits expressed in electrocytes. Two of these channels, eslack1 and eslack2, closely resemble K_{Na} channels encoded by the slack gene in mammalian systems, and the third channel, eslick, shares the highest homology to the slick channel in rat. By expressing fluorescent protein-tagged K_{Na} channel subunits in electrocytes, we showed all three types of K_{Na} channels are expressed on the anterior side of cells, separated by >1 mm from the Na_v channels which are restricted to the posterior membrane. We also examined the functional differences among the three K_{Na} channels by expressing them in *X. laevis* oocytes. Recordings of whole-cell currents showed that eslick currents are activated more rapidly than eslack1 currents. To explore which conductances play key roles in

determining the firing frequency of electrocytes, we used qRT-PCR to measure the mRNA levels of genes encoding ion channels and Na^+/K^+ ATPases in EO from fish with different EODf. The transcription levels of eslick, $Na_v1.4a$, $K_{ir}6.2$ and Na^+/K^+ ATPase increased with EODf, while transcription levels of eslack1, eslack2, $Na_v1.4b$ did not correlate with EODf.

MATERIALS AND METHODS

Animals and tissue harvesting

E. virescens (glass knifefish) were obtained from tropical fish importers (Gunpowder Aquatics, Wimauma, FL), and housed in tanks in a recirculating aquarium system at 28 ± 1°C with water conductivity 100-150 µS/cm. They were kept under 12 hour light: 12 hour dark cycle and fed *ad libitum* with live blackworms. The EO tissue was harvested by cutting off ~2 cm section of the tail and removing the overlying skin. Skeletal muscle tissue was dissected from the hypaxial muscle after fish were euthanized by immersion in 2% eugenol solution in aquarium water.

All methods described were approved by the Institutional Animal Care and Use Committee of The University of Oklahoma and complied with the guidelines given in the Public Health Service Guide for the Care and Use of Laboratory Animals.

EOD frequency measurements

Fish were transferred to the EOD recording tank with two recording wires attached to the two opposite end walls and a ground wire located at one of the side walls. They were allowed to move freely while EODs were differentially amplified with a Cygnus FLA-01 amplifier (Delaware Water Gap, PA) and EODf of the amplified signal was measured with a RadioShack digital multimeter set in frequency mode. To

prevent effects of temperature and water conductivity on the fish's EOD frequency, the recording tank was placed in the aquarium room and filled with water from the same aquarium system where the fish was kept. Representative EOD waveforms recorded from two fish are shown in Fig.1E.

Molecular Biology

Reagents

The pSP64 Poly(A) vector, ImProm-II™ Reverse Transcription System and GoTaq® DNA polymerase were purchased from Promega (Madison, WI). The RNA Clean & Concentrator™-5 was purchased from Zymo Research (Irvine, CA). The SMARTer® RACE 5'/3' Kit was purchased from Clontech Laboratories, Inc. (Mountain View, CA). All other molecular biology reagents were purchased from Thermo Fisher Scientific (Waltham, MA).

RNA and cDNA preparation

Tissues were homogenized using LabGEN 125 homogenizer (Cole-Parmer). Total RNA was extracted using TRIzol® reagent and purified using RNA Clean & Concentrator™-5. Genomic DNA contamination was removed by incubating the total RNA with DNaseI at room temperature for at least 15 minutes. RNA quality was assessed by loading and running total RNA in a 1% agarose gel containing 0.5% bleach and SYBR® Green II RNA Gel Stain (Aranda et al., 2012). One microgram of EO total RNA was reverse transcribed to cDNA with oligo$(dT)_{15}$ primer using ImProm-II™ Reverse Transcription System. The concentration of RNA and cDNA was measured by Qubit fluorometer 2.0 (Thermo Fisher Scientific).

Cloning and sequencing of genes encoding *E. virescens* K_{Na} channels

cDNAs of interest were amplified by polymerase chain reaction (PCR) and 5'/3' rapid amplification of cDNA ends (RACE). All PCR and RACE products were initially analyzed on 1% agarose gels stained with SYBR® Safe DNA Gel Stain, purified and cloned into TOPO TA vector or pRACE vector. In each cloning, plasmids extracted from ten isolated individual colonies were sequenced by the Biology Core Molecular Lab at University of Oklahoma. Sequence results were used as a query to search the rat protein database using the online NCBI blastx tool to determine the molecular identity of amplified products (Altschul et al., 1990).

eSlack1

A ~500-bp fragment of eslack1 was amplified by nested PCRs using Platinum® Taq High Fidelity DNA Polymerase with two pairs of degenerate primers designed against the highly conserved regions of published nucleotide sequences of *slack* in other species (external primer pair: forward 5'-ARAGYTTYACCTWYGCYKCCTTY-3' and reverse 5'- RYYTTYTSNBGYARMAGRTGGCA-3'; internal primer pair: forward 5'-AYAARAARTAYGGWGTRTGTHTG-3' and reverse 5'- GGMGAGCTSCCRATRTABGGMGA-3'). The thermocycler conditions were 94°C for 2 min, 30 cycles of 94°C for 30 s 55°C for 30 s and 68°C for 3 min, followed by a final extension step of 68°C for 10 min. The missing 5'end of eslack1 cDNA was amplified by the following reactions: 1) A ~1-kb fragment was amplified by a 5'RACE reaction with a slack degenerate primer (5'-GGMGAGCTSCCRATRTABGGMGA-3') and an universal primer provided by the SMARTer® RACE 5'/3' Kit. 2) A ~500-bp fragment was amplified in a PCR with a forward degenerate primer (5'- GCCWTCBCAGCTSCTGGTGGT -3') targeting the signature sequence of the K^+ selectivity filter and an eslack1-specific

reverse primer (5'-GCAAAGTCCTTCACCGCCCA-3') designed from the partial cDNA fragment. 3) A 5'RACE PCR was carried out with an eslack1 reverse primer (5'-TCACCTGACTGTCTGCCTCACATGGAC -3') and the universal primer to amplify the start codon as well as the 5'untranslated region (UTR). The missing 3'end of eslack1 including the stop codon and 3'UTR was amplified by a 3'RACE reaction with an eslack1 forward primer (5'- CTACCCGTCCACAGCATCATCACTAGC-3') and the universal primer. Sequences of the five eslack1 fragments were aligned into a single contig (Geneious software, Biomatters Ltd, Auckland NZ). The full-length cDNA of eslack1 was amplified with a forward primer (5'- ATATATAAGCTTTCTTTATTACC GAAGGTGTCCCTCCG-3') derived from the 5'UTR and a reverse primer (5'-TATATATCTAGAGTTTCGGTTGATCAGGTCAGTTTAAAC-3') derived from the 3'UTR. It was cut at the HindIII and XbaI sites introduced in the primers and cloned into pSP64 Poly(A) vector. Sequence of the insertion was confirmed to match the five overlapping PCR products. eSlack1 cDNA contains 3495 nucleotides.

eSlack2

The presence of eSlack2 was noted when sequencing the TOPO TA vectors inserted with the ~500-bp PCR product amplified with a forward degenerate primer targeting the K^+ selectivity filter signature sequence and a reverse eslack1-specific primer. Insert sequences from ten plasmids were aligned and assembled into two contigs using the Geneious software. The two contigs share 78.8% homology in nucleotide sequence, with residue differences dispersed along the entire region, and both of them share the highest homology with rat slack (NCBI BLAST). We next performed 5' and 3' RACE reactions to amplify the missing 5' and 3' ends. A ~1.5-kb

product was amplified in the 5'RACE reaction with a gene-specific reverse primer (5'-GAGCTGACGCAGAGCACCACGTGTTT-3'), and a ~5 kb product was amplified in the 3'RACE reaction with a gene-specific forward primer (5'- GCGTACCCACTCTG CCATGTTCAACC-3'). Sequences of the three PCR products were aligned to a single contig using Geneious. Full-length eslack2 cDNA was amplified with a forward primer (5'-ATATATGTCGACCTTCTTTACAATGATGGGAC-3') targeting the 5'UTR and a reverse primer (5'-TATATAGGATCCCATTGGACAGTATGAATGAC-3') targeting the 3'UTR. It was cut at the SalI and BamHI sites introduced to the primers and cloned into pSP64 Poly(A) vector. Sequence of the insert corresponded to the consensus sequence of the aligned contig. eslack2 is composed of 3093 nucleotides.

eSlick

When amplifying the 3'end of eslack2 with an eslack2-specific forward primer (5'- TCTGGTGGTGGTGGACAAGGAGAGC-3') and the universal primer, we detected a ~2.5-kb fragment. The RACE PCR product was cloned and sequenced as described. The nucleotide sequence was then blasted against the rat protein database in NCBI, and shown to share the highest homology with rat slick but not slack. Then a 5'RACE PCR was performed to amplify the missing 5'end of the slick transcript using a gene-specific reverse primer (5'- ACGTCCTTATCCACAGATCCTCCTCGG-3'). A ~4-kb DNA fragment was amplified, cloned and sequenced. Sequences of the two DNA fragments were aligned to a single contig containing potential start codon at the 5' region and stop codon at the 3' end. Full-length eslick cDNA was amplified with a forward primer (5'- ATATATGTCGACTTTAGAGGAACGCATACTTAGC-3') designed against the 5'UTR and a reverse primer (5'- TATATAGGATCCTAAGT

AGTCAGATCAGTAGGGC-3') designed against the 3'UTR. It was cut at the SalI and BamHI sites introduced in the primers and cloned into pSP64 Poly(A) vector. eslick cDNA contains 3510 nucleotides.

Reverse transcription PCR analysis of gene expression in EO and muscle

To identify the expression patterns of target genes in EO and muscle, Reverse Transcription PCR was performed using GoTaq® DNA polymerase with one microliter EO or muscle cDNA. Genes of interest and their specific primers are listed in Table 1. Thermocycling conditions included 95°C for 2 min, 35 cycles of 95°C for 30 s, 55°C for 30 s, and 72°C for 1 min or 2 min (depending on the size of amplicons), and a final extension at 72°C for 5 min. After gel electrophoresis, PCR products were visualized using the Safe Imager™ 2.0 (Thermo Fisher Scientific). Gel images were taken with the same exposure time.

Real-time PCR for mRNA quantitation in EO

One microgram of total RNA extracted from EOs from 11 adult *E. virescens* with EOD frequencies (192Hz, 202Hz, 206Hz, 229Hz, 250Hz, 300Hz, 333Hz, 350Hz, 380Hz, 395Hz, 426Hz) spanning the species' natural range was reverse transcribed to cDNA with oligo$(dT)_{15}$ primer using ImProm-II™ Reverse Transcription System. cDNA was diluted to 20 ng/µl. Gene-specific primers were designed using the GenScript online software to constrain the primer length to ~20 bases, melting temperature (Tm) to the range of 58-60°C, and amplicon size to ~100 bp (Table 2). Each reaction contained 100 ng cDNA, 25 ul 2× Power SYBR® Green Master Mix, 200 nM of forward and reverse primer, and nuclease-free H_2O to reach a total volume of 50 µl. Experiments were run in an Applied Biosystems 7500 Real-time PCR system using

the default run method for Power SYBR® Green cDNA two step kit: hold at 95°C for 10 min and 40 cycles amplification (denature at 95°C for 15 s, and anneal/extend at 60°C for 1 min). Each sample had three technical replicates. The specificity of primers was assessed by both melt curve analysis and gel electrophoresis of qPCR product. The expression level of all target genes was normalized to the endogenous control β-actin. EO cDNA from fish with the lowest EOD frequency (192 Hz) was used as the calibrator sample. Reactions without cDNA template were performed as negative controls. All negative controls showed no amplification or amplification starting more than eight cycles later than the reactions with cDNA template. In each experimental run, the standard curve was generated using 500, 100, 20, 4, 0.8 ng EO cDNA from a fish with 202 Hz EOD frequency. All target genes and β-actin had standard curves with R^2>0.97. The slopes of standard curves were used to estimate the amplification efficiencies, which were in the range between 95% and 105%. Data were analyzed using Applied Biosystems 7500/7500 Fast software. Standard deviations were calculated by following the Applied Biosystems guide to perform relative quantification of gene expression using the relative standard curve method.

Gene phylogeny analysis

E. virescens slack1, *slack2*, and *slick* cDNA sequences were translated and aligned with protein sequences of the SLO family channels in nematode, zebrafish, mouse, rat and human using ClustalW. Then the phylogenetic relationship was analyzed using the Geneious software (version 7.1.7). The consensus tree was obtained by using the neighbor-joining method, Jukes Cantor amino acid substitution model and resampled 1000 times with the Bootstrapping method. Human voltage-gated K^+ channel

subfamily A member 1 ($hK_v1.1$) was included as the outgroup. Channels included in the phylogenetic analysis were *Caenorhabditis elegans* Slo1channel (NCBI accession number: Q95V25); *Danio rerio* Slo1 channel (NP_001139072); *Mus musculus* Slo1 channel (NP_001240287); *Rattus norvegicus* Slo1 channel (NP_114016); *Homo sapiens* Slo1 channel (AAI44497); *Caenorhabditis elegans* Slo2 channel (AAD51350); *Danio rerio* Slack channel (XP_009293403); *Danio rerio* Slick channel (XP_017214614); *Mus musculus* Slack channel (NP_780671); *Mus musculus* Slick channel (NP_001074496); *Rattus norvegicus* Slack channel (NP_068625); *Rattus norvegicus* Slick channel (NP_942057); *Homo sapiens* Slack channel (NP_065873); *Homo sapiens* Slick channel (NP_940905); *Mus musculus* Slo3 channel (O54982); *Homo sapiens* Slo3 channel (NP_001027006); *Homo sapiens* $K_v1.1$ channel (NP_000208).

Expression of recombinant K_{Na} channels in electrocytes

We constructed recombinant eSlack1, eSlack2 and eSlick channels tagged with the red fluorescent protein (mCherry) at their N-terminus. mCherry was PCR-amplified from u-mCherry (a gift from Scott Gradia; Addgene plasmid # 29769). The polylinker sequences between ion channels and mCherry were GGSGGGSGGSGS for eSlack1/ eSlick and GGSGGGSG for eSlack2 (Perestenko and Henley, 2006; Shi et al., 1999). mCherry-eSlack1, mCherry-eSlack2 and mCherry-eSlick were assembled and cloned into the pOX vector using the NEBuilder® HiFi DNA Assembly Master Mix (New England Biolabs® Inc.) then subcloned into the pmaxCloning™ vector (Lonza). Prior to EO injection, the fish were anesthetized by exposing them to 0.01% clove oil until losing equilibrium but still maintaining opercular beating (< 2 min total). A single 25 µl bolus of 5 µg/µl plasmid in 150 mM KCl was injected into the fish's EO in the tail

using a microliter syringe. The injected fish was then transferred back to its home tank until its mobility was fully recovered. The expression of mCherry-tagged ion channels was examined on the 10^{th} day after injection using epifluorescence and confocal microscopy.

Image acquisition

To examine the expression of mCherry-eSlack1, mcherry-eSlack2 and mCherry-eSlick in electrocytes, we harvested the EO using the same procedure as described earlier (Ban et al., 2015). Live electrocytes were first examined on a Zeiss Apotome.2 microscope with a X5/0.16NA dry objective and processed by Zeiss AxioVision Rel.4.8.2. Structured illumination was used to create optical sections of the sample. Then we used a LeicaTCS SP8 laser scanning confocal microscope with a X25/0.95NA dipping objective to acquire high-resolution images. mCherry was excited by a 561-nm laser line and autofluorescence of the electrocyte was excited by a 488-nm laser line (Ban et al., 2015). The images were acquired as serial sections and processed by the software Leica Application Suite Advanced Fluorescence (LAS AF) 3.3.0.10134. Electrocytes not expressing mcherry-tagged eSlack/Slick subunits were used as controls and imaged under the same settings.

Xenopus laevis oocytes expressing mCherry-tagged K_{Na} channels were incubated in ND96 saline and imaged using a LeicaTCS SP8 laser scanning confocal microscope with a X10/ 0.3NA dry objective. Brightness and contrast of all images were adjusted using ImageJ for 64-bit Windows (version 1.51s; National Institute of Health).

Electrophysiology

eSlack/Slick cDNA was subcloned into pOX vector (a generous gift of Dr. Lawrence B. Salkoff, Washington University, St. Louis, USA). In vitro transcribed RNA (cRNA) was prepared using the mMESSAGE mMACHINE^{TM} T3 Transcription Kit (Thermo Fisher Scientific). We used an Agilent 2100 Bioanalyzer to examine the quality and concentration of cRNA. Defolliculated *X. laevis* oocytes in stage VI were obtained from Ecocyte Bioscience (Austin, TX) and incubated in modified Barth's saline containing the following in mM: 88 NaCl, 1 KCl, 2.4 $NaHCO_3$, 0.82 $MgSO_4$, 0.33 $Ca(NO3)_2 \cdot 4H_2O$, 0.41 $CaCl_2 \cdot 2H_2O$, 5 HEPES, 2.5 CH3COCOONa, and 50 μg/ml gentamycin at pH 7.5. Oocytes were injected with 46 nl of nuclease-free water containing ~80 ng of cRNA and studied 4 to 5 days post injection.

Whole-cell currents from oocytes were recorded using a standard two-electrode configuration (Markham et al., 2013), with an Axoclamp 900 amplifier controlled by a Digidata 1440 interface and pCLAMP10 software (Molecular Devices, Sunnyvale, CA). Data were sampled at 100 kHz and filtered at 10 kHz. Electrodes were pulled from 1.2 mm o.d. thin-wall borosilicate glass tubing, filled with 2 M NaCl or KCl and had resistances of 0.5-1.2 MΩ. Oocytes were incubated in ND96 saline (in mM: 96 NaCl, 2 KCl, 1 $MgCl_2$, 1.8 $CaCl_2 \cdot 2H_2O$ and 5 HEPES, pH to 7.5). To measure channel activation, oocytes were held at -90 mV, then depolarized by 400-ms voltage steps ranging from -90 mV to +80 mV in 10-mV increments every 5 s. In some experiments, cells were depolarized by a 500-ms pulse to +20 mV from a holding potential of -90 mV every 10 s to examine the effects of NaCl and KCl on the amplitude of whole-cell currents. The activation τ for eSlack and eSlick currents was estimated using the

Clampfit fitting functions. Current traces from the start point to the peak point just before the plateau stage were fitted to a standard single-term exponential growth function. The time required to reach 62.8% of the final value was calculated as the activation τ.

RESULTS

Molecular identities of K_{Na} channels in *E. virescens* electrocytes

Mammalian K_{Na} channels are encoded by two highly similar paralogous genes, *Slo2.1* (*Slick*, *kcnt2*) and *Slo2.2* (*Slack*, *kcnt1*) belonging to the *Slo* gene family (Bhattacharjee et al., 2003; Joiner et al., 1998). In *E. virescens* EOs, we cloned three genes similar to the mammalian *Slo2* genes. Phylogenetic analysis (Fig. 2A) of channels in the SLO family show that two genes have the strongest homology with mammalian *slack* genes, and the third gene is more closely related to *slick* genes. The open reading frames (ORFs) of the two *E. virescens slack* genes encode two proteins that consist of 1164 and 1030 amino acids with 68.6% homology. Amino acid differences between the two *slack* transcripts were dispersed along the entire sequence, suggesting they are not likely generated by RNA alternative splicing. Given the evidence that duplication of voltage-gated sodium and potassium channel genes has occurred in multiple gymnotiform species (Few and Zakon, 2007; Zakon et al., 2006), gene duplication is more likely the mechanism giving rise to the two slack transcript variants in *E. virescens*. We designated the duplicated *slack* genes in *E. virescens* as e*slack1* (ORF: 3495 nt) and e*slack2* (ORF: 3093 nt), respectively.

Electric organs (EOs) are developmentally derived from muscle (Bennett, 1970). With the development and maturation of EOs, electrocytes eliminate the coupling

between contraction and excitability (Gallant et al., 2014; Unguez and Zakon, 1998). Due to the myogenic origin of EO tissue, we examined the expression pattern of eSlack1, eSlack2, and eSlick in *E. virescens* muscle and EO by reverse transcription PCR and found that eSlack1 and eSlack 2 are expressed in both EO and muscle, whereas Slick is expressed solely in the EO (Fig. 2B).

Sequence and Structure of *E. virescens* K_{Na} Channels

The *E. virescens* 1164 amino acid-long eSlack1 and 1030 amino acid-long eSlack2 channel subunits share 74.3% and 70.8% homology to rat Slack-A, respectively (Brown et al., 2008). Both eSlack1 and eSlack2 subunits are predicted to contain six membrane-spanning domains (S1-S6) with a pore-forming loop between S5 and S6, and an extensive cytoplasmic C-terminal region (Fig. 3) (Hite et al., 2015; Hofmann and Stoffel, 1993; Joiner et al., 1998; Krogh et al., 2001). Slack channels are activated by intracellular Na^+ ions, and the sensitivity of these channels to Na^+ is determined by the presence of a Na^+ coordination motif in the second RCK domain. This motif contains six amino acids in rat Slack subunits (DNKPDH), with aspartic acid (D) and histidine (H) in the beginning and ending positions, respectively (Zhang et al., 2010). In the homologous position, *E. virescens* Slack-1 and Slack-2 subunits have the sequence DNQPDDH and DNPPDNH, respectively, making them putative Na^+-binding sites (Fig. 3A). There is great divergence between *E. virescens* Slack-1 and Slack-2 in the N- and C- terminus. eSlack2 appears to have a C-terminal tail approximately 100 amino acids shorter than eSlack1 and all other identified Slack and Slick subunits in mammals (Fig. 2A). The N-terminus is where amino acid differences are most frequently found between eSlack1 and eSlack2. The N-terminus of eSlack2 is highly similar to that of

mouse and rat Slack-A. In mammals, RNA alternative splicing gives rise to three Slack transcripts, Slack-A, Slack-B and Slack-M, which are regulated by alternative promoters and differ in the residues in the N-terminus (Brown et al., 2008). eSlack1 has a unique N-terminus which is not identical to any known mammalian Slack isoforms (Fig. 3).

The ORF of *E. virescens* Slick encodes a protein composed of 1142 amino acids, sharing 66.6% homology with rat Slick subunits. It has an N-terminus closely resembling that of eSlack2 and rat Slick, six membrane-spanning domains (S1-S6) with a pore-forming loop between S5 and S6, and an extensive C-terminal region (Fig. 3). At the homologous position of the Na^+ coordination motif of rat Slick subunit (DNPPDMH) (Thomson et al., 2015), *E. virescens* Slick has the sequence DNPPEPQ, which shares four of seven residues with rat Slick, and does not end with histidine. Histidine may be not necessary for binding Na^+, consistent with the finding in rat Slick that mutation of the aspartic acid residue dramatically decreased the channel's sensitivity to Na^+, whereas histidine substitution barely changed the channel's function (Thomson et al., 2015). Rat and human Slick channels are ATP-regulated channels, and can be directly inhibited by intracellular ATP. The molecular determinant of ATP sensitivity is the presence of the "Walker A motif" (GxxxxGKT) on the distal C-terminus of Slick subunits (Bhattacharjee et al., 2003; Walker et al., 1982). The residues at the homologous position of the Walker A motif in rat Slick are not very conservative between rat and *E. virescens* Slick. And we could not find a motif having the signature residues of Walker A motif in the C-terminus of *E. virescens* Slick subunits. Whether *E.*

virescens Slick channels are regulated by intracellular ATP levels needs to be determined by future electrophysiology studies.

Expression pattern of K_{Na} channels in electrocytes

The subcellular localization of ion channels plays a key role in determining the bioelectrical properties of excitable cells, especially for electrocytes, which have been shown to be highly polarized, with quite different posterior and anterior membranes. Our previous immunohistochemical studies revealed that K_{Na} channels are located on the anterior side, separated by >1 mm from cholinergic receptors and Na^+ channels that are restricted to the posterior membrane (Ban et al., 2015). Protein sequence alignment between peptide immunogen and the three *E. virescens* K_{Na} subunits showed that the K_{Na} channel antibody used in that study only targeted the eSlack1 subunit. Due to the lack of specific commercially-available antibodies and the failure of multiple custom-generated antibodies to produce specific labeling, we took the approach of visualizing the location of eSlack2 and eSlick subunits by expressing fluorescent protein-tagged constructs of these ion channel subunits in electrocytes. It has been shown that direct injection of naked DNA plasmids produces expression of transgene in fish muscle (Sudha et al., 2001). Electrocytes of *E. virescens* can reliably express fluorescent protein tagged actin following bulk injection of expression vectors into the EO (Michael Markham and Harold Zakon: unpublished observations). Because electrocytes exhibit autofluorescence with excitation and emission spectra similar to those of green fluorescent protein (GFP), red fluorescent protein (mCherry) was used to construct the recombinant ion channels.

mCherry was fused to the N-terminus of eSlack/Slick subunits and separated by a flexible polylinker containing a glycine polypeptide with serine inserts to allow the proper folding and function of both molecules (Nuwer et al., 2010; Perestenko and Henley, 2006; Shi et al., 1999). Fluorescent protein fusion proteins can potentially affect the normal localization of the target protein. To ensure N-terminal mCherry fusion does not affect the trafficking of eSlack/Slick subunits to the plasma membrane, we examined the expression of these recombinant ion channels in *Xenopus laevis* oocytes and showed that all of them could be successfully expressed on cell membranes (Fig. 4). Next, we injected mCherry-eSlack/Slick expression vectors into the EO and found that mCherry-eSlack1 was localized on the anterior side, mimicking the distribution of endogenous eSlack1 detected by immunohistochemistry (Ban et al. 2015) (Fig. 5B), suggesting that N-terminal mCherry fusion does not affect the normal localization of eSlack/Slick subunits. Similar to mcherry-eSlack1, the expression of mCherry-eSlack2 and mCherry-eSlick was only detected on the anterior side (Fig. 5C and D). Our results indicate that the three *E. virescens* K_{Na} channel subunits have identical expression patterns, only on the anterior side of electrocytes.

Characteristics of K_{Na} channel currents

Markham et al. recorded whole-cell currents from *E. virescens* electrocytes and demonstrated the existence of the outward noninactivating Na^+-activated K^+ currents (I_{KNa}) (Markham et al., 2013). To determine how the three K_{Na} channels identified here contribute to outward K^+ currents, we expressed the three K_{Na} channels in *X. laevis* oocytes to characterize and compare their electrophysiological properties. Both eSlack1 and eSlick constructs produced robust outward K^+ currents with strong outward

rectification. Whole-cell currents from cells injected with eSlack1 cRNA showed much slower activation than those injected with eSlick cRNA (Fig. 6A). At test potentials positive to -40 mV, eSlack1 activated with a slow component that increased with time (Fig. 6A and B). The τ-V relationship for the rate of eSlack1 activation shows that eSlack1 currents activated slower as membrane potential becomes more depolarized until +10 mV, after which activation becomes more rapid with more depolarized membrane potentials (Fig. 6C). In contrast, eSlick shows rapid activation. Whole-cell currents in eSlick- injected oocytes activated instantaneously with step changes in voltage to test potentials positive to -70mV (Fig. 6A and B). According to the τ-V relationship of eSlick activation, the τ decreases with more depolarized membrane potentials until +20 mV, when it reached a plateau (Fig. 6D). We used water-injected oocytes as controls. As reported previously, control cells express an endogenous Ca^{+}-activated Cl^{-} current, the magnitude of which is much smaller than in cells expressing exogenous currents (Fig. 6A) (Cristofori-Armstrong et al., 2015). Unlike eSlack1 and eSlick, oocytes injected with eSlack2 cRNA expressed currents indistinguishable from those of control cells (Fig. 6A). The C-terminal tail of eSlack2 is approximately 100 amino acids shorter than eSlack1 and eSlick. Since mCherry-eSlack2 can be expressed on the plasma membrane of both *X. laevis* oocytes and electrocytes, the absence of currents is not likely due to the difficulty of trafficking eSlack2 into the plasma membrane. A likely possibility is that eSlack2 cannot form functional homotetrameric channels without the intact C-terminus.

The activity of mammalian slack and slick channels is regulated by the intracellular levels of Na^{+} and Cl^{-}. We therefore examined the effects of elevated $[Na^{+}]_i$

on the activity of eSlack1 and eSlick channels. Thomson et al. showed that filling low-resistance microelectrodes with 2 M NaCl allows Na^+ to diffuse into the cell and thereby increases $[Na^+]_i$ (Garg et al., 2013; Thomson et al., 2015). We applied the same method to increase $[Na^+]_i$ and measured the amplitude of currents when the cell was depolarized to +20 mV repetitively from -90 mV every 10 s. The peak amplitude of eSlack1 and eSlick currents immediately after impaling the cell was higher than that of control cells, suggesting that eSlack1 and eSlick have basal levels of activity at intraoocyte Na^+ concentrations of ~10 mM (Weber, 1999) (Fig. 7A). During 9 min of recording, the peak amplitude of both eSlack1 and eSlick at a membrane potential of +20 mV was elevated with NaCl diffusing into the cell (Fig. 7A and C). To distinguish the role of Na^+ and Cl^- in increasing current amplitude, we also used microelectrodes filled with 2 M KCl and measured the peak amplitude of both eSlack1 and eSlick over 9 min. The eSlack1current remained constant with an increased intracellular level of KCl. In contrast, eSlick showed increased current magnitudes with KCl-filled electrodes (Fig. 7B and C). The peak current of control cells at +20 mV kept constant during 9-min loading of either 2 M NaCl or 2 M KCl (Fig. 7). These results suggest that eSlack1 has an absolute requirement for Na^+ to increase the channel's open probability, whereas eSlick may be more sensitive to intracellular Cl^- levels. The other possible reason for the increase of eSlick current with KCl diffusing into the cell is that a dramatic increase in the intracellular concentration of K^+ shifted the equilibrium potential for K^+ more negative. Future studies should use inside-out patch clamp to examine the K_{Na} channel's dependence on Na^+ and Cl^-.

Positive correlation between EODf and the transcription level of eSlick in the EO

E. virescens has considerable animal-to-animal variability in EOD frequency (200-500 Hz) (Fig. 1E) (Scheich, 1977). Previous studies in a closely related species, *Steropygus macrurus*, have shown that the transcription levels of potassium channels in the EO are correlated with EODf (Few and Zakon, 2007). This led us to examine whether the mRNA levels of e*slack1*, e*slack2* and e*slick* genes in the EO vary across fish with different EOD frequencies. We extracted RNA from the EO of 10 fish with different EOD frequencies (192 Hz, 202 Hz, 206 Hz, 229 Hz, 250 Hz, 300 Hz, 333 Hz, 350 Hz, 380 Hz, 395 Hz, 426 Hz) spanning the species' natural range, and measured the transcription levels of the three K_{Na} channel genes with real-time PCR. We found that only the transcription level of eslick was positively correlated with EOD frequency (Fig. 8A and supplementary Fig. 1A-C)). We also divided the fish into two groups with high (> 300 Hz; n=5) and low (≤ 300 Hz; n=5) EOD frequencies, and compared the mean transcription level of the three K_{Na} channel genes between the two groups. A significant difference between fish with high and low EOD frequencies was found in the transcription level of eslick (high frequency: 3.52 ± 0.58, n = 5; low frequency: 1.94 ± 0.28, n = 5; one-way ANOVA, p = 0.04), but not eslack1 (high frequency: 1.51 ± 0.40, n = 5; low frequency: 0.96 ± 0.23, n = 5; one-way ANOVA, p = 0.26) or eslack2 (high frequency: 2.31 ± 0.31, n = 5; low frequency: 1.83 ± 0.95, n = 5; one-way ANOVA, p = 0.65) (Fig. 8C).

Transcription levels of $Na_v1.4a$, $K_{ir}6.2$ and Na^+/K^+ ATPase increase with EODf

In addition to the Na^+-activated K^+ current observed in electrocytes, whole-cell recordings of endogenous currents in electrocytes also indicated the existence of an

inwardly rectifying K^+ (K_{ir}) current and a voltage-gated Na^+ (Na_v) current (Markham et al., 2013). The firing frequency of electrocytes is maintained by the coordination between ion channels involved in generating APs and the Na^+/K^+ ATPases, which are responsible for restoring the ionic gradients after each AP. The Na_v channels in the EO of *E. virescens* are encoded by a pair of duplicated genes, $Na_v1.4a$ and $Na_v1.4b$, which are orthologs of the mammalian muscle-specific $Na_v1.4$ gene (Zakon et al., 2006). The Kir channels are ATP-sensitive potassium (K_{ATP}) channels encoded by the KCNJ11 gene (Michael Markham: unpublished data). In reverse transcription PCR, we noted that Nav1.4b and Kir6.2 are expressed in both muscle and EO, whereas $Na_v1.4a$ and the α-subunit of Na^+/K^+ ATPases are predominantly expressed in the EO (data not shown). We reasoned that EOD frequency might also be correlated with expression levels of these ion channels and Na^+/K^+ ATPases.

With real-time PCR, we measured the mRNA levels of these genes from the EO of 10 fishes that were mentioned earlier. Results showed that the transcription levels of $Na_v1.4a$, $K_{ir}6.2$ and Na^+/K^+ ATPase increased exponentially with EOD frequency (Fig. 8B1, B3 and B4, and supplementary Fig. 1D, F and G). No correlation between the transcription level of $Na_v1.4b$ and EOD frequency was detected (Fig. 8B2 and supplementary Fig. 1E). When comparing the mean transcription level of genes between the two groups of fish with high and low EOD frequencies, significant differences were detected in $Na_v1.4a$ (high frequency: 3.89 ± 0.72, $n = 5$; low frequency: 1.38 ± 0.17, $n = 5$; one-way ANOVA, $p < 0.01$), $K_{ir}6.2$ (high frequency: 3.18 ± 0.55, $n = 5$; low frequency: 1.16 ± 0.13, $n = 5$; one-way ANOVA, $p < 0.01$) and Na^+/K^+ ATPase (high frequency: 6.84 ± 1.28, $n = 3$; low frequency: 1.57 ± 0.61, $n = 5$;

one-way ANOVA, $p < 0.01$), but not $Na_v1.4b$ (high frequency: 1.28 ± 0.19, $n = 5$; low frequency: 1.32 ± 0.19, $n = 5$; one-way ANOVA, $p = 0.89$) (Fig. 8C).

DISCUSSION

E. virescens electrocytes are unique because they terminate their APs using K_{Na} channels rather than voltage-gated K^+ (K_v) channels, as is the case in all other electric fish where electrophysiological data are available (Few and Zakon, 2007; Markham et al., 2013). In this study, we discovered the presence of three K_{Na} channel subunits expressed in electrocytes, eSlack1, eSlack2 and eSlick. Functional potassium channels are tetramers of four subunits, and channels can consist of homotetramers or heterotetramers. All three K_{Na} channels in *E. virescens* elecrocytes are expressed on the anterior side, raising the possibility that they form heterotetrameric K_{Na} channels.

Heterotetrameric K^+ channels have functional properties that are typically intermediate between the properties of homomeric channels for each subunit. In the present study, eslick currents were much faster than eslack currents and therefore better suited for higher frequency electrocytes. The positive correlation of eslick expression with EODf suggests two possibilities. One is that the ratio of eslick homotetrameric channels to eslack1 homotetrameric channels increases as EODf increases. A second possibility is that the ratio of eslick to eslack1subunits within heterotetramers increases with EOD frequency. Additionally, the failure of eslack2 expressed alone to produce functional KNa channels strongly suggests that this subunit occurs only within heterotetramers.

In mammalian systems, RNA alternative splicing gives rise to multiple Slack variant transcripts, Slack-A, Slack-B and Slack-M, which are regulated by alternative

promoters and differ in the residues in their N-terminus (Brown et al., 2008). The N-terminus of Slack-B is necessary for the trafficking of Slick subunits into the plasma membrane and they can form heterotetrameric K_{Na} channels (Chen et al., 2009). eSlack2 and eSlick share similar N-terminal sequences with rat Slack-A and Slick. eSlack1 has a unique N-terminus, which is not identical to the N-terminus of any known mammalian Slack and Slick subunit. Heterogeneous expression of *E. virescens* K_{Na} channels in *X. laevis* oocytes showed that eSlack1 and eSlick can form functional homotetrameric K_{Na} channels and, although eSlack2 can be successfully trafficked into the plasma membrane, it could not conduct currents, which is likely due to the shorter C-terminal tail. Future biochemical studies with immunoprecipitation are necessary to examine the interactions among the three *E. virescens* K_{Na} channel subunits and the possibility that they form heterotetrameric ion channels.

Similar to mammalian K_{Na} channels, the opening of eSlack1 channels requires $[Na^+]_i$, whereas eSlick channels' opening appears to be more dependent on intracellular levels of Cl^-. These characteristics offer K_{Na} channels several advantages over K_v channels in cells with high firing rates. The accumulation of intracellular Na^+ with high-frequency stimulation may result in the enhanced activation of K_{Na} channels which may serve as a negative feedback mechanism to stabilize the membrane potential. Additionally, K_{Na} channels may play a protective role against the inhibition of Na^+/K^+ ATPases under hypoxic conditions. The natural habitats of *E. virescens* include regions of low-oxygen waters and these fish are reported to have higher tolerance to hypoxic stress. Hypoxia-induced inhibition of Na^+/K^+ ATPases results in the increase of intracellular levels of Na^+ and Cl^-, which may activate K_{Na} channels to ameliorate the

detrimental effects caused by osmotic imbalance, thus increasing the cell's ability to react to hypoxic stress.

It was thought that *E. virescens* would reduce its EOD frequency in response to energetic constraints such as food deprivation and hypoxic stress. Surprisingly, these fish respond to metabolic stress by decreasing EOD amplitude but not frequency (Reardon et al., 2011; Sinnett and Markham, 2015). *E. virescens* modulate the amplitude of EOD by controlling the trafficking of Na_v channels on the plasma membrane of electrocytes (Markham et al., 2009). It is a challenge for electrocytes to maintain firing rate when Na^+ influx is reduced. The dependence of K_{Na} channels on $[Na^+]_i$ rather than the change of membrane potential allow electrocytes to scale the amplitude of K^+ currents to the reduced Na^+ conductance during the resting time or under energetic constraints and to mainitain the shape of AP. Our results showed that eSlack1 and eSlick channels could be activated by intraoocyte Na^+ concentration of ~10 mM (Fig. 7B). The high sensitivity of K_{Na} channels allows electrocytes to repolarize as usual when Na^+ influx is reduced, thus maintaining the cell's characteristic firing rate and enforcing the fidelity of EODf as a signal to define the individual's gender, identity and social status (Helfman et al., 2009; Hopkins, 1974).

In *E. virescens,* electrogenesis is energetically expensive, exceeding 25% of the fishes' daily energy budget (Lewis et al., 2014; Markham et al., 2016; Salazar et al., 2013). The Na^+ influx during each AP exceeds 10 μA. The number of ATP molecules required by Na^+/K^+ ATPases to restore the ionic gradients after each AP is approximately 2×10^{10}, which is about 100 times higher than that estimated for human neurons (Hallermann et al., 2012; Howarth et al., 2012a; Lewis et al., 2014).

Simultaneous APs of approximately 1000 electrocytes at several hundred Hertz creates extreme energetic demands for each electrocyte individually, and for the EO as a whole. Thus the ion channels expressed in the cells must support high-frequency firing, and more importantly adapt the cell's electrical activities to its metabolic state. The expression of ATP-sensitive K^+ (K_{ATP}) channels may enable electrocytes to couple their excitability to the availability of ATP. Rat Slick contains an ATP-binding motif in its C-terminal tail and can be directly inhibited by intracellular ATP (Bhattacharjee et al., 2003). Whether eslick is an ATP-sensitive K^+ (K_{ATP}) channel should be examined in future research. Electrocytes also express an ATP-sensitive inwardly rectifying $K_{ir}6.2$ channel that forms functional complexes with a sulphonylurea receptor (e.g., SUR1) belonging to the ATP-binding cassette (ABC) superfamily. The $K_{ir}6.2$-SUR1 complex in other systems has been shown to be inhibited by physiological levels of ATP, thereby increasing the channel's open probability as the intracellular concentration of ATP falls (Inagaki et al., 1995). The relationship between the availability of ATP and the activity of the $K_{ir}6.2$-SUR1 complex in electrocytes needs to be further studied to determine its precise role in electrocyte function. One appealing hypothesis is that the presence of these potential K_{ATP} channels may form an endogenous protective system to stabilize the cell's bioelectrical properties under energetic constraints.

In *E. virescens*, EODf is individually specific, ranging from 200 to 600 Hz. We demonstrated that in fish with higher EOD frequencies, electrocytes apparently fulfill the fast-spiking requirement by increasing the transcription level of some ion channels but not all of them. Importantly, a gene's mRNA level does not always predict its protein abundance, and we have not yet determined whether the abundance of

corresponding proteins in electrocytes also correlates with EODf due to the lack of specific antibodies targeting most of the ion channels in electrocytes. However, the same biophysical strategy to enable the fast-spiking capability seems to be adopted by electrocytes from different species of electric fish. In *Sternopygus macrucrus*, a weakly electric fish species with lower EODf (50-200 Hz), the transcription levels of two K_v channel subunits in EO vary with the fish's EODf. In *E. virescens*, we measured the mRNA level of $Na_v1.4a$, $Na_v1.4b$, eslack1, eslack2, eslick, $K_{ir}6.2$ and Na^+/K^+ ATPase in EO from fish with different EODf and found out that transcription levels of only $Na_v1.4a$, eslick, $K_{ir}6.2$ and Na^+/K^+ ATPase are positively correlated to EODf. These genes likely contribute to the increased electrical excitability of EO compared to muscle. $Na_v1.4b$, eslack1, eslack2 and $K_{ir}6.2$ showed similar transcription level in both muscle and EO, whereas $Na_v1.4a$ and Na^+/K^+ ATPase were predominantly expressed in EO and eslick was expressed exclusively in EO.

Given the faster activation kinetics for eslick compared to eslack1 and eslack2, the correlation of eslick with EODf is consistent with briefer APs required as EODf increases. Higher expression of Na^+/K^+ ATPases at higher EODfs also is easily understood for higher frequency EODs, as increased rates of AP generation will require more rapid restoration of ionic gradients following each AP. We have not yet determined the biophysical properties of $Na_v1.4a$ and $Na_v1.4b$ in this system, but it seems likely that $Na_v1.4a$ currents would have faster kinetics given the association of $Na_v1.4a$ expression levels with EODf.

Understanding the mechanisms regulating ion channel expression levels as firing rates change is important not only in the context of electric sensory and

communication signals in fish, but also for understanding how the performance of fast-spiking cells is tuned and perhaps optimized in other systems such as auditory processing networks. This is especially true because in both cases a tradeoff between firing rates and metabolic cost appears to be a major force that shapes the operational properties and functional limits of these systems (Howarth et al., 2012b). Additionally, it is well known that excitable cells modify the expression patterns of ionic conductances to maintain a particular functional state (Marder and Goaillard, 2006), but the cellular mechanisms that govern this process remain elusive. A similar question arises in the case of electrocytes as in the present study. Do electrocytes respond to a given firing rate determined by the pacemaker nucleus by some cell-autonomous mechanism that appropriately tunes the expression levels of the necessary ion channels, or does some extrinsic mechanism regulate both pacemaker firing rate and electrocyte ion channel expression? Only additional research following on the findings presented here can address these questions.

REFERENCES

Altschul, S.F., Gish, W., Miller, W., Myers, E.W., Lipman, D.J., 1990. Basic local alignment search tool. Journal of molecular biology 215, 403-410.

Aranda, P.S., LaJoie, D.M., Jorcyk, C.L., 2012. Bleach gel: a simple agarose gel for analyzing RNA quality. Electrophoresis 33, 366-369.

Ban, Y., Smith, B.E., Markham, M.R., Ban, Y., 2015. A highly-polarized excitable cell separates sodium channels from sodium-activated potassium channels by more than a millimeter. Journal of neurophysiology, jn. 00475.02014.

Bean, B.P., 2007. The action potential in mammalian central neurons. Nature Reviews Neuroscience 8, 451-465.

Bee, M.A., 2004. Within-individual variation in bullfrog vocalizations: Implications for a vocally mediated social recognition system. The Journal of the Acoustical Society of America 116, 3770-3781.

Bee, M.A., Kozich, C.E., Blackwell, K.J., Gerhardt, H.C., 2001. Individual variation in advertisement calls of territorial male green frogs, Rana clamitans: implications for individual discrimination. Ethology 107, 65-84.

Bennett, M.V., 1970. Comparative physiology: electric organs. Annual review of physiology 32, 471-528.

Bhattacharjee, A., Joiner, W.J., Wu, M., Yang, Y., Sigworth, F.J., Kaczmarek, L.K., 2003. Slick (Slo2. 1), a rapidly-gating sodium-activated potassium channel inhibited by ATP. The Journal of neuroscience 23, 11681-11691.

Brown, M.R., Kronengold, J., Gazula, V.R., Spilianakis, C.G., Flavell, R.A., Von Hehn, C.A., Bhattacharjee, A., Kaczmarek, L.K., 2008. Amino-termini isoforms of the Slack K^+ channel, regulated by alternative promoters, differentially modulate rhythmic firing and adaptation. The Journal of physiology 586, 5161-5179.

Chen, H., Kronengold, J., Yan, Y., Gazula, V.-R., Brown, M.R., Ma, L., Ferreira, G., Yang, Y., Bhattacharjee, A., Sigworth, F.J., 2009. The N-terminal domain of Slack determines the formation and trafficking of Slick/Slack heteromeric sodium-activated potassium channels. The Journal of Neuroscience 29, 5654-5665.

Coetzee, W.A., Amarillo, Y., Chiu, J., Chow, A., Lau, D., McCormack, T., Morena, H., Nadal, M.S., Ozaita, A., Pountney, D., 1999. Molecular diversity of K^+ channels. Annals of the New York Academy of Sciences 868, 233-255.

Cristofori-Armstrong, B., Soh, M.S., Talwar, S., Brown, D.L., Griffin, J.D., Dekan, Z., Stow, J.L., King, G.F., Lynch, J.W., Rash, L.D., 2015. Xenopus borealis as an alternative source of oocytes for biophysical and pharmacological studies of neuronal ion channels. Scientific reports 5, 14763.

Davidson, S.M., Wilkinson, G.S., 2002. Geographic and individual variation in vocalizations by male Saccopteryx bilineata (Chiroptera: Emballonuridae). Journal of Mammalogy 83, 526-535.

Erisir, A., Lau, D., Rudy, B., Leonard, C., 1999. Function of specific K^+ channels in sustained high-frequency firing of fast-spiking neocortical interneurons. Journal of neurophysiology 82, 2476-2489.

Few, W.P., Zakon, H.H., 2007. Sex differences in and hormonal regulation of Kv1 potassium channel gene expression in the electric organ: molecular control of a social signal. Developmental neurobiology 67, 535-549.

Fitzsimmons, L.P., Barker, N.K., Mennill, D.J., 2008. Individual variation and lek-based vocal distinctiveness in songs of the screaming piha (Lipaugus vociferans), a suboscine songbird. The Auk 125, 908-914.

Forrest, T., Eubanks, M.D., 1995. Variation in the flash pattern of the firefly, Photuris versicolor quadrifulgens (Coleoptera: Lampyridae). Journal of insect behavior 8, 33-45.

Gallant, J.R., Traeger, L.L., Volkening, J.D., Moffett, H., Chen, P.-H., Novina, C.D., Phillips, G.N., Anand, R., Wells, G.B., Pinch, M., 2014. Genomic basis for the convergent evolution of electric organs. Science 344, 1522-1525.

Garg, P., Gardner, A., Garg, V., Sanguinetti, M.C., 2013. Structural basis of ion permeation gating in Slo2. 1 K^+ channels. The Journal of general physiology 142, 523-542.

Hahn, A.H., Guillette, L.M., Hoeschele, M., Mennill, D.J., Otter, K.A., Grava, T., Ratcliffe, L.M., Sturdy, C.B., 2013. Dominance and geographic information contained within black-capped chickadee (Poecile atricapillus) song. Behaviour 150, 1601-1622.

Hallermann, S., de Kock, C.P., Stuart, G.J., Kole, M.H., 2012. State and location dependence of action potential metabolic cost in cortical pyramidal neurons. Nature neuroscience 15, 1007-1014.

Helfman, G., Collette, B.B., Facey, D.E., Bowen, B.W., 2009. The diversity of fishes: biology, evolution, and ecology. John Wiley & Sons.

Hite, R.K., Yuan, P., Li, Z., Hsuing, Y., Walz, T., MacKinnon, R., 2015. Cryo-electron microscopy structure of the Slo2. 2 Na^+-activated K^+ channel. Nature 527, 198-203.

Hofmann, K., Stoffel, W., 1993. TMbase-A database of membrane spanning protein segments.

Hopkins, C.D., 1974. Electric communication: functions in the social behavior of Eigenmannia virescens. Behaviour, 270-305.

Howarth, C., Gleeson, P., Attwell, D., 2012a. Updated energy budgets for neural computation in the neocortex and cerebellum. Journal of Cerebral Blood Flow & Metabolism 32, 1222-1232.

Howarth, C., Gleeson, P., Attwell, D., 2012b. Updated energy budgets for neural computation in the neocortex and cerebellum. J Cereb Blood Flow Metab 32, 1222-1232.

Inagaki, N., Tsuura, Y., Namba, N., Masuda, K., Gonoi, T., Horie, M., Seino, Y., Mizuta, M., Seino, S., 1995. Cloning and functional characterization of a novel ATP-sensitive potassium channel ubiquitously expressed in rat tissues, including pancreatic islets, pituitary, skeletal muscle, and heart. Journal of Biological Chemistry 270, 5691-5694.

Jiang, T., Liu, R., Metzner, W., You, Y., Li, S., Liu, S., Feng, J., 2010. Geographical and individual variation in echolocation calls of the intermediate leaf-nosed bat, Hipposideros larvatus. Ethology 116, 691-703.

Joiner, W.J., Tang, M.D., Wang, L.-Y., Dworetzky, S.I., Boissard, C.G., Gan, L., Gribkoff, V.K., Kaczmarek, L.K., 1998. Formation of intermediate-conductance calcium-activated potassium channels by interaction of Slack and Slo subunits. Nature neuroscience 1, 462-469.

Kaczmarek, L.K., Bhattacharjee, A., Desai, R., Gan, L., Song, P., von Hehn, C.A., Whim, M.D., Yang, B., 2005. Regulation of the timing of MNTB neurons by short-term and long-term modulation of potassium channels. Hearing research 206, 133-145.

Kazial, K.A., Burnett, S.C., Masters, W.M., 2001. Individual and group variation in echolocation calls of big brown bats, Eptesicus fuscus (Chiroptera: Vespertilionidae). Journal of Mammalogy 82, 339-351.

Kitchen, D.M., Seyfarth, R.M., Fischer, J., Cheney, D.L., 2003. Loud calls as indicators of dominance in male baboons (Papio cynocephalus ursinus). Behavioral ecology and sociobiology 53, 374-384.

Krogh, A., Larsson, B., Von Heijne, G., Sonnhammer, E.L., 2001. Predicting transmembrane protein topology with a hidden Markov model: application to complete genomes. Journal of molecular biology 305, 567-580.

Lewis, J.E., Gilmour, K.M., Moorhead, M.J., Perry, S.F., Markham, M.R., 2014. Action Potential Energetics at the Organismal Level Reveal a Trade-Off in Efficiency at High Firing Rates. The Journal of Neuroscience 34, 197-201.

Marder, E., Goaillard, J.-M., 2006. Variability, compensation and homeostasis in neuron and network function. Nat. Rev. Neurosci. 7, 563.

Markham, M.R., Ban, Y., McCauley, A.G., Maltby, R., 2016. Energetics of sensing and communication in electric fish: A blessing and a curse in the Anthropocene? Oxford University Press.

Markham, M.R., Kaczmarek, L.K., Zakon, H.H., 2013. A sodium-activated potassium channel supports high-frequency firing and reduces energetic costs during rapid

modulations of action potential amplitude. Journal of neurophysiology 109, 1713-1723.

Markham, M.R., McAnelly, M.L., Stoddard, P.K., Zakon, H.H., 2009. Circadian and social cues regulate ion channel trafficking. PLoS biology 7, e1000203.

Medina, I., Francis, C.D., 2012. Environmental variability and acoustic signals: a multi-level approach in songbirds. Biology Letters 8, 928-931.

Nuwer, M.O., Picchione, K.E., Bhattacharjee, A., 2010. PKA-induced internalization of slack K_{Na} channels produces dorsal root ganglion neuron hyperexcitability. The Journal of Neuroscience 30, 14165-14172.

Perestenko, P.V., Henley, J.M., 2006. 7 Visualization of AMPAR Trafficking and Surface Expression. The Dynamic Synapse: Molecular Methods in Ionotropic Receptor Biology, 119.

Reardon, E.E., Parisi, A., Krahe, R., Chapman, L.J., 2011. Energetic constraints on electric signalling in wave-type weakly electric fishes. Journal of Experimental Biology 214, 4141-4150.

Salazar, V.L., Krahe, R., Lewis, J.E., 2013. The energetics of electric organ discharge generation in gymnotiform weakly electric fish. The Journal of experimental biology 216, 2459-2468.

Scheich, H., 1977. Neural basis of communication in the high frequency electric fish, Eigenmannia virescens (jamming avoidance response). Journal of comparative physiology 113, 181-206.

Seabra, S.G., André, G., Quartau, J.A., 2008. Variation in the acoustic properties of the calling songs of Cicada barbara and C. orni (Hemiptera: Cicadidae) at the individual and population levels. ZOOLOGICAL STUDIES-TAIPEI- 47, 1.

Shao, L.R., Halvorsrud, R., Borg-Graham, L., Storm, J.F., 1999. The role of BK-type Ca^{2+}-dependent K^{+} channels in spike broadening during repetitive firing in rat hippocampal pyramidal cells. The Journal of Physiology 521, 135-146.

Shi, S.-H., Hayashi, Y., Petralia, R.S., Zaman, S.H., Wenthold, R.J., Svoboda, K., Malinow, R., 1999. Rapid spine delivery and redistribution of AMPA receptors after synaptic NMDA receptor activation. Science 284, 1811-1816.

Sinnett, P.M., Markham, M.R., 2015. Food deprivation reduces and leptin increases the amplitude of an active sensory and communication signal in a weakly electric fish. Hormones and behavior 71, 31-40.

Sudha, P.M., Low, S., Kwang, J., Gong, Z., 2001. Multiple tissue transformation in adult zebrafish by gene gun bombardment and muscular injection of naked DNA. Marine Biotechnology 3, 119-125.

Thomson, S.J., Angela, H., Sanguinetti, M.C., 2015. Identification of the Intracellular Na^+ Sensor in Slo2. 1 Potassium Channels. Journal of Biological Chemistry, jbc. M115. 653089.

Unguez, G.A., Zakon, H.H., 1998. Reexpression of myogenic proteins in mature electric organ after removal of neural input. The Journal of neuroscience 18, 9924-9935.

Walker, J.E., Saraste, M., Runswick, M.J., Gay, N.J., 1982. Distantly related sequences in the alpha-and beta-subunits of ATP synthase, myosin, kinases and other ATP-requiring enzymes and a common nucleotide binding fold. The EMBO journal 1, 945.

Weber, W.-M., 1999. Ion currents of Xenopus laevis oocytes: state of the art. Biochimica et Biophysica Acta (BBA)-Biomembranes 1421, 213-233.

Yuan, A., Santi, C.M., Wei, A., Wang, Z.-W., Pollak, K., Nonet, M., Kaczmarek, L., Crowder, C.M., Salkoff, L., 2003. The Sodium-Activated Potassium Channel Is Encoded by a Member of the Slo Gene Family. Neuron 37, 765-773.

Zakon, H.H., Lu, Y., Zwickl, D.J., Hillis, D.M., 2006. Sodium channel genes and the evolution of diversity in communication signals of electric fishes: convergent molecular evolution. Proceedings of the National Academy of Sciences of the United States of America 103, 3675-3680.

Zhang, Z., Rosenhouse-Dantsker, A., Tang, Q.-Y., Noskov, S., Logothetis, D.E., 2010. The RCK2 domain uses a coordination site present in Kir channels to confer sodium sensitivity to Slo2. 2 channels. The Journal of Neuroscience 30, 7554-7562.

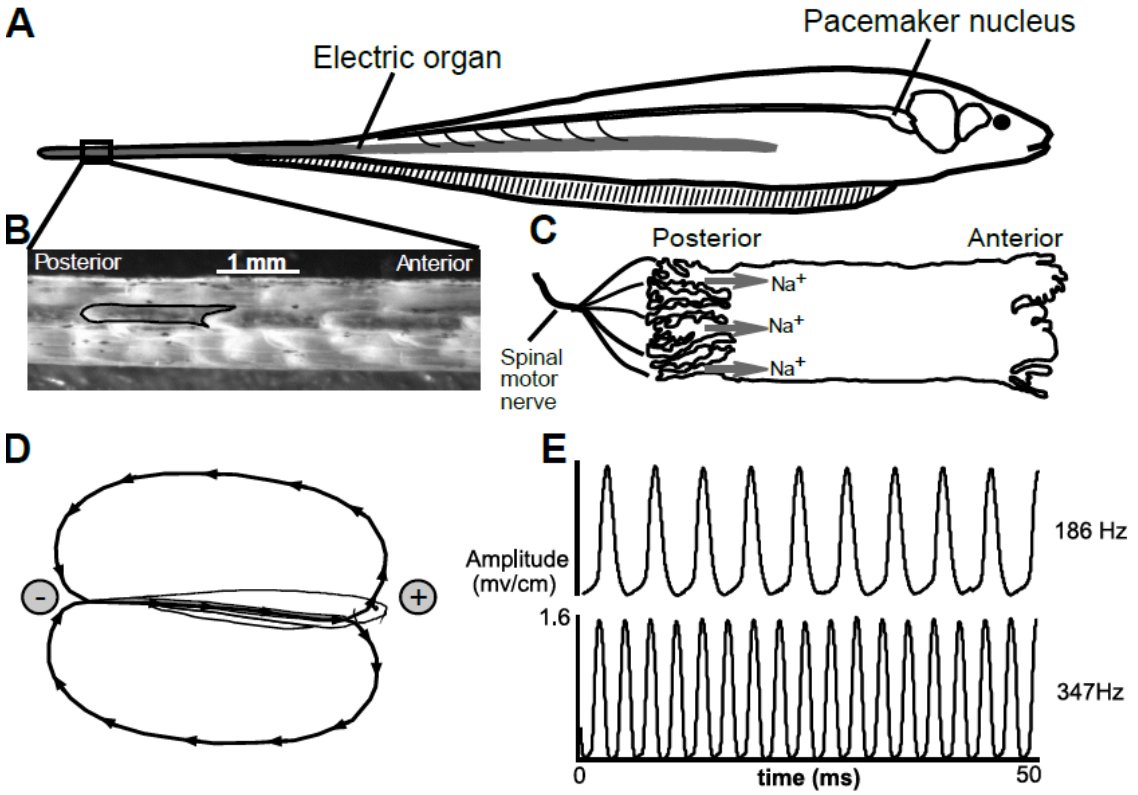

Fig. 1. EOD generation in *E. virescens*. *A:* The EO runs longitudinally along the fish body and extends into the caudal tail filament. *B:* A section from the tail with skin removed to expose the EO. A single electrocyte is outlined in black. *C:* Schematic of an electrocyte. Electrocytes are highly polarized cells approximately 1.5 mm in anterior-posterior length and 0.6 mm in diameter. Electrocyte APs are controlled by the medullary pacemaker nucleus via spinal motor neurons innervating on the posterior membrane of each electrocyte. The cell's innervated posterior face is deeply invaginated and occupied by cholinergic receptors and voltage-gated Na^+ (Na_v) channels. The activation of cholinergic synapses causes an inward Na^+ current. *D:* The Na^+ current moves toward the head, followed by a return path from head to tail in the surrounding water. *E:* The EOD waveforms recorded from fish with high and low EOD frequency. Panels A-D were adapted from Ban et al., 2015.

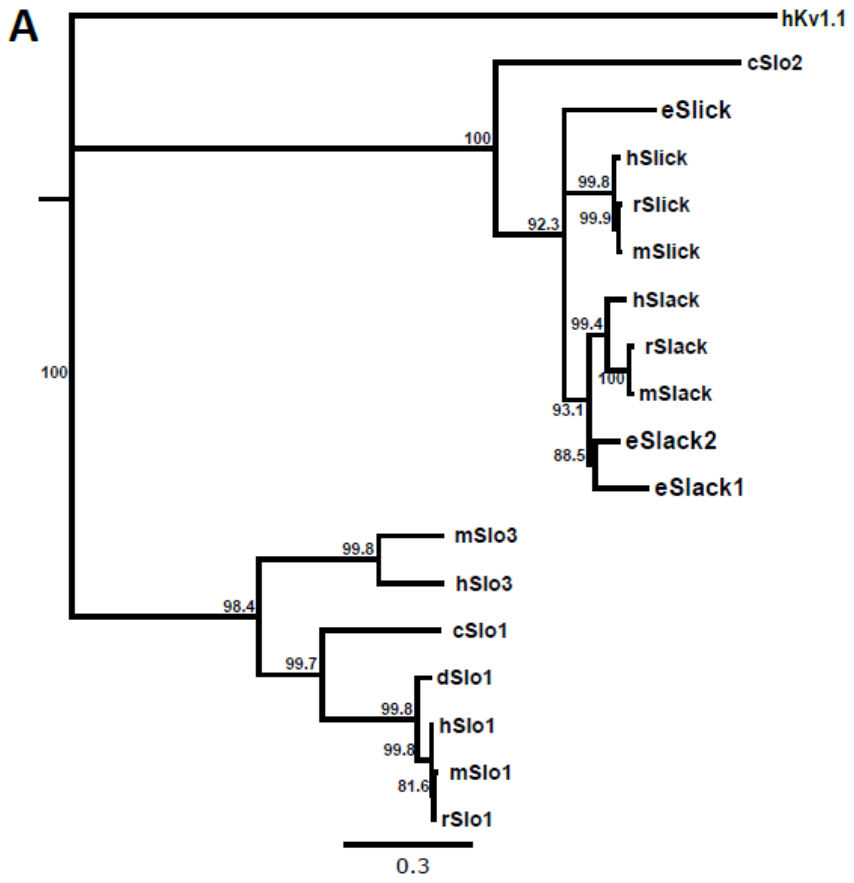
A
hKv1.1
cSlo2
eSlick
hSlick
rSlick
mSlick
hSlack
rSlack
mSlack
eSlack2
eSlack1
mSlo3
hSlo3
cSlo1
dSlo1
hSlo1
mSlo1
rSlo1
100
99.8
99.9
92.3
99.4
100
93.1
88.5
100
99.8
98.4
99.7
99.8
99.8
81.6
0.3

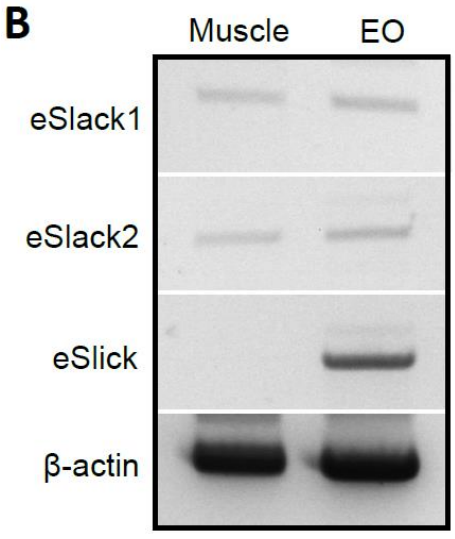
B
Muscle
EO
eSlack1
eSlack2
eSlick
β-actin

Fig. 2. Molecular identities of *E. virescens* K_{Na} channel genes. *A:* A rooted neighbor-joining phylogenetic tree for the high-conductance potassium channels in the SLO family. The family of SLO channels includes Slo1 (the "big" potassium (BK) K_{Ca} channel), Slo2.1 (the Slick K_{Na} channel), Slo2.2 (the Slack K_{Na} channel), and Slo3 (the large-conductance pH-sensitive K^+ channel). Human Kv1.1 was used as the outgroup. (h: *Homo sapiens*; r: *Rattus norvegicus*; m: *Mus musculus*; d: *Danio rerio*; c: *Caenorhabditis elegans*; e: *Eigenmannia virescens*). *B:* Expression pattern of *E. virescens* K_{Na} channels in muscle and EO. eSlack1 and eSlack2 were amplified from the cDNA of both muscle and EO, whereas eSlick was only amplified from EO cDNA. Primers and amplicon sizes are listed in table 1.

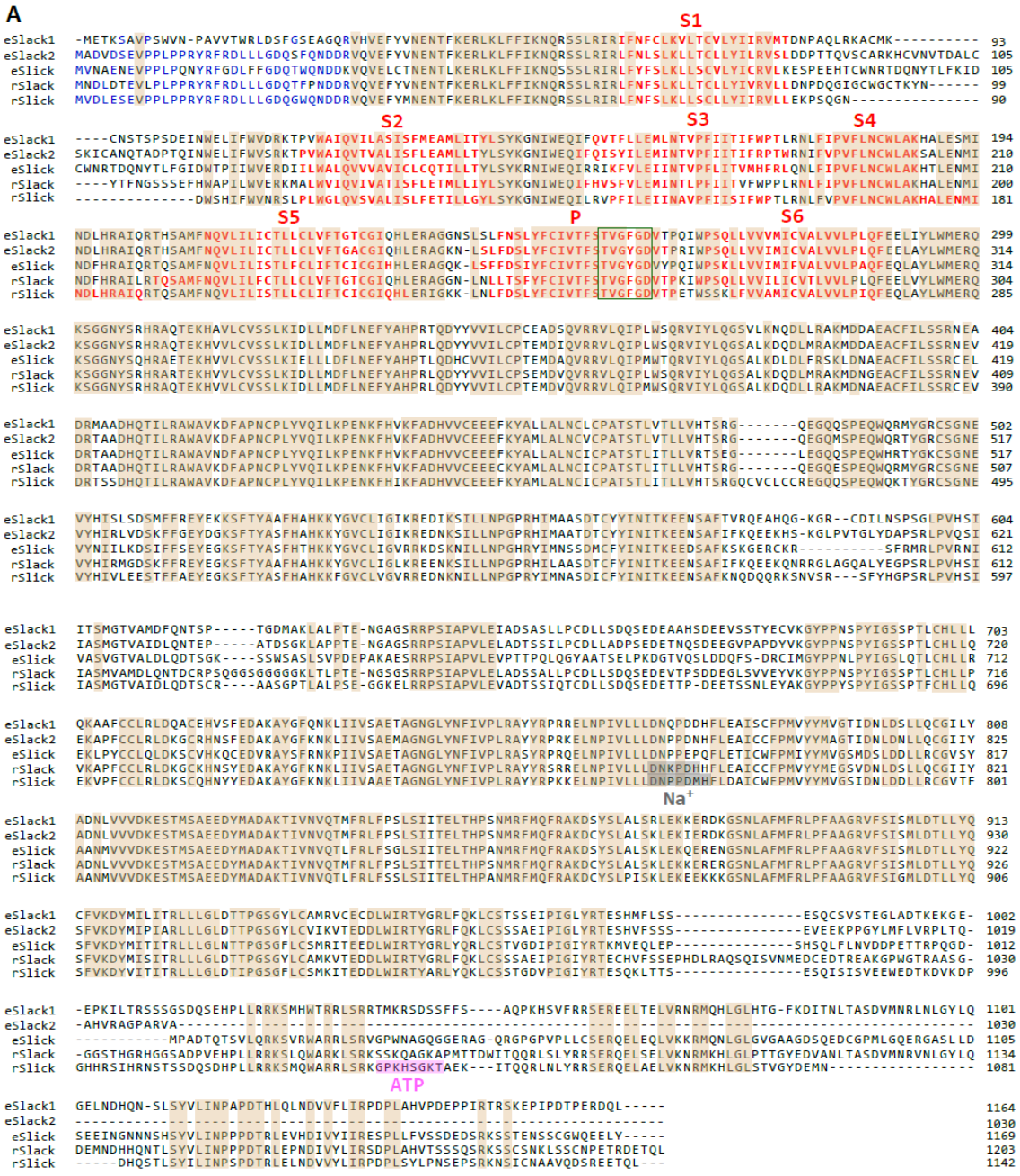
A
S1
S2
S3
S4
S5
P
S6
ATP
Na+

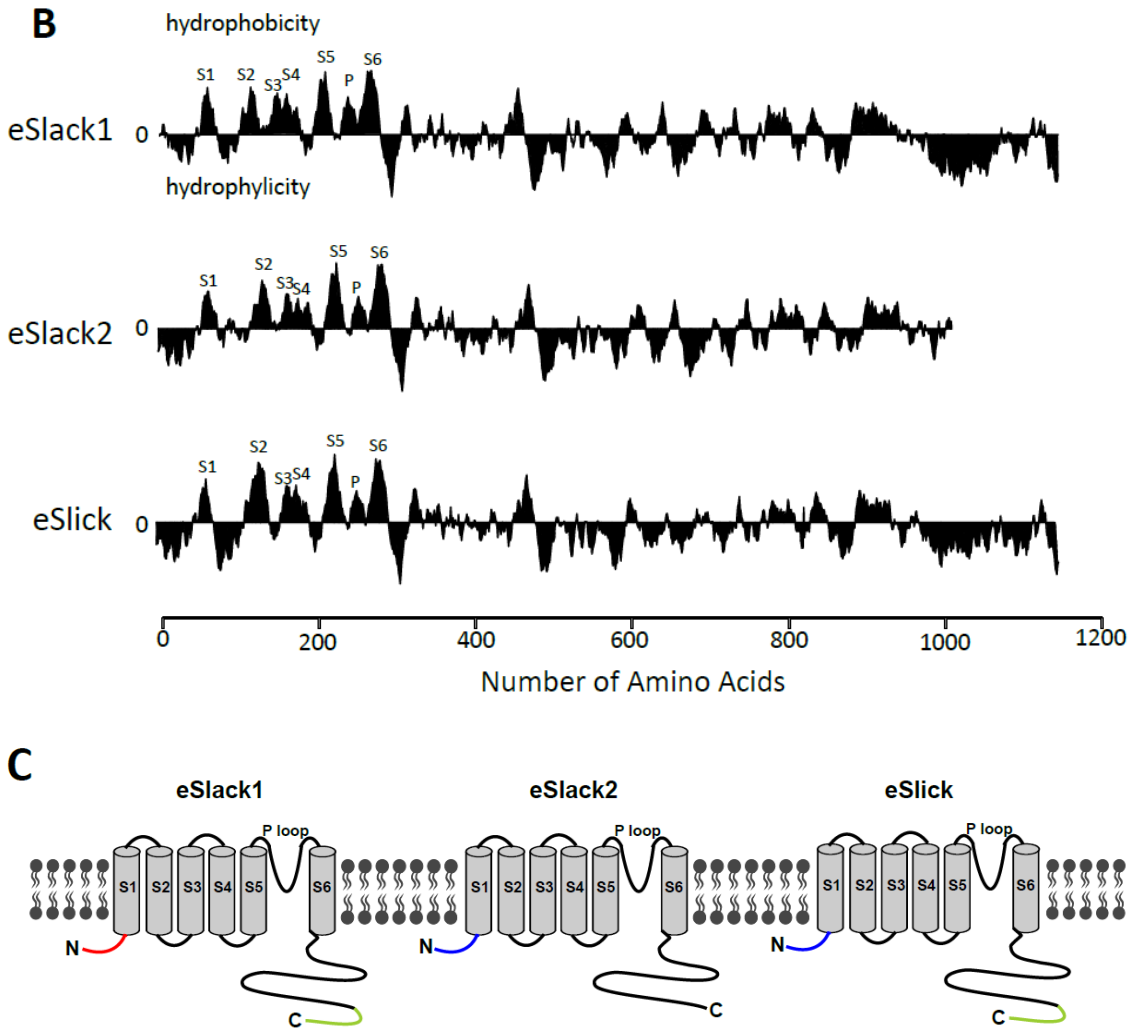

Fig. 3. Sequence and structure of *E. virescens* K_{Na} channels. *A:* Multiple-sequence alignment was run by the Clustal W program using the *Geneious* software. Identical amino acids among all five sequences are shaded in brown except the C-terminal tail, where residues shared by eSlack1, eSlick, rSlack and eSlick are also highlighted. Gaps are represented by dashed lines. In the cytoplasmic N-terminus, identical residues are colored in blue. Red residues represent the membrane-spanning domains (S1-6) and the pore region (P) of the five K_{Na} channels. Within the pore-forming loop, the conserved residues determining the channel's specific selectivity to K^+ ions are highlighted with a green box. Residues shaded in gray represent the Na^+ coordination motifs in rat Slack and Slick. Residues composing the ATP-binding motif of rat Slick are shaded in magenta. Dashed lines indicate gaps. *B:* Kyte-Doolittle hydrophilicity plot of *E. virescens* K_{Na} channels (window size of 19 amino acids). *C:* Schematic representation of *E. virescens* K_{Na} channel subunits. eSlack2 and eSlick have an identical N-terminus (blue), which is different from that of eSlack1(red). The C-terminal tail of eSlack2 is shorter than that of eSlack1 and eSlick (green).

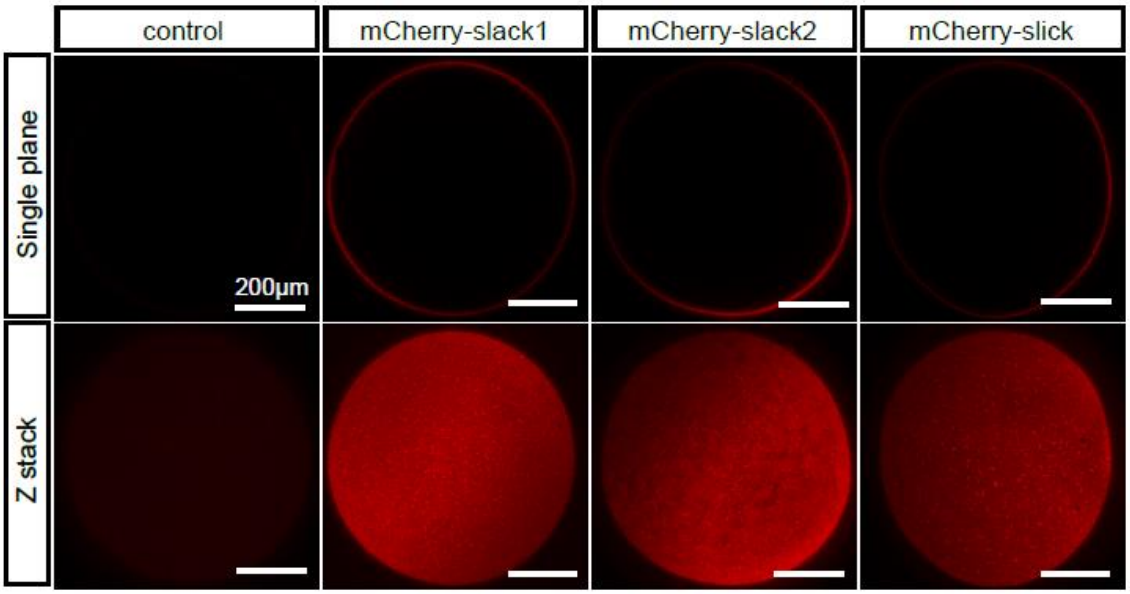

Fig. 4. Expression of mCherry-tagged K_{Na} channels on the plasma membrane of *X. laevis* oocytes. Top panel: Images of *X. laevis* oocytes expressing mCherry-tagged K_{Na} channels taken at the focal plane of the maximal circumference of the cells. Bottom panel: Z stack images of *X. laevis* oocytes expressing mCherry-tagged *E. virescens* K_{Na} channels rendered with maximum intensity projection.

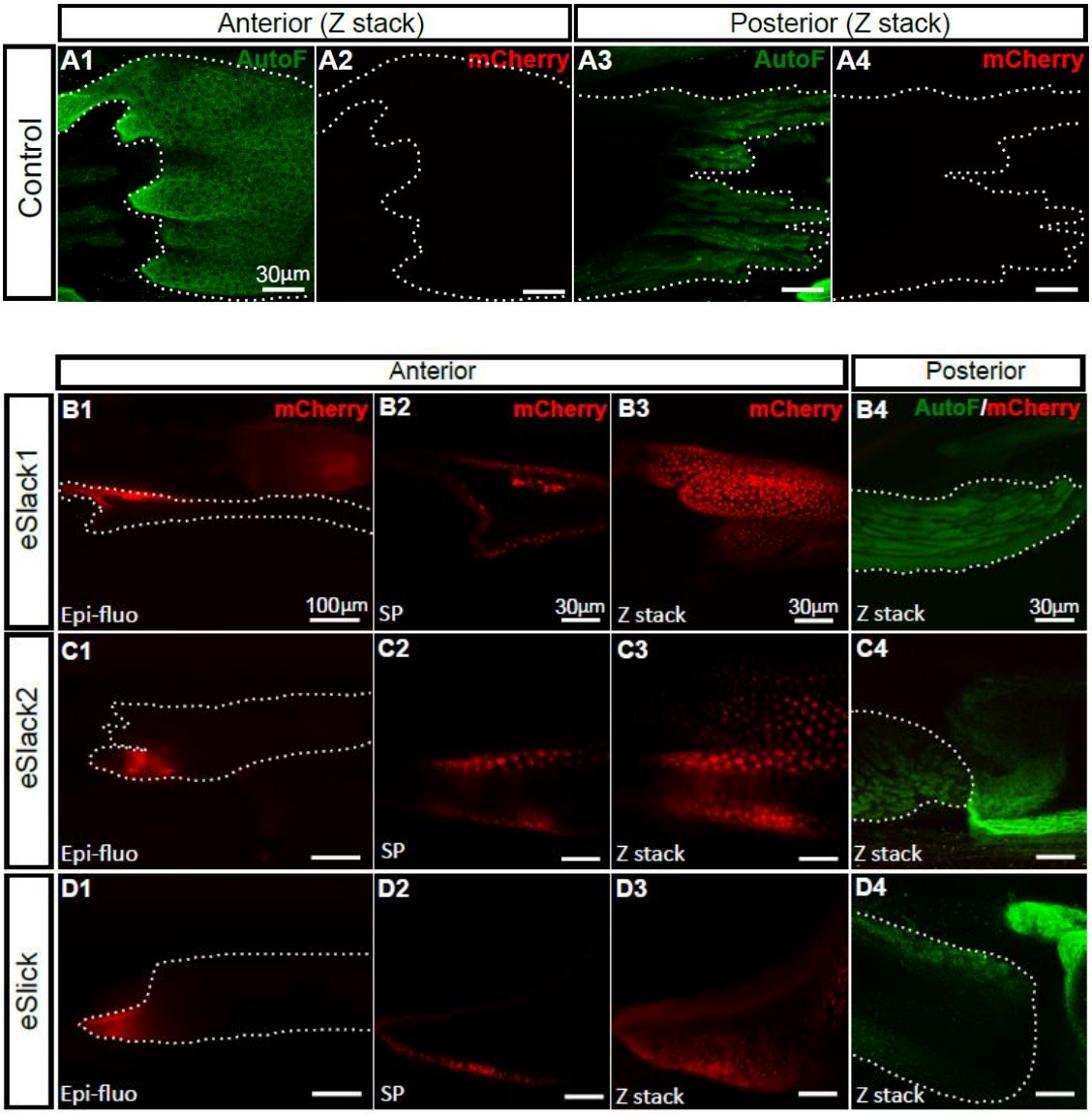

Fig. 5. Distribution of K_{Na} channels in electrocytes. *A:* z stack images of a control electrocyte without expressing mCherry-tagged K_{Na} channels. Tissue autofluorescence (green) was excited by a 488-nm laser. *B-D:* Images of electrocytes expressing mCherry-eSlack/Slick plasmids revealed that all three types of K_{Na} channel subunits are only localized in the anterior region of cells. Images in B1, C1 and D1, acquired using an epifluorescent microscope, show a larger field of view. Other images in B-D were acquired with a laser-scanning confocal microscope. Images displayed in B2, C2 and D2 are single optical sections showing the anterior face from cells expressing recombinant K_{Na} channels (red). B3, C3 and D3 are z stack images rendered from the serial optical sections shown in B2, C2 and D2. Merged images of autofluorescence (green) and mCherry (red) in C4, D4 and E4 revealed that recombinant K_{Na} channels are not expressed on the posterior membrane of electrocytes. White dotted lines indicate the boundaries of electrocytes.

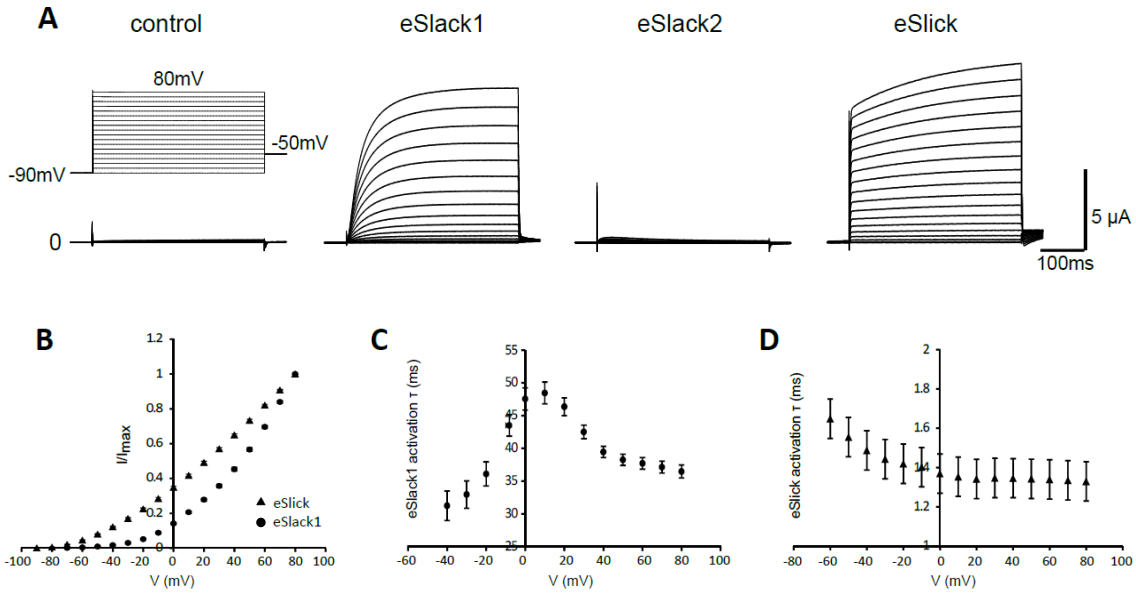

Fig. 6. Whole-cell recordings of *X. laevis* oocytes expressing *E. virescens* K_{Na} channels. *A:* Whole-cell currents recorded when oocytes were depolarized by 400-ms voltage steps ranging from -90 mV to +80 mV in 10-mV increments every 5 s from a holding potential of -90 mV. *B:* Current-voltage relationships of oocytes expressing eSlack1 (circle; n=13) and eSlick (triangle; n=10) channels. Current amplitude was measured as the mean amplitude during the last 30 ms of each pulse, divided by the maximal current amplitude. *C-D:* Activation time constant (τ) of eSlack1 (C; n=13) and eSlick (D; n=10) currents was plotted as a function of membrane potential.

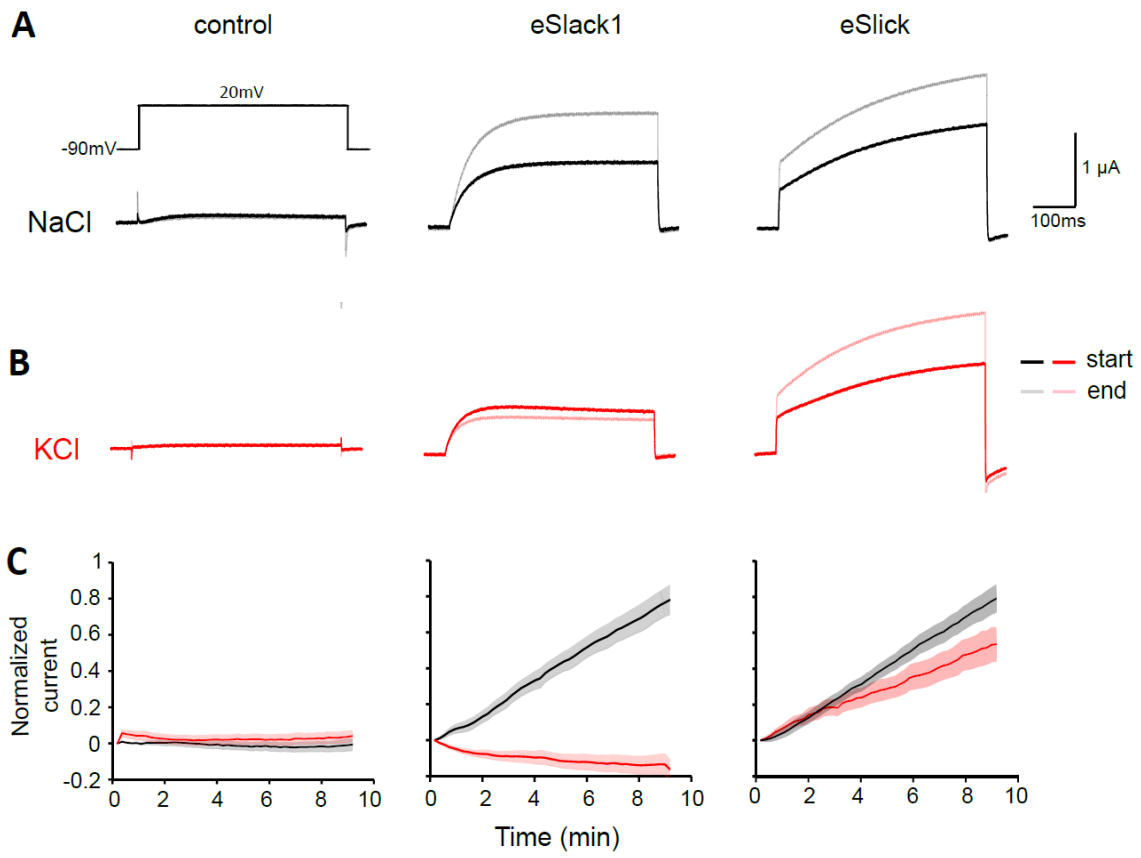

Fig. 7. Comparison between eSlack1 and eSlick whole-cell currents recorded with microelectrodes filled with 2 M NaCl or KCl. Oocytes were depolarized by a 500-ms pulse to +20 mV from a holding potential of -90 mV every 10 s. *A:* With both microelectrodes filled with 2 M NaCl, whole-cell currents recorded from control oocytes (left), oocytes expressing eSlack1 channels (middle), and oocytes expressing eSlick channels (right) immediately after impaling the cell (start; black) and after 9 min of loading (end; gray). *B:* Whole-cell currents recorded from the three types of oocytes mentioned above immediately after impaling the cell (start; red) and 9 min after (end; pink), with both microelectrodes filled with 2 M KCl solution. *C:* Current amplitudes were normalized to the current recorded at "start," taking the log (base 2). Normalized current amplitudes from control cells (left), cells expressing eSlack1 (middle) and cells expressing eSlick (right) were plotted against time with 2 M NaCl (black) or KCl (red) loaded to the cell. Measurements from 8 cells in each group were analyzed. Standard error is shown as gray or pink shading.

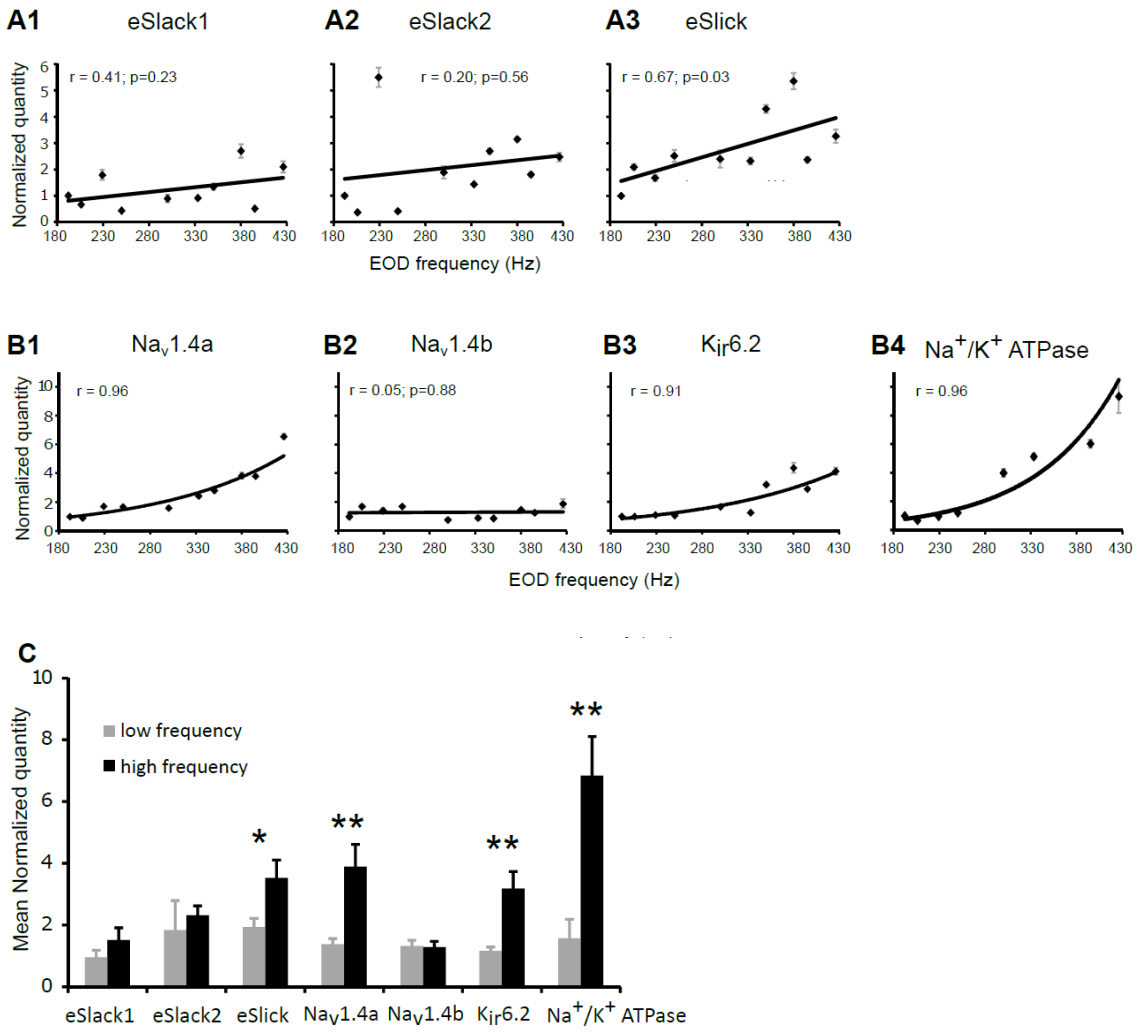

Fig. 8. qRT-PCR quantification of ion channel genes in EOs from *E. virescens* with different EODf. *A-B:* The normalized transcription levels of target genes were plotted against EOD frequency. *A:* The transcription levels of eSlack1 (A1) and eSlack2 (A2) in the EO were not significantly correltaed with EOD frequency. The transcription level of eSlick significantly increased with EOD frequency (A3). *B:* The transcription levels of $Na_v1.4a$ (B1), $K_{ir}6.2$ (B3) and Na^+/K^+ ATPase (B4) in EO from fish with different EOD frequencies can be fitted by exponential curves. There was no correlation between the normalized amounts of $Na_v1.4b$ (B2) transcripts in EO and EOD frequency. *C:* Comparison of the mean transcription levels of genes between low (< 300 Hz) and high (> 300 Hz) frequency EOs. The average amounts of eSlick, $Na_v1.4a$, $K_{ir}6.2$ and Na^+/K^+ ATPase in high-frequency EOs were higher than those in low-frequency EOs. There was no significant difference in the mean transcription levels of eSlack1, eSlack2 and $Na_v1.4b$ between high-and low-frequency EOs. Statistically significant differences are marked by asterisks: One-way ANOVA, one asterisk, $P < 0.05$; two asterisks, $P < 0.01$.

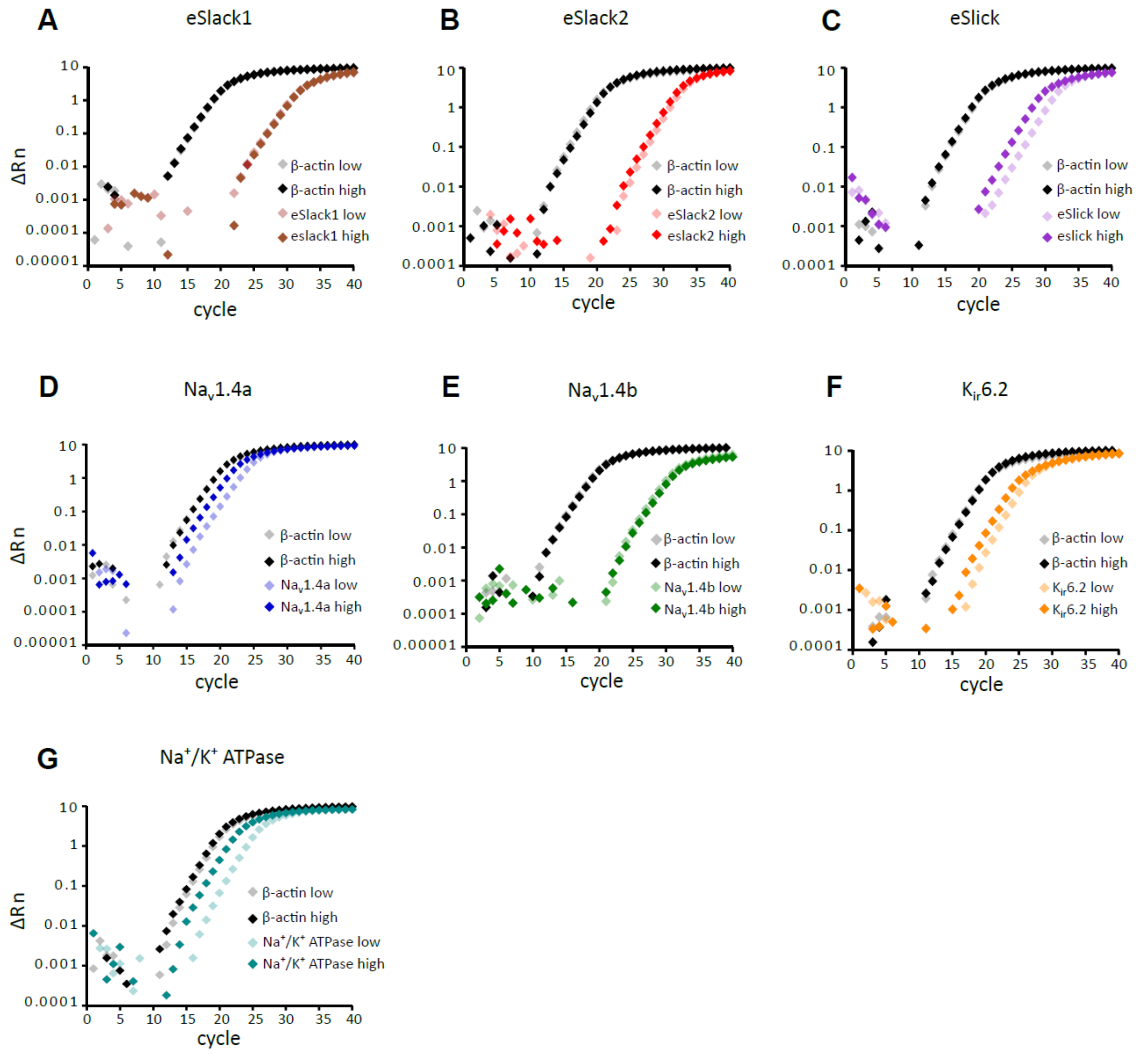

Supplementary Fig. 1. Amplification of the target genes and endogenous control β-actin from EO cDNA of a fish with low EODf and a fish with high EODf. The amplifications of β-actin, eSlack1 (A), eSlack2 (B), and Nav1.4b (E) from EO cDNAs of fish with high and low EODf look identical. eSlick (C), Nav1.4a (D), Kir6.2 (F), and Na^+/K^+ ATPase (G) started amplifying and reached the amplification plateau phase earlier when using EO cDNAs from a fish with high EODf than EO cDNAs from a fish with low EODf.

Table 1. Primers used in reverse transcription PCR

Gene	Primers (F: forward; R: reverse)	Amplicon Size (bp)
β-actin	F 5'-GTATTGTCACTAACTGGG-3' R 5'- CATAGCTTTTCTCCAGAG-3'	501
eSlack1	F 5'-TGTCTTCCACCTACGAGTGC-3' R 5'-CCTCTCTGATCGACGAAACA-3'	1157
eSlack2	F 5'-GGGTTCTGCAGATTCCTCTC-3' R 5'-CCTCTGATGACGAGAACACG-3'	1881
eSlick	F 5'-ATACCCTGTTCGGGATTGAC-3' R 5'-TGTGAACGCAGCTCTTATCC-3'	1845

Table 2. Primers used in qRT- PCR

Gene	Primers (F: forward; R: reverse)	Amplicon Size (bp)
β-actin	F 5'-ATGAGGAAATCGCTGCTCTC-3' R 5'- CCAACAATGGAAGGGAAGAC-3'	103
$Na_v1.4a$	F 5'-CAGCAAGGACAGAAAGGACA-3' R 5'- CAATGGGCACATTCAGAACT-3'	107
$Na_v1.4b$	F 5'-AAACTGAAGGAGGAGGAGGA-3' R 5'- CTTTGGGTTCAGGCTCTTC-3'	98
$K_{ir}6.2$	F 5'-TGTTACCGACATCCACTCGT-3' R 5'- GCAGACACGCATTCTTCTGT-3'	105
Na^+/K^+ ATPase	F 5'-CAGGAGACCTGGTGGAGATT-3' R 5'- ACTCTCCGGTCAGAGAGGAA-3'	105
eSlack1	F 5'-AAGAGCATGCACTGGACAAG-3' R 5'- CCTCTCTGATCGACGAAACA-3'	108
eSlack2	F 5'-GATCCCAATCGGACTGTACC-3' R 5'- CGCACGAGGAACATCAAATA-3'	93
eSlick	F 5'-ATACCCTGTTCGGGATTGAC-3' R 5'- GGCATATGACTGCAACAACC-3'	93

Chapter 4: Conclusion and future directions

The glass knifefish *E. virescens* generates constant high-frequency EODs for navigation and communication. EODs are generated by the synchronous APs of electrocytes in the EO, thus the energetic cost of EOD production arises primarily from the energy consumed by Na^+/K^+ ATPases to restore the ionic gradients after each AP in electrocytes (Bean, 2007). The influx of Na^+ ions during each AP exceeds 10 μA and the amount of ATP molecules required by Na^+/K^+ ATPases to extrude these Na^+ ions is estimated to be two orders of magnitude more than that estimated for mammalian neurons (Attwell and Laughlin, 2001; Howarth et al., 2012; Lewis et al., 2014b). The combination of high firing rates and large ionic currents creates extreme energetic demand for each electrocyte, and for the EO as a whole. Recent experimental and theoretical estimates suggest the cost of EOD production exceeds 30% of the total energy budget (Lewis et al., 2014b; Salazar et al., 2013). This work studied the cellular and molecular mechanisms that enable the electrocyte's functional capacity to maintain high firing rates while managing the extremely large inward Na^+ currents by investigating electrocyte morphology together with the molecular identity, kinetic properties, density and subcellular localization of its ion channels.

3D reconstructions of *E. virescens* electrocytes showed that they are large multi-nucleated cells approximately 1.5 mm in anterior-posterior length and 0.6 mm across on both the lateral-medial axis and the ventral-dorsal axis. The posterior region is deeply invaginated and vascularized with dense layers of vesicles beneath the membrane, while the anterior membrane is relatively smooth, with sparse vascularization and fewer vesicles. The dense vascularization occupying the posterior face facilitates the exchange

of nutrients and metabolic waste, consistent with the presence of high concentrations of mitochondria in the posterior region (Schwartz et al., 1975).

E. virescens electrocytes initiate the AP with Na_v channels and repolarize the AP with K_{Na} channels. The expression pattern of ion channels and ion transporters in electrocytes is highly compartmentalized. Cholinergic receptors and Na_v channels are restricted to the posterior membrane, while K_{Na} channels and $K_{ir}6.2$ channels are localized on the anterior membrane. Na^+/K^+ ATPases are distributed on both the posterior and anterior faces.

The densely packed vesicles beneath the posterior membrane are likely associated with trafficking of Na_v channels and Na^+/K^+ ATPases through the action of ACTH to modulate EOD amplitude following the circadian rhythm (Markham et al., 2009). The lack of vesicles on the anterior membrane suggests that K_{Na} channels are not cycled into and out of membrane in the same manner as Na_v channels. These results are consistent with earlier studies on the effects of ACTH on the ionic currents of *E. virescens* electrocytes. Application of ACTH increased the amplitude of both Na_v and K_{Na} currents. The increase of Na_v currents was a direct effect of ACTH regulating the trafficking of Na_v channels; however, the increase of K_{Na} currents was a secondary effect caused by the increase in Na_v currents (Markham et al., 2013).

The large inward Na^+ currents during each AP together with the high firing rates create significant demands on the Na^+/K^+ ATPases. The invaginations on the posterior side provide more membrane surface area for the expression of high densities of Na^+/K^+ ATPases. The extensive posterior membrane would also increase membrane

capacitance and decrease resistance, which would facilitate current flow during the AP (Schwartz et al., 1975).

K_{Na} channels that repolarize the AP in *E. virescens* electrocytes have not yet been identified in other gymnotiform electric fish in which APs are terminated by classical K_v channels. I identified three types of K_{Na} channel subunits, eSlack1 and eSlick, closely related to K_{Na} channel subunits in other vertebrates, and a novel subunit eSlack2, which is about 100 amino acids shorter. eSlack1 and eSlack2 are expressed in both skeletal muscle and EO while eSlick is expressed only in EO. Whole-cell currents recorded from *X. laevis* oocytes expressing these K_{Na} channels revealed that eSlick currents activated much more rapidly than eSlack1 currents. eSlack2 could not form functional homomeric ion channels, although the subunits could be successfully trafficked to the plasma membrane.

The EOD frequency in *E. virescens* is individually specific. Using qRT-PCR to determine the transcription levels of electrocyte ion channels and Na^+/K^+ ATPases across fish with different EOD frequencies revealed that the mRNA levels of $Na_v1.4a$, eSlick K_{Na} subunit, $K_{ir}6.2$ and Na^+/K^+ ATPase were positively correlated with EOD frequency, while the mRNA levels of $Na_v1.4b$, eSlack1 and eSlack2 K_{Na} subunits were not correlated with EOD frequency. These results suggest that the expression levels of some ion channels in electrocytes are precisely tuned to the cell's firing frequency. Electrocytes are developed from muscle. Most ion channels and ion transporters existed in electrocytes are also present in muscle fibers. However, we found Slick K_{Na} channels, $Na_v1.4a$, and Na^+/K^+ ATPases were predominantly expressed in electrocytes. The expression of these three proteins in electrocytes are not only associated with the

individual variance in EODf, but also contribute to the increased excitability of electrocytes than muscle.

Previous patch-clamp studies of K_{Na} channels in other taxa suggested that channel activation required $[Na^+]_i$ that far exceeds that normally existing in bulk cytoplasm (Dryer, 1994). K_{Na} channels in mammalian neurons were suggested to be closely clustered with Na^+ channels that allow localized accumulation of Na^+ ions sufficient to activate K_{Na} channels without increasing $[Na^+]_i$ in the bulk cytoplasm (Budelli et al., 2009; Hage and Salkoff, 2012). In contrast, K_{Na} channels in *E. virescens* electrocytes do not require proximal sources of Na^+ influx, as all three types of K_{Na} channel subunit are expressed exclusively on the anterior membrane, separated from the Na_v channels on the posterior membrane by more than 1 mm (Ban et al., 2015). This raises the important question of how K_{Na} channels are activated in electrocytes.

Two hypotheses have been proposed to explain how K_{Na} channels are activated in electrocytes. The first hypothesis assumed the activation of *E. virescens* K_{Na} channels requires highly concentrated Na^+, just like K_{Na} channels in other vertebrates. During each AP or sustained high-frequency firing, electrocytes would experience a significant increase in $[Na^+]_i$ in the anterior region, which would be sufficient to activate K_{Na} channels. The other hypothesis assumed electrocytes K_{Na} channels to be more sensitive to $[Na^+]_i$ than other previously identified K_{Na} channel isoforms. Computational simulation of electrocyte APs and Na^+ dynamics indicated that K_{Na} channels were activated by Na^+ concentrations of approximately 15 mM (Ban et al., 2015). By expressing the three K_{Na} channel subunits in *X. laevis* oocytes, we found eSlack1 and eSlick can be activated by intraoocyte Na^+ concentrations of ~10 mM. These results

support the second hypothesis that electrocyte's K_{Na} channel has a higher sensitivity to intracellular Na^+.

To fully understand the activation mechanisms of electrocyte's K_{Na} channels, it is necessary to clarify whether the three K_{Na} channel subunits form heteromeric ion channels and to examine the Na^+ sensitivity of *E. virescens* K_{Na} channels. Heterogeneous expression of *E. virescens* K_{Na} channels in *X. laevis* oocytes showed that eSlack1 and eSlick can form functional homomeric K_{Na} channel and, although eSlack2 could be successfully expressed on the plasma membrane, it could not conduct currents. The difficulty of eSlack2 to form functional K_{Na} channels is probably due to its shorter C-terminal tail. To test this possibility in future experiments, eSlack2 chimeras with the C-terminal tail replaced by the C-terminal tail of eSlack1 and eSlick could be expressed in *X. laevis* oocytes. The presence of whole-cell currents induced by the expression of eSlack2 chimeras would indicate the necessity of an intact C-terminal tail in channel's normal gating properties.

The other possibility is that the function of eSlack2 requires the presence of other K_{Na} channel subunits, eSlack1 and/or eSlick. In mammalian neurons, Slick and the Slack-B isoform can form heteromeric K_{Na} channels (Chen et al., 2009). It is impossible to examine the interactions between the K_{Na} channel subunits by purifying these proteins directly from electrocytes due to the lack of antibodies specific to *E. virescens* Slack and Slick subunits. The interaction could be characterized by expressing recombinant K_{Na} channel subunits fused to peptide tags or fluorescent proteins in *X. laevis* oocytes. One approach would be to express the three types of K_{Na} subunit fused to different immunoreactive peptide tags (e.g. His tag, Myc Tag and HA tag) in oocytes

and use co-immunoprecipitation and western blot to examine protein interactions. The other approach would be to fuse the three types of K_{Na} subunit to cyan fluorescent protein (CFP), yellow fluorescent protein (YFP) and red fluorescent protein (RFP), respectively, express them together in *X. laevis* oocytes and perform single-molecule imaging with total internal reflection fluorescence (TIRF) microscopy.

To precisely determine the Na^+ dependence of electrocyte K_{Na} channels, future experiments could use the inside-out patch clamp method to examine the Na^+ sensitivity of each K_{Na} channel subunit that are expressed in *X.laevis* oocytes. However, the channel's activity as measured *in vitro* may not mimic its activity *in vivo*, as the channel's Na^+ sensitivity may be modulated by other intracellular factors such as NAD^+ (Tamsett et al., 2009) and the perfusion saline would not perfectly match the intracellular environment. Additionally, if the three K_{Na} channel subunits assemble into heterotetrameric complexes, the heteromeric K^+ channel may have different kinetic properties and Na^+ sensitivity from homomeric K_{Na} channels. Due to the lack of antibodies specific to eSlack2 and eSlick subunit, it is impossible to determine the relative density of each subunit in electrocytes, making it extremely hard to mimic the composition of K_{Na} channels in an exogenenous expression system. Alternatively, the activity of K_{Na} channels can be examined in electrocytes. Fluorescent indicators of Na^+ and/or K^+ could be loaded into a single electrocyte, then high-speed imaging can be performed to monitor the temporal and spatial dynamics of $[Na^+]_i$ and $[K^+]_i$ while the cell is stimulated to generate high-frequency APs. This approach would not only allow studying the activity of K_{Na} channels *in vivo*, but also would help to determine how ion

channels and Na^+/K^+ ATPases coordinate to manage the large influx of Na^+ ions under sustained high-frequency firing.

E. virescens electrocytes generate APs constantly at high frequency ranging from 200 to 500 Hz. Some neurons in mammalian brain, such as certain neocortical and hippocampal interneurons and neurons in the auditory pathway located in the brainstem, are also able to generate APs at very high frequency (>600 Hz) (Erisir et al., 1999; Kaczmarek et al., 2005). Results of the present research will not only contribute to understanding of the biophysical mechanisms allowing the generation of sustained high-frequency firing in electrocytes but also to the understanding of general strategies adopted by excitable cells to achieve the fast-spiking phenotype. The bioelectrical properties of electrogenic cells such as neurons, myocytes, and electrocytes depend on cell morphology and the subcellular localization and functional properties of ion channels responsible for AP generation. Among various ion channels, the number and characteristics of K^+ channels have been suggested to be key determinants of spiking rate (Faber and Sah, 2003; Few and Zakon, 2007; Massengill et al., 1997). More than 100 types of K^+ channel subunits with different biophysical properties have been identified to date (Coetzee et al., 1999). Fast-activating K^+ channels give cells the ability to spike quickly (Hasenstaub et al., 2010); for example, fast-spiking cortical and hippocampal neurons often incorporate voltage-gated K^+ channels of the K_v3 subfamily, which show fast activation and deactivation kinetics (Erisir et al., 1999; Lien and Jonas, 2003; Rudy and McBain, 2001). The present study identified the expression of a fast-activating Slick K_{Na} channels in *E. virescens* electrocytes and demonstrated the role of these channels in supporting the generation of high-frequency APs by showing that the

spiking rate of electrocytes is correlated with the transcription level of Slick K_{Na} channels but not the transcription level of the slow-activating Slack1 K_{Na} channels.

Besides functional requirements, minimizing the metabolic cost of AP generation is likely another major constraint governing the kinetics and density of ion channels (Hasenstaub et al., 2010). K^+ channels with faster activation kinetics will enable higher firing rates, but at the expense of increased energy consumption due to the more extensive overlap between the inward Na^+ currents and the outward K^+ currents. *E. virescens* electrocytes incorporate K_{Na} channels to meet the fast-spiking requirement and to minimize the wasteful energy during AP generation. Results from a computational simulation to compare the energetic efficiency of model electrocytes expressing K_{Na} channels and $K_v3.1$ channels indicated that K_{Na} channels made the generation of 500-Hz APs ~30% more energetically efficient by reducing the overlap between the depolarizing Na^+ and repolarizing K^+ currents (Markham et al., 2013).

Molecular adaptations that maximize electrocyte spiking functions while minimizing metabolic costs may also occur in other ion channels and transporters, such as $K_{ir}6.2$ channels and Na^+/K^+ ATPases. *E. virescens* electrocytes express Kir6.2 channels and a type of sulphonylurea receptor (SUR) which belongs to the ATP-binding cassette (ABC) superfamily (R. Maltby and M.R. Markham; unpublished data). In other systems, the activity of $K_{ir}6.2$-SUR complex is inhibited by physiological levels of ATP, and the channel's open probability increases as the intracellular concentration of ATP falls (Inagaki et al., 1995). The presence of ATP-sensitive $K_{ir}6.2$ channels in electrocytes may form an endogenous protective system to stabilize the cell's bioelectrical properties under energetic constraints. Studies of the molecular evolution

of Na^+/K^+ ATPases in weakly electric fish suggested the presence of positive selection in the α2 subunit of Na^+/K^+ ATPase within lineages with higher EOD frequencies (H. Riedmann and M.R. Markham; unpublished data). In *E. virescens* electrocytes, approximately 6×10^{10} Na^+ ions enter the cell during each AP. Efficient removal of these Na^+ ions during the 1-2 millisecond interspike interval requires high densities of Na^+/K^+ ATPases or extremely fast Na^+/K^+ ATPases or both. Results of the present study showed that higher transcription levels of $K_{ir}6.2$ and Na^+/K^+ ATPase were present in electrocytes with higher firing rates. Future studies focusing on the properties of the $K_{ir}6.2$-SUR complex and the consequences of those amino acid substiutions that are under positive selection in electrocyte Na^+/K^+ ATPases are necessary to fully understand the molecular adaptations that maximize electrocyte's spiking ability while minimizing the energetic costs. Discoveries arising from continued investigation of the molecular mechanisms of fast-spiking in electrocytes will likely have important implications for the mechanisms that balance the metabolic costs with the information coding advantage of fast-spiking neurons in central neural systems (Howarth et al., 2012).

REFERENCES

Attwell, D., Laughlin, S.B., 2001. An energy budget for signaling in the grey matter of the brain. Journal of Cerebral Blood Flow & Metabolism 21, 1133-1145.

Ban, Y., Smith, B.E., Markham, M.R., Ban, Y., 2015. A highly-polarized excitable cell separates sodium channels from sodium-activated potassium channels by more than a millimeter. Journal of neurophysiology, jn. 00475.02014.

Bean, B.P., 2007. The action potential in mammalian central neurons. Nature Reviews Neuroscience 8, 451-465.

Budelli, G., Hage, T.A., Wei, A., Rojas, P., Jong, Y.-J.I., O'Malley, K., Salkoff, L., 2009. Na^+-activated K^+ channels express a large delayed outward current in neurons during normal physiology. Nature neuroscience 12, 745-750.

Coetzee, W.A., Amarillo, Y., Chiu, J., Chow, A., Lau, D., McCormack, T., Morena, H., Nadal, M.S., Ozaita, A., Pountney, D., 1999. Molecular diversity of K^+ channels. Annals of the New York Academy of Sciences 868, 233-255.

Dryer, S.E., 1994. Na^+-activated K^+ channels: a new family of large-conductance ion channels. Trends in neurosciences 17, 155-160.

Erisir, A., Lau, D., Rudy, B., Leonard, C., 1999. Function of specific K^+ channels in sustained high-frequency firing of fast-spiking neocortical interneurons. Journal of neurophysiology 82, 2476-2489.

Faber, E., Sah, P., 2003. Ca^{2+}-activated K^+ (BK) channel inactivation contributes to spike broadening during repetitive firing in the rat lateral amygdala. The Journal of physiology 552, 483-497.

Few, W.P., Zakon, H.H., 2007. Sex differences in and hormonal regulation of K_v1 potassium channel gene expression in the electric organ: molecular control of a social signal. Developmental neurobiology 67, 535-549.

Hage, T.A., Salkoff, L., 2012. Sodium-activated potassium channels are functionally coupled to persistent sodium currents. The Journal of Neuroscience 32, 2714-2721.

Hasenstaub, A., Otte, S., Callaway, E., Sejnowski, T.J., 2010. Metabolic cost as a unifying principle governing neuronal biophysics. Proceedings of the National Academy of Sciences 107, 12329-12334.

Howarth, C., Gleeson, P., Attwell, D., 2012. Updated energy budgets for neural computation in the neocortex and cerebellum. Journal of Cerebral Blood Flow & Metabolism 32, 1222-1232.

Inagaki, N., Tsuura, Y., Namba, N., Masuda, K., Gonoi, T., Horie, M., Seino, Y., Mizuta, M., Seino, S., 1995. Cloning and functional characterization of a novel ATP-sensitive potassium channel ubiquitously expressed in rat tissues, including pancreatic islets, pituitary, skeletal muscle, and heart. Journal of Biological Chemistry 270, 5691-5694.

Kaczmarek, L.K., Bhattacharjee, A., Desai, R., Gan, L., Song, P., von Hehn, C.A., Whim, M.D., Yang, B., 2005. Regulation of the timing of MNTB neurons by short-term and long-term modulation of potassium channels. Hearing research 206, 133-145.

Lewis, J.E., Gilmour, K.M., Moorhead, M.J., Perry, S.F., Markham, M.R., 2014. Action Potential Energetics at the Organismal Level Reveal a Trade-Off in Efficiency at High Firing Rates. The Journal of Neuroscience 34, 197-201.

Lien, C.-C., Jonas, P., 2003. K_v3 potassium conductance is necessary and kinetically optimized for high-frequency action potential generation in hippocampal interneurons. The Journal of neuroscience 23, 2058-2068.

Markham, M.R., Kaczmarek, L.K., Zakon, H.H., 2013. A sodium-activated potassium channel supports high-frequency firing and reduces energetic costs during rapid modulations of action potential amplitude. Journal of neurophysiology 109, 1713-1723.

Markham, M.R., McAnelly, M.L., Stoddard, P.K., Zakon, H.H., 2009. Circadian and social cues regulate ion channel trafficking. PLoS biology 7, e1000203.

Massengill, J.L., Smith, M.A., Son, D.I., O'dowd, D.K., 1997. Differential expression of K4-AP currents and K_v3. 1 potassium channel transcripts in cortical neurons that develop distinct firing phenotypes. The Journal of neuroscience 17, 3136-3147.

Salazar, V.L., Krahe, R., Lewis, J.E., 2013. The energetics of electric organ discharge generation in gymnotiform weakly electric fish. The Journal of experimental biology 216, 2459-2468.

Rudy, B., McBain, C.J., 2001. Kv3 channels: voltage-gated K^+ channels designed for high-frequency repetitive firing. Trends in neurosciences 24, 517-526.

Schwartz, I., Pappas, G., Bennett, M., 1975. The fine structure of electrocytes in weakly electric teleosts. Journal of neurocytology 4, 87-114.

Tamsett, T.J., Picchione, K.E., Bhattacharjee, A., 2009. NAD^+ activates K_{Na} channels in dorsal root ganglion neurons. The Journal of Neuroscience 29, 5127-5134.